Gas Sensors Based on Perovskite Structured Material

Dissertation

der Mathematisch-Naturwissenschaftlichen Fakultät

der Eberhard Karls Universität Tübingen

zur Erlangung des Grades eines

Doktors der Naturwissenschaften

(Dr. rer. nat.)

vorgelegt von

Abdulaziz Alharbi

aus Alrass, Saudi Arabia

Tübingen

2020

Gedruckt mit Genehmigung der Mathematisch-Naturwissenschaftlichen Fakultät der Eberhard Karls Universität Tübingen.

Tag der mündlichen Qualifikation:	12.05.2020
Dekan:	Prof. Dr. Wolfgang Rosenstiel
1. Berichterstatter:	Prof. Dieter Kölle
2. Berichterstatter:	Dr. Nicolae Barsan

Table of Contents

Abstract (English) 5

Abstract (German) 7

List of Abbreviations 9

List of Symbols 10

1. Introduction and motivation 11

2. Background 14

2.1 Dissolved Gas Analysis (DGA) online monitoring 14

2.1.1 Gas extraction methods 14

2.1.2 Detection of dissolved gases 14

2.1.3 Interpretation of DGA Data 16

2.2 Semiconducting metal-oxide gas sensors (SMOX) 19

2.3 General aspects of perovskites 24

2.3.1 Structural properties 24

2.3.2 Surface reactions 25

2.3.3 Catalytic Properties of $LaFeO_3$ 27

2.4 Adsorption and reaction of analytes on metal oxide surfaces 29

2.4.1 CO_2 29

2.4.2 Hydrocarbons 31

2.5 Using Operando Spectroscopy for Understanding the Gas Sensing Mechanism 32

3. Materials and Experimental Methods 34

3.1 Sample preparation 34

3.1.1 Material synthesis 34

3.1.2 Sensor fabrication 37

3.2 Experimental Techniques 38

3.2.1 Structural and Morphological Characterizations 38

3.2.2 DC Resistance Measurements 38

3.2.3 Operando DRIFT Spectroscopy 39

3.2.4 Catalytic Conversion Measurements 41

4. Gas Sensing Properties 43

4.1 Material characterization 43

4.1.1 Solid state reaction 43
4.1.2 Sol gel 45
4.2 Gas sensing performance 46
4.2.1 Sensors based on solid state reaction 46
4.2.2 Sensors based on sol gel 49
4.3 Solid state vs Sol gel synthesis of the LFO based gas sensor 51
4.4 Gas sensing properties of LFO(600) 53
4.4.1 Selectivity 53
4.4.2 Humidity effect 56
4.4.3 CO_2 background 57
4.4.4 Cross Sensitivity 58
4.4.5 Non-Stoichiometric Compound 59
4.5 Conclusion 61
5. Investigations of the ethylene and acetylene sensing mechanism 62
5.1 Investigation of Ethylene and Acetylene Surface Reactions 63
5.1.1 CO_2 reactivity on LFO surface 65
5.1.2 Hydrocarbons reactivity on LFO surface 76
5.2. The role of platinum in the gas sensing mechanism 91
5.2.1 DC resistance measurements 91
5.2.2 DRIFT investigations 93
5.2.3 The origin of CO_2 98
5.3. Gas sensing mechanism 101
5.4 Conclusion 105
6. Summary 106
7. Outlook 108
8. References 109

Abstract (English)

Gas sensing using metal oxides can be a highly cost effective and reliable technology in a variety of medical and industrial applications. However, selectively sensing a specific gas in a complex gas mixture continues to be a significant challenge in many applications, in particular for closely related analyte gases such as acetylene and ethylene. For example, the specific individual concentrations of dissolved gases (C_2H_2, C_2H_4, CH_4, C_2H_6, CO, CO_2 and H_2) that emerge in electrical power transformer oils provide critical diagnostic information about the transformer's stable operation and safety. It is therefore useful to have sensors that can selectively differentiate between these individual gases. To achieve this, I used the $LaFeO_3$ perovskite and investigated its gas sensing mechanism in detail.

The powders of $LaFeO_3$ perovskite were obtained by two different synthesis methods, namely solid state reactions and sol gel processes. I then used this material as an active sensing layer during exposure to dissolved gases. All of my sensors showed a significant response to unsaturated hydrocarbons, namely acetylene and ethylene, but not to the other gases that I tested. I further improved this high selectivity of my sensors, to only detect acetylene and not ethylene, by controlling the operating temperature. The effects of different background conditions, such as humidity and CO_2 levels, on the $LaFeO_3$ sensors were also characterized.

To understand the origin of the sensing mechanism of my sensors, I combined catalytic conversion measurements with simultaneously performed operando DRIFT (Diffuse Reflectance Infrared Fourier Transform) spectroscopy and DC resistance measurements. I applied the operando investigation technique to the relevant analytes, CO_2, C_2H_4 and C_2H_2, in order to identify the type and role of different

adsorbates in mediating selective gas sensing. DRIFT spectra revealed that at 150°C, the reaction with both acetylene and ethylene resulted in surface formate species; at higher temperatures, this was the case only for acetylene. Accordingly, the $LaFeO_3$ responds to both gases at 150°C but only to acetylene at 250°C. Finally, I could identify the mechanism by which the formate species are responsible for the sensor response, and the essential additional role played by Pt electrodes used in my sensors in the detection of ethylene and the temperature dependent selectivity.

Abstract (German)

Gassensorik mit Metalloxiden kann eine sehr kosteneffektive und verlässliche Technologie für eine Vielzahl medizinischer und industrieller Anwendungen darstellen. Jedoch stellt das selektive Erkennen eines spezifischen Gases in einer komplexen Gasmischung, nach wie vor eine große Herausforderung dar. In besonderem Maße gilt dies bei eng verwandten Analytgasen, wie Acetylen und Ethylen. Ein Anwendungsbeispiel hierfür bildet die Quantifizierung einzelner Analyte (C_2H_2, C_2H_4, CH_4, C_2H_6, CO, CO_2 and H_2) in der Gasphase von Transformatorenöl, wodurch kritische diagnostische Informationen zum stabilen und sicheren Betrieb von Hochspannungstransformatoren erhalten werden können. Daher ist eine Notwendigkeit für Sensoren gegeben, die selektiv zwischen diesen Einzelgasen unterscheiden können. Um solche Sensoren zu verwirklichen, habe ich $LaFeO_3$ Perovskite eingesetzt und deren Gassensormechanismus im Detail untersucht.

Die $LaFeO_3$ Pulver wurden mithilfe zweier unterschiedlicher Synthesemethoden realisiert, namentlich durch eine Festphasenreaktion und durch ein Sol-Gel Verfahren. Ich verwendete diese Materialen dann als aktive, gassensitive Schicht unter Exposition gegenüber der gelösten Analytgase. Alle von mir getesteten Sensoren zeigten signifikante Sensorantworten auf ungesättigte Kohlenwasserstoffe, namentlich Acetylen und Ethylen, jedoch keine Antworten auf andere hier getestete Gase. Des Weiteren konnte ich die hohe Selektivität dieser Sensoren durch Kontrolle der Betriebstemperatur weiter verbessern, so dass ausschließlich Acetylen, kein Ethylen, von den Sensoren gemessen werden konnte. Die $LaFeO_3$ Sensoren wurden bezüglich des Einflusses verschiedener Hintergrundbedingungen, wie variierende Feuchtigkeit und CO_2 Konzentration, charakterisiert.

Um die Herkunft der gassensorischen Eigenschaften dieser Sensoren zu verstehen, führte ich kombinierte Messungen des katalytischen Umsatzes mit simultaner operando-DRIFT (Diffuse Reflectance Infrared Fourier Transform) Spektroskopie und Gleichstrom-Widerstandsmessungen durch. Diese „operando“-Techniken wendete ich für alle relevanten Analyte (CO_2, C_2H_4 und C_2H_2) an, um die Art und die Rolle der unterschiedlichen Oberflächenabsorbate als Vermittler der selektiven Gassensorantwort zu identifizieren. DRIFT Spektren zeigten, dass bei 150°C die Reaktion mit sowohl Acetylen, wie auch Ethylen, an der Oberfläche zur Bildung von Formiaten führte; bei höheren Temperaturen jedoch geschah dies ausschließlich bei der Reaktion mit Acetylen. Entsprechend, reagierte $LaFeO_3$ bei 150°C auf beide Gase, bei 250°C jedoch nur auf Acetylen. Schlussendlich konnte ich den Mechanismus, durch den die Formiatspezies sich für die Sensorantwort verantwortlich zeigt, identifizieren und die zusätzliche, aber grundlegende Rolle der hierbei verwendeten Platinelektroden bei der Detektion von Ethylen und dessen temperaturabhängiger Selektivität beleuchten.

List of Abbreviations

LFO	$LaFeO_3$
DGA	Dissolved Gas Analysis
C_2H_2	Acetylene
C_2H_4	Ethylene
CH_4	Methane
C_2H_6	Ethane
CO	Carbon monoxide
CO_2	Carbon dioxide
H_2	Hydrogen
DRIFT	Diffuse Reflectance Infrared Fourier Transform
a.u.	Arbitrary units
S.S.	Sensor signals
ppm	Parts per million
r.h.	Relative humidity
SEM	Scanning Electron Microscopy
SMOX	Semiconducting Metal Oxide
VOCs	Volatile Organic Compounds
XRD	X-ray Diffraction
LFO @ Pt – electrode	LFO deposited on the substrates with Pt electrodes
LFO @ Au – electrode	LFO deposited on the substrates with Au electrodes

List of Symbols

$e\Delta V_s$	Band bending
k	Boltzmann constant
n_b	Concentration of electrons in the conduction band
n_s	Concentration of electrons in the conduction band at the surface
e	Elementary charge of an electron
V_s	Surface potential
ΔV_s	Change of the surface potential
R_{air}	Resistance in the clean air
R_{gas}	Resistance in the presence of a target Gas
T	Temperature

1. **Introduction and motivation**

Gas sensing is critical in many medical and industrial applications [1]. The ideal sensor is one that is cost effective but highly reliable. Moreover, since multiple gases are common in a variety of applications, the selectivity of the sensor to a specific gaseous compound, as opposed to others simultaneously present, becomes absolutely necessary [2]. However, if a sensor is unable to distinguish between these many different compounds, then false indications about the nature of the problem can occur, increasing the costs of maintenance and repairs.

In recent years, the method known as Dissolved Gas Analysis (DGA) has attracted much attention [3–6]. The method measures the dissolved gases that are present in transformer oil. Examples of such gases are acetylene (C_2H_2), ethylene (C_2H_4), methane (CH_4), ethane (C_2H_6), carbon monoxide (CO), carbon dioxide (CO_2), and hydrogen (H_2). These gases are generated by the decomposition processes of insulation materials when the transformer has faults. Measuring the concentration of such gases provides critical information about the transformer health status [7]. Depending on the type of fault, different types of decomposition processes can occur. For example, the presence of the hydrocarbons (e.g. ethylene and acetylene) and hydrogen in a certain concentration is an indication of thermal and electrical defects. Among the dissolved gases, acetylene and ethylene are generally considered to be the most important ones in transformer oil diagnostics, especially because they indicate significant characteristic signs of arcing and thermal faults [8]. Detecting and monitoring acetylene and ethylene, which are colorless and flammable hydrocarbons, without interference by other related gases is therefore of considerable interest in a wide range of industrial applications, even beyond the one that I focus on here (power transformer oil).

On-line monitoring of DGA in power transformer oil has many advantages such as an early indication of unusual behavior of power transformer which helps to avoid serious risks which makes the maintenance cost very small compared to unexpected shutdown of the power transformer. It can additionally be part of standard data collection routines during normal operation. This can allow engineers to analyze and plan routine maintenance activities more efficiently and cost-effectively.

Many studies have been conducted to improve the detection of the above-mentioned gases in terms of sensitivity and selectivity. Recently, Q. Zhang et al. have reviewed the wide use of a gas sensor based on tin oxide (SnO_2) for detecting typical fault characteristic gases extracted from power transformer oil [9]. Different preparation methods and dopant additions have been used to enhance the sensing performance of such tin oxide sensors. Moreover, WO_3 [10] and ZnO [11,12] have been employed to detect some of the same gases. Despite the huge amount of work carried out, selectivity remains a main challenge for developing practical sensors based on metal oxides to detect these gases independently and individually.

Perovskites have been considered as a promising candidate for gas sensing applications due to their high selectivity to specific gases, low operating temperatures as compared to single metal oxide materials, and their suitability for deployment under harsh environments and catalytic activity [13–15]. More details about perovskites will be given in section 2.3.

In this work, I used different preparation methods (solid state reaction and sol gel) to produce $LaFeO_3$ (LFO) with a perovskite-type structure. I investigated the sensing performance of LFO-based gas sensing materials in order to enhance the selectivity for unsaturated hydrocarbons, namely acetylene and ethylene, without interference by other gases, including CH_4, C_2H_6, CO, CO_2, and H_2. This exceptional property

could be further improved to be only selective to acetylene alone by controlling the operating temperatures of the sensor. Moreover, I explored the interaction between the gas being sensed and the surface of the perovskite using a combination of simultaneous operando DRIFT (Diffuse Reflectance Infrared Fourier Transform) spectroscopy and DC resistance measurements. I aimed to evaluate the adsorbed species on the material's surface during the progress of the reaction, and to define their role in the electrochemical properties of the gaseous interaction. In addition, the catalytic properties of the sensitive layer (perovskite) and other sensor's parts (electrodes) to the hydrocarbons have been considered in order to find out their role in enhancing the sensing performance of the sensor in particular the selectivity. As a result, I developed a deep mechanistic insight of the sensing process afforded by my LFO sensors.

2. Background

2.1 Dissolved Gas Analysis (DGA) online monitoring

To reach an accurate and effective online DGA monitoring, I mainly need three things; a gas extraction technique, a sensor to detect dissolved gases, and a method to interpret the DGA data. In this section, I provide an overview of each part including its working principles and a brief comparison between different techniques.

2.1.1 Gas extraction methods

There are many techniques to extract (degas) dissolved gases from oil. For example, there is a class of vacuum extraction methods using a Toepler pump or non-mercury vacuum pumps. It uses a repetitive vacuum extraction principle to separate gases from oil [16]. Another common degassing technique is based on the headspace principle by direct contact between the oil and a small gas phase above or through a membrane separating the two phases [17,18]. The latter method is widely used by manufacturers, such as Vaisala and SIEMENS [19].

2.1.2 Detection of dissolved gases

Once the gas extraction is achieved, the type and the concentrations of the gases can be determined by various gas detection technologies. Such technologies are varied and range from standard gas chromatography to the ones based on optical principles, with potential advantages and disadvantages associated with each approach, as summarized in Table 1.

Table 1. Comparison between different gas detection technologies [19–22].

Technology	Advantages	Disadvantages
Semiconducting metal–oxide	• Most widely used sensors • High responses • Good stability • Corrosive atmospheres	• Low gas selectivity
Gas chromatography	• Wide range of fault gases • Highest accuracy • Repeatability	• Can be used only in the laboratory, due to the complexity of the equipment • Long time required to complete a test • Expensive • An expert is needed to conduct the test and interpret the data
Thermal conductivity detector	• Fast response • Stable • Wide measuring range • Simple construction • Robust	• Sensitive to interfering gases • Reaction due to heating wire • Heating element reacts with gas
Combustion cell detector	• Often used for H_2 detection • High detection precision • Good repeat • Response capability	• Limited lifespan • High cost • Detection error
Infrared absorption detector	• Often used for CO_2 detection • No sample separation	• Not all gases have IR absorption • Sequential monitoring is slower on • multi point analyzers • User expertise required
Fourier-transform infrared	• Simultaneous multi-gas measurement	• Accuracy influenced by moisture
Electrochemical gas sensor	• Small size • Working at high temperature	• Frequent calibrations needed • Short/limited life time • Single gas measurement • Cross sensitivity to other gases
Photoacoustic Spectroscopy	• Wide range of fault gases • Detecting Low gas concentrations • Low maintenance cost	• Concentration accuracy influenced by the external temperature and pressure, and by vibration • Results are sensitive to the wave number range of the optical filters and their absorption characteristics

While the scope of this work precludes detailed analysis of each technique listed in Table 1, my focus will be on the semiconducting metal oxides (SMOX) approach. This is because SMOX is a promising candidate for analyzing dissolved gases in transformer oil due to its reliability, simplicity, and cost-efficiency in comparison to other techniques [23]. However, the major drawbacks of this sensor type are the low selectivity and strong cross interference, and this is exactly what I address in this work. I will show that I can achieve selectivity with my proposed LFO sensors. More details about SMOX will appear in section 2.2.

2.1.3 Interpretation of DGA Data

When abnormal concentrations of dissolved gases are detected, different types of faults can occur, such as partial discharge (PD), arcing, overheating, and thermal decomposition [24]. To identify the type of fault, many methods, such as the Key Gas Method (KGM), the Doernenburg Ratio Method (DRM), the Rogers Ratio Method (RRM), the IEC Ratio Method (IRM), the Duval Triangle Method (DTM), and the Duval Pentagon Method (DPM), have been proposed to interpret the DGA data [25–27].

The main differences between the various methods mentioned above are based on the used gases and identification principle. For example, an identification of the fault can be obtained by using the individual gas concentrations, such as in the case of KGM. Most interpretation methods, however, use different gas concentration ratios to identify the fault. Recently, Bustamante et al. [19] have summarized the main features of such methods, as shown in Table 2.

Table 2. Comparison between different interpretation methods for DGA Data. The table is adapted from [19].

Method	Description	Fault Identification and Normal Aging	Gas Used
Key Gas Method (KGM)	Uses individual gas concentrations to identify the fault	Partial discharge (PD), arcing, overheated oil, overheated cellulose	CO, H_2, C_2H_2, C_2H_4
Doernenburg Ratio Method (DRM)	Uses four gas concentration ratios: CH_4/H_2,C_2H_2/C_2H_4,C_2H_2/CH_4,C_2H_6/C_2H_2	Thermal decomposition, PD, arcing	H_2, C_2H_2, CH_4, C_2H_6, C_2H_4
Rogers Ratio Method (RRM)	Uses three gas concentration ratios: CH_4/H_2,C_2H_2/C_2H_4,C_2H_4/C_2H_6	Normal aging, PD, arcing, low temperature fault, thermal fault <700°C, thermal fault >700°C	H_2, C_2H_2, CH_4, C_2H_6, C_2H_4
IEC Ratio Method (IRM)		PD, low energy discharge, high energy discharge, thermal faults <300°C, between 300 and 700°C, and >700°C	H_2, C_2H_2, CH_4, C_2H_6, C_2H_4
Duval Triangle Method (DTM)	Uses three gases corresponding to the increasing energy content or temperature of the faults	PD, low energy discharge, high energy discharge, thermal faults <300°C, between 300 and 700°C, and >700°C	C_2H_2, CH_4, C_2H_4
Duval Pentagon Method (DPM)	Uses five gases corresponding to the increasing energy content or temperature of the faults	Normal aging, PD, low energy discharge, high energy discharge, thermal faults <300°C, between 300°C and 700°C, and >700°C	H_2, C_2H_2, CH_4, C_2H_6, C_2H_4

The DTM is quite a common and well established method to identify faults in transformer insulation materials [28,29]. The DPM is a relatively new method, and it was developed to enhance the DTM results. Figure 1 shows how the DMT works in order to figure out the fault type. Three different gases (C_2H_2, C_2H_4, and CH_4) are used in this method, and the concentration ratios of the three gases are calculated using the following equations:

$$\%C_2H_2 = \frac{100 \cdot x}{x+y+z} \quad (1)$$

$$\%C_2H_4 = \frac{100 \cdot y}{x+y+z} \quad (2)$$

$$\%CH_4 = \frac{100 \cdot z}{x+y+z} \quad (3)$$

Where x, y and z are the gas concentrations (in ppm) of C_2H_2, C_2H_4, and CH_4, respectively.

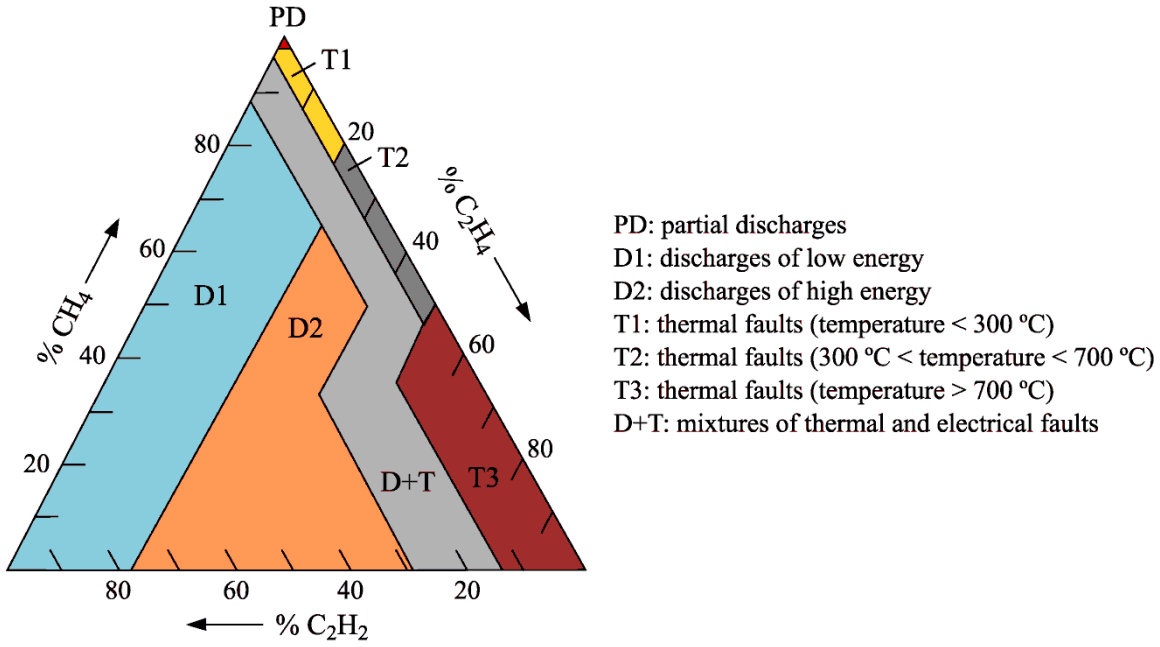

Figure 1. Duval Triangle and list of faults detectable by DGA. The figure is adapted from [19]

2.2 Semiconducting metal-oxide gas sensors (SMOX)

The working principle of semiconducting metal-oxide (SMOX) gas sensors is based on the change of the semiconductors' electrical properties when they are exposed to analytes. The first observation of such phenomena was in the 1950s [30]. Later, in 1962, Seiyama was the first to use this principle to detect some gases using ZnO thin film [31]. In the same year, Taguchi patented his gas detecting device based on SnO_2, which was able to detect the inflammable gas by determining the electrical resistance change of the semiconductor [32].

Normally, such a sensor consists of four parts including: a sensitive layer, electrodes, heater, and substrate (Figure 2). A substrate (such as Al_2O_3) with electrodes on the front side is generally used to measure the resistance of the sensitive material. The heater, which is often placed on the back side of the substrate, is used to control the operating temperature.

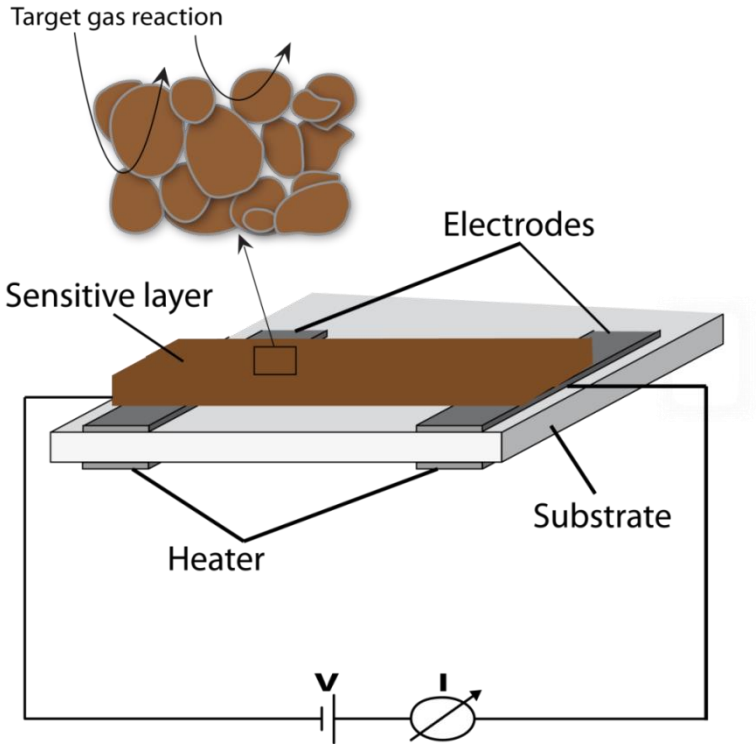

Figure 2. Schematic of a SMOX sensor.

For a typical SMOX sensor as described above and during the gas exposure, a contact between the analyte and the sensor parts (the sensitive material, electrodes, and the substrate) takes place. Beside the sensitive material, the electrodes (such as platinum) can have significant catalytic effects, thereby playing an important role in the sensing mechanism itself for some gases. Such possible contribution will be addressed in my study (see section 5.2). Finally, the substrate (alumina) is chemically inactive, and, therefore, no significant contribution in the reaction is expected.

At the level of the sensitive material itself, the measured resistance of a SMOX sensor is a total of three different resistances: the bulk resistance, grain-grain contact resistance, and grain–electrode contact resistance. The bulk resistance is controlled by the free charge carries (n_b) and constant; the latter two resistances depend on the surface concentration of free charge carriers, which are governed by the respective surface band bending. In the case of grain-electrode contact, the difference in the work function between the sensing and the electrode materials determines the surface band bending. Finally, in grain-grain contact, the band bending is strongly influenced by the atmosphere composition [33,34].

Because the used sensitive material in my study is a thick porous film, the measured resistance between the sensitive material and the electrodes is negligible due to the large number of grain–grain contributions. As a result, the overall resistance of the thick porous film is controlled primarily by back-to-back Schottky barriers at the grain-grain boundaries. It is worth noting here that in thin compact films, however, the bulk and the contact resistances between the sensitive material and the electrodes play a significant contribution in overall resistance [33,34].

The above implies that in the applications with thick porous films where grain-grain contact is most important, the semiconductor type (n- or p-type) plays an important role in understanding the mechanism of conductance change in SMOX sensors. In what follows, I describe the working principles of each type of SMOX sensor. This is important because I will later focus on p-type SMOX sensors which are not use as commonly as n-type SMOX sensors in the gas sensing field.

In an n-type semiconductor: In air and at a normal operating temperature range of the SMOX sensor (100 to 400°C), the oxygen adsorption process on the material surface can take place. A depletion layer is then formed as a result of a buildup of negative surface charge (yellow region in Figure 3), which leads to an upwards band bending as shown in the left side of Figure 3. As a consequence, only electrons with sufficient energy are able to overcome the potential barrier at the grain boundaries and can participate in the conduction mechanism. By exposing the sensor to a reducing gas, oxygen ions are removed from the surface, and trapped electrons return to the bulk of the solid. The conduction then increases due to a reduction in potential barrier energy (see right side of Figure 3).

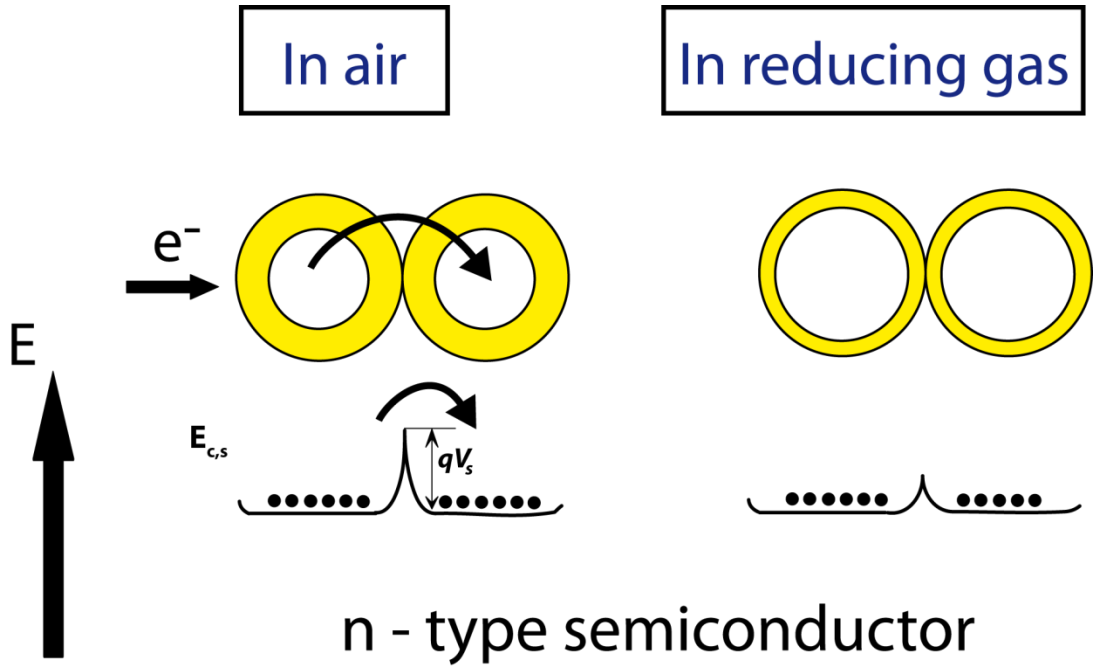

Figure 3. The grains in the sensing layer with the depletion region (yellow color) and the corresponding energy band diagram in air (left side) and under reducing gas exposure (right side).

By applying Schottky approximation, the conductance of the sensor is based on the number of electrons in the conduction band (CB) at the surface of the grains (n_s), which can be described by a Boltzmann distribution at $V = V_s$:

$$n_s = n_b \exp\left(-\frac{eV_s}{kT}\right) \qquad (4)$$

The resistance of the sensing layer depends exponentially on the surface band bending (eV_s):

$$n_s \; \alpha \; \exp\left(\frac{eV_s}{kT}\right) \qquad (5)$$

Based on that, the sensor signals (S.S) can be defined as:

$$S.S = \frac{R_{air}}{R_{gas}} = \exp\left(\frac{e\Delta V_s}{kT}\right) \qquad (6)$$

This means that the magnitude of the so-formed back-to-back Schottky barriers, which is indicated the band bending change, controls the conduction process.

In a p-type semiconductor: The conductance is controlled by the accumulation layer which is completely different from the depletion layer. In this case, the current flows through the accumulation layer (grey region in Figure 4). The space charge layer is more conductive than the inner part of the grains, which is in contrast to the case of n-type SMOX. The change in the surface band bending depends on the hole concentration, which is the main free charge carrier in p-type semiconductors, in the sensing layer. As a result, the sensor signals of p-type SMOX can be written as:

$$S.S = \ln\left(\frac{R_{\text{air}}}{R_{\text{gas}}}\right) = -\left(\frac{e\Delta V_s}{2kT}\right) \quad (7)$$

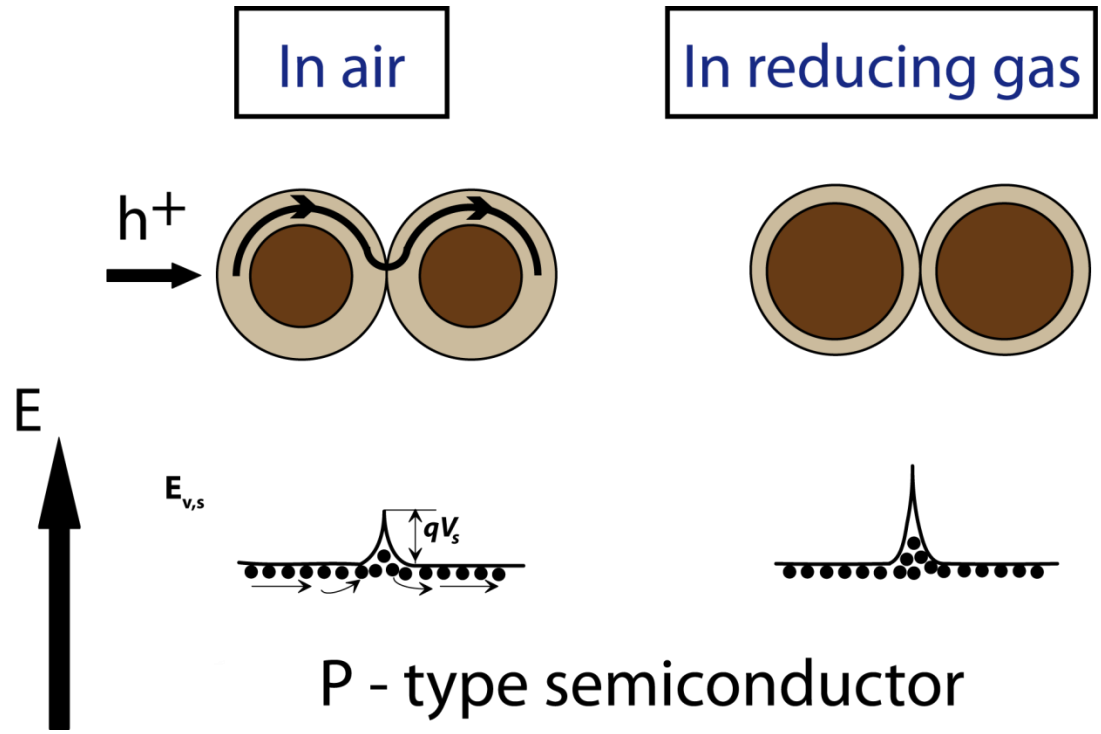

Figure 4. The grains in the sensing layer with the accumulation region (grey color) and the corresponding energy band diagram in air (left side) and under reducing gas exposure (right side).

By exposing the sensor to a reducing gas, oxygen ions are removed from the surface, and trapped electrons return to the lattice. The resistance then increases due to the upward band bending increases and, therefore, a reduction in the number of holes as free surface carries.

2.3 General aspects of perovskites

Perovskites are employed successfully for various applications in catalysis [35,36], in fuel cells (SOFCs) [37], and in photovoltaics [38]. Also, they have been used in gas sensors [39,40], the first report being proposed by Obayashi et al [41]. At that time, they were exposed to ethanol and carbon dioxide, and a response was only observed for ethanol.

2.3.1 Structural properties

In general, perovskites have interesting electrical and thermal stability properties [42]. The general formula for a perovskite structure is ABO_3, where A is a trivalent rare earth cation, such as La, Sm, Nd, and so on (with or without its partial substitution by a divalent alkaline earth cation, such as Ca, Sr, Ba, and so on), and B is a transition element, such as Mn, Co, Fe, and so on. A special property of this class of materials is the rich variety of possible A and B site cations.

The ideal perovskite-type structure is cubic. In this structure, the B cation is in a six-fold coordination and the A cation is in a twelvefold coordination with the anions. The Figure 5a shows one possibility of the perovskite structure where the B cation is in the center. Alternatively, the structure can be viewed with the corner-sharing octahedral units that form the skeleton of the structure, whose body-center position is occupied by the A cation [42].

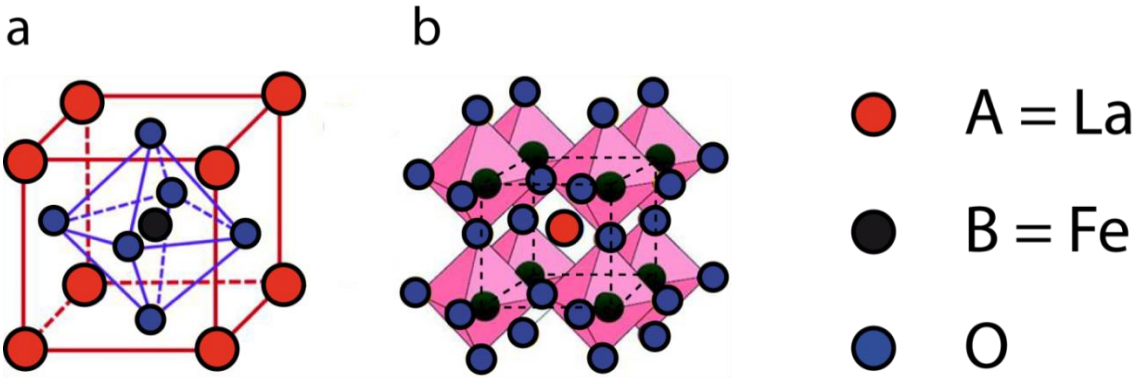

Figure 5. The perovskite structure: the center of the unit cell is cation a) B or b) A. The figure is adapted from [42].

One of the most common compounds in perovskites is Lanthanum ferrite $LaFeO_3$ (LFO). It is a p-type semiconducting material with a band gap of 2.1 eV.

2.3.2 Surface reactions

2.3.2.1 Adsorption types

The adsorption of gaseous species on the material's surface can affect its electronic state as I explained in section 2.2. Therefore, the physical and chemical properties can be influenced. Based on the strength of the adsorption, three types of interaction are proposed, namely physisorption, chemisorption, and ionosorption.

Physisorption can occur in all gas – solid interaction, but it is the weakest one of all three adsorption types ($E_B < 0.518$). It is controlled by van der Waals potentials, and there is no bonding between adsorbate and adsorbent. This means that molecular structures stay essentially the same. As a result, no charge transfer with the surface takes place [43].

In chemisorption, species are quite strongly adsorbed on a solid surface ($E_B > 0.518$). In such interaction, the adsorbed molecules can also undertake a dissociative process as has been seen during H_2 adsorption on transition metals. In a

chemisorption mechanism localized charge transfer takes place (covalent bonding), which affects the electron affinity of the sensing material. However, in contrast to a chemical bond, the chemisorbed species can move along the surface, resulting in a statistical distribution or an occurrence only at certain geometrical surface sites [43,44].

In ionosorption, the process can be considered as a special case of chemisorption. In this mechanism, however, a delocalized electron transfer takes place at the surface instead of a localized one, leading to the band bending of the surface, which in turn results in a resistance change. This process plays a key role in gas sensing mechanisms. Adsorption of oxygen on metal oxide surfaces is a common example for this type of mechanism [45].

2.3.2.2 Adsorption of Oxygen on $LaFeO_3$

The oxygen adsorption mechanism on metal oxide surfaces plays a significant role in determining the sensing properties of SMOX gas sensors. Therefore, it is quite beneficial to address such adsorption process of LFO in this section. This would provide a basis for a more detailed characterization of sensing behavior in my work. Liu et al studied the adsorption of O_2 on LFO (010) surface using Density function theory (DFT) [46]. They found that the surface states are near Fermi energy level and mainly caused by Fe 3d orbital. Moreover, the adsorbed O_2 on Fe ion is much more stable than that on La and O ions, and the bonding mechanism of adsorbed O_2 on surface Fe ions is the strong interaction between O 2p and Fe 3d orbital. This finding is in line with the experimental results suggesting that the catalytic activity of perovskites is mainly controlled by the B-site metal [42,47,48]. In my work, I will

demonstrate experimentally that the surface iron ions of LFO are also the main active sites in the gas adsorption mechanism (see section 5.1.1).

2.3.3 Catalytic Properties of $LaFeO_3$

For a good gas response to occur, an oxide must exhibit both an appropriate semiconducting characteristic as well as a surface that can catalyze reactions with neutral target molecules. This makes considering the catalytic properties of LFO quite essential in order to understand its gas sensing mechanisms.

The catalytic activity of most perovskites can be improved by partial substitution of the A-site to induce oxygen nonstoichiometry [49,50]. However, this is not always the case because the catalytic properties of $LaFeO_3$ for the low hydrocarbons conversion strongly depend on the catalyst elemental composition. The stoichiometric $LaFeO_3$ shows the best catalytic activity for the low hydrocarbons compared to different nonstoichiometric compounds of the same material [51].

Velichkova and co-authors [52] studied the effects of different A-cations (Yttrium and lanthanum) in $AFeO_3$ perovskites on the catalytic oxidation of hydrocarbons. They found that LFO indicated more efficient catalytic activity of hydrocarbons than $YFeO_3$. The authors attributed this to the ability of La to stabilize the perovskite crystal structure, leading to an intensive conversion of Fe ions between the different oxidation states (Fe^{4+}/Fe^{3+}). This activates the hydrocarbon and oxygen molecules more effectively than $YFeO_3$.

A kinetic study through varying the O content and the crystal size has been used to confirm the significance of the site requirements for the methane combustion on LFO perovskite catalysts [53]. This study concluded that three types of reactions based on active sites of the catalysts take place, as shown in Figure 6. First, if the Fe atoms

highly coordinate with O, total combustion of CH_4 is likely. Second, Fe moderately coordinated with O leads to partial oxidation. Third, Fe highly coordinated with vacancy sites leads to carbon formation.

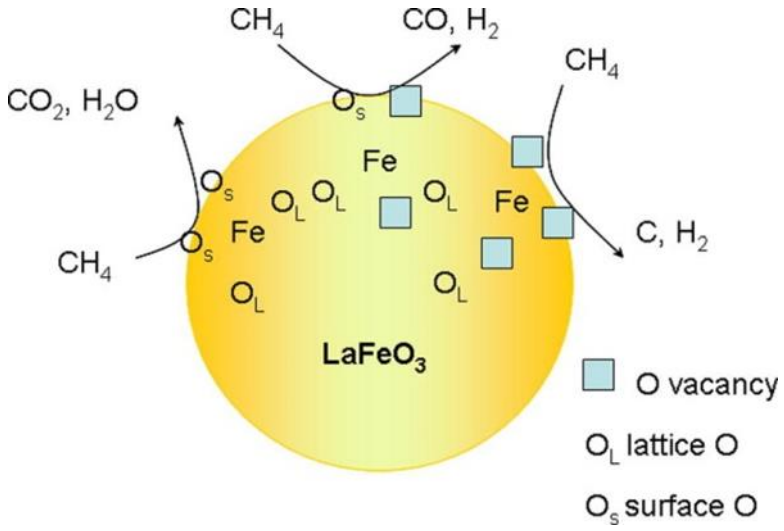

Figure 6. The Fe coordination number with oxygen on $LaFeO_3$ surface governs the selectivity to total and partial oxidation as well as methane decomposition. The figure is adapted from [53].

2.4 Adsorption and reaction of analytes on metal oxide surfaces

Adsorption and reaction of different molecules of the surface of metal oxides is a broad topic. In this section, I narrow my focus to only two kinds of analytes, namely CO_2 and hydrocarbons, because I will focus on these gases in my investigations.

2.4.1 CO_2

In general, adsorption of CO_2 on metal oxide surfaces forms typically different configurations of carbonates and bicarbonates (Figure 7), and this fact is well addressed in the literature [54,55]. In particular, to identify the type of different carbonate species, the values of splitting (Δv_3) have been successfully used [56].

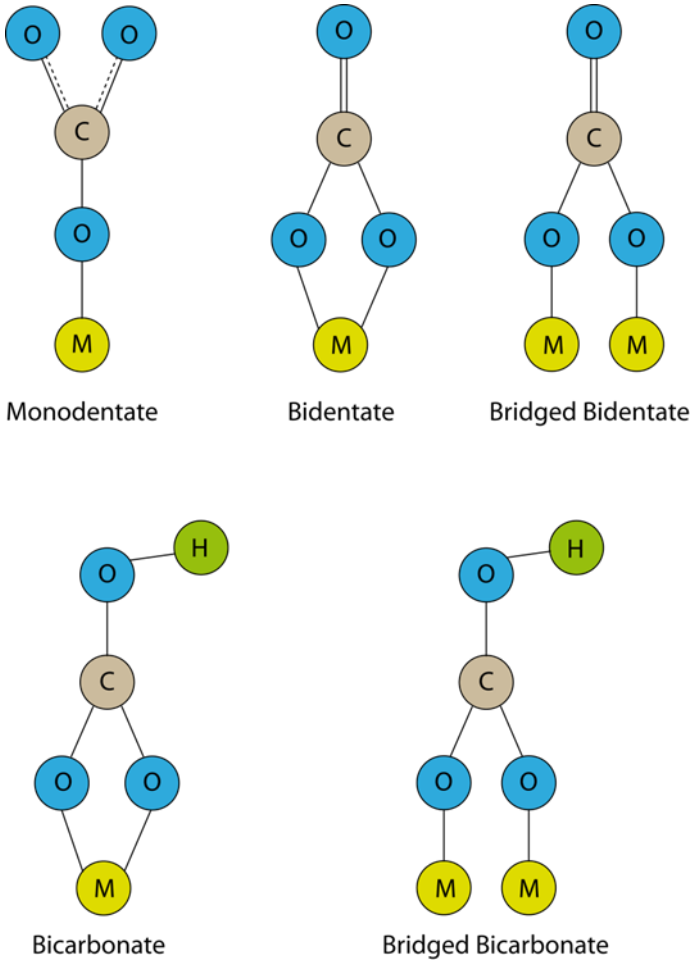

Figure 7. Various configurations of surface carbonate and bicarbonate.

To briefly explain that, the free carbonate ion has one Raman active vibration at 1063 cm^{-1}, which is related to the symmetric CO stretching (v_1), and three infrared active vibrations as follows:

- Out of plane deformation (v_2) at 879 cm^{-1}
- Asymmetric CO stretching (v_3) at 1415 cm^{-1}
- In plane deformation (v_4) at 680 at cm^{-1}

When a free carbonate is chemisorbed on a metal oxide surface with at least one coordinating cation, a splitting of the doubly degenerate v_3 and v_4 vibrations takes place. Moreover, the vibration of v_1 becomes infrared active. However, the v_1 and v_2 vibrational frequencies are similar for all different types of carbonates and do not undergo energy splitting. Therefore, the identification of different configurations of carbonate species is only made on the basis of the splitting of the vibration Δv in v_3 or v_4. The value of splitting is greatly dependent on the number of coordinating cations and the polarizing power of cations, which is proportional to z/r^2 (z is the charge of a cation and r is ionic radius) [54]. Because the v_4 is vibrating in the low frequency region where strong metal-oxide stretching vibrations are expected, v_4 is quite difficult to be detectable in adsorption studies. As a consequence, the splitting value of v_3 is the only one vibration that can be effectively used to distinguish between the different types of surface species.

The first experimental use of this principle was by Nakamoto et al [56]. They succeeded to distinguish between bidentate and monodentate carbonate on the cobalt oxide surface. As a general rule of such classification, the average splitting values with around 100, 300 and 400 cm^{-1} could be assigned to monodentate, bidentate, and bridged carbonates, respectively. For irregular carbonate

configurations, such as polydentate configurations, splitting values were quite similar to monodentate splitting values, or even smaller. However, polydentate carbonates are adsorbed on the surface much stronger than monodentate ones.

2.4.2 Hydrocarbons

The surface chemistry reaction of hydrocarbons on metal oxide surfaces is much more complicated than for CO_2. However, the type of surface species depends mainly on the temperature and the surface activity [21]. For example, the adsorption of olefin (alkene) compounds on the metal oxide surface in the range of temperature from 150°C to 200°C can yield to various carboxylate-like compounds, such as formates, as shown in Figure 8.

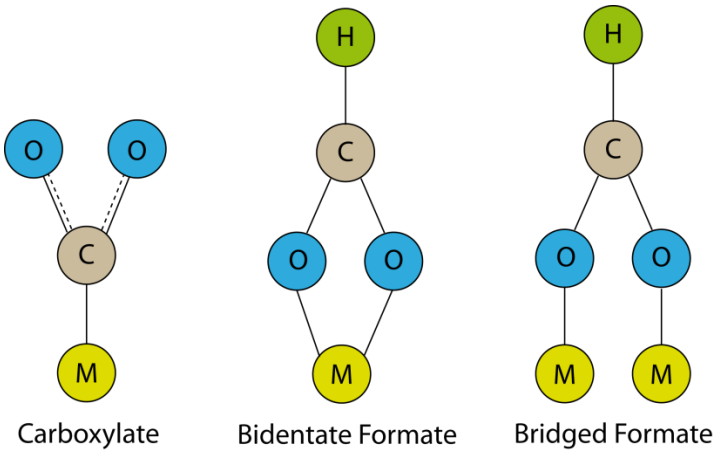

Figure 8. Different configurations of surface carboxylate and formate.

2.5 Using Operando Spectroscopy for Understanding the Gas Sensing Mechanism

Understanding the gas sensing mechanism is so significant for further development of practical sensors. To reach that understanding, exploring the interaction between the gas being sensed and the surface of the sensing material is crucial, because such interaction can give clues as to why the compound can be so selective for only one or two gases. Specifically, increasing our ability to evaluate the adsorbed species on the material's surface during the progress of the reaction is a vital key in order to define their role in electrochemical properties of the gaseous interaction.

One of the best possibilities for understanding the mechanistic interaction mentioned above is to use in situ tools where the material is behaving as it would do in real life. This also increases the ability of isolating intermediated species, by applying a series of experiments probing each step in the gas interaction cycle with the material. As a result, the correlation between the presence of a surface's species and the influence on the chemical and electrical properties can be obtained. For example, in previous work, Arantxa Davó-Quiñonero et al [57] combined an operando DRIFT cell with mass spectroscopy to study the role of hydroxyl groups in the oxidation of CO over CuO/CeO catalysts. They found that the hydroxyl group on the material surface can play a key role in catalytic mechanisms by determining the type of carbonate species that are formed on the material surface during CO chemisorption. Hydroxyls prompt the formation of bicarbonates, which are responsible for increasing the CO oxidation rates. In a similar vein, a technique combining ambient-pressure X-ray photoelectron spectroscopy (AP-XPS) and DRIFT spectroscopy was recently used to study the reactivity of CO_2 on cobalt-based perovskites [58]. The authors of that study

investigated the effect of the bulk perovskite chemistry and electronic structure on the surface during the reaction with CO_2.

In lab, we combine operando DRIFT spectroscopy with DC resistance measurements to investigate the surface chemistry change of the sensing material simultaneously with its resistance measurements upon target gas exposure allowing us significant insight about the chemistry change at the surface. This helps us to interpret the reaction mechanism and find out the origin of the gas sensing mechanism of the sensor.

3. Materials and Experimental Methods

3.1 Sample preparation

In this section, the preparation methods of the sensitive material powders will be explained. The fabrication technique, which is used to fabricate my sensor, is also taken into account.

3.1.1 Material synthesis

Perovskites are highly reactive towards CO_2 and humidity during preparation [59]. Therefore, the preparation of such materials in ambient air leads to hydroxylation and formation of carbonates, which will mainly be present on the surface. High temperature treatments are needed. However, this may lead to a decreased surface area, which is not desired for gas sensing. It is important to balance between ensuring hydroxylation and the presence of carbonates on one side and having relatively high surface area with homogeneity on the other side. I have used two synthesis approaches (solid state reaction and sol gel) to prepared LFO with a perovskite structure. Five different powders were made from each method based on the calcination temperatures, namely LFO(500), LFO(600), LFO(700), LFO(800) and LFO(900) – the number in the parentheses indicates the calcination temperature. Moreover, non-stoichiometric compounds of LF_xO(600) were synthesized by reducing the amount of iron as x = 0.95, 0.90, 0.85 and 0.80.

3.1.1.1 Solid state reaction

Fixed amounts of constituent oxides La_2O_3 and Fe_2O_3 were used to prepare LFO. Sodium hydrogen carbonate ($NaHCO_3$) was added in a (5:1) ratio to the total metal oxides, and the mixture was then fired in an alumina crucible for 10 hours at different temperatures between 500 and 900°C. The resulting powders were cooled down to room temperature and washed with distilled water to take out all traces of sodium compounds. Finally, the powders were dried at 70°C for 12 hours. This process is shown schematically in Figure 9.

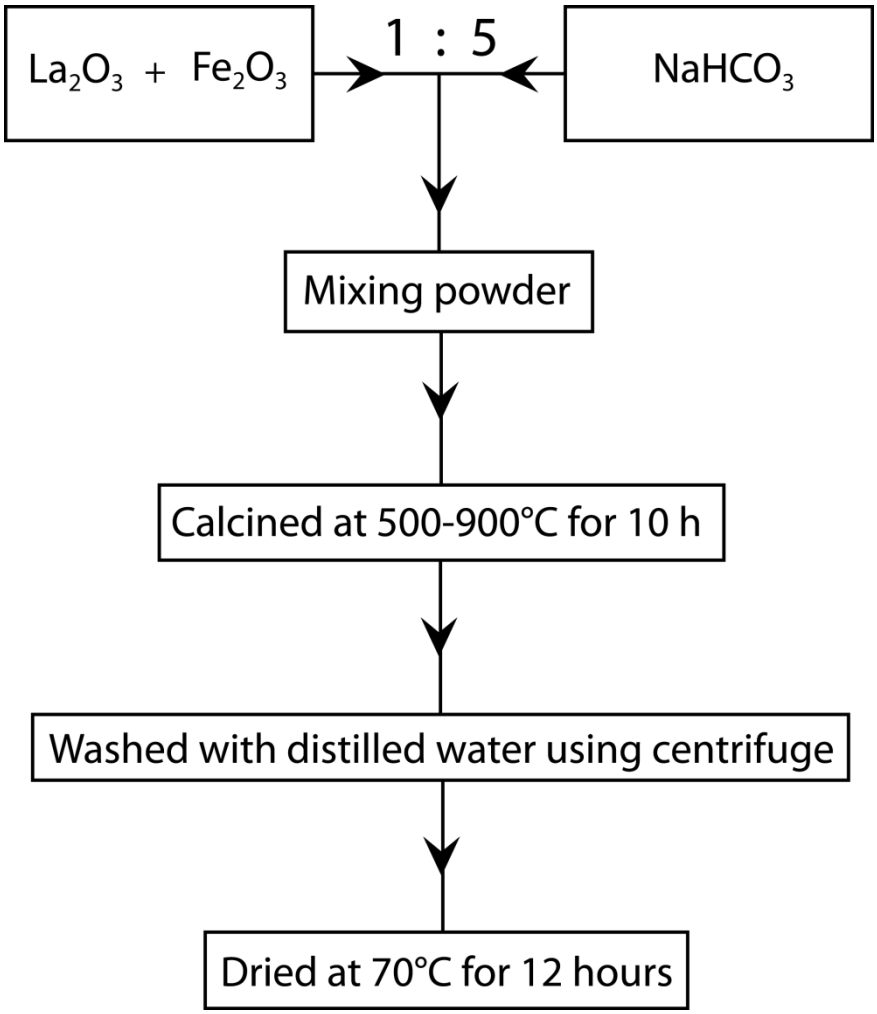

Figure 9. Schematic representation of LFO powder preparation by solid state reaction.

3.1.1.2 Sol Gel

The amounts of $La(NO_3)_3 \cdot 6H_2O$, $Fe(NO_3)_3 \cdot 6H_2O$, and citric acid were used to prepare LFO based materials. The amount of citric acid was added in a (1:1) ratio to the total metal nitrates, and the mixture was then dissolved in distilled water. The slurry was mixed for one hour using magnetic stirring. After that, the solution was neutralized at a pH of around 6 or 7 by adding ammonium hydroxide. Then, it was kept stirring overnight. The resulting gel was dried at 90°C for 4 hours and then fired in an alumina crucible for 2 h at different temperatures from 500 to 900°C. This process is shown schematically in Figure 10.

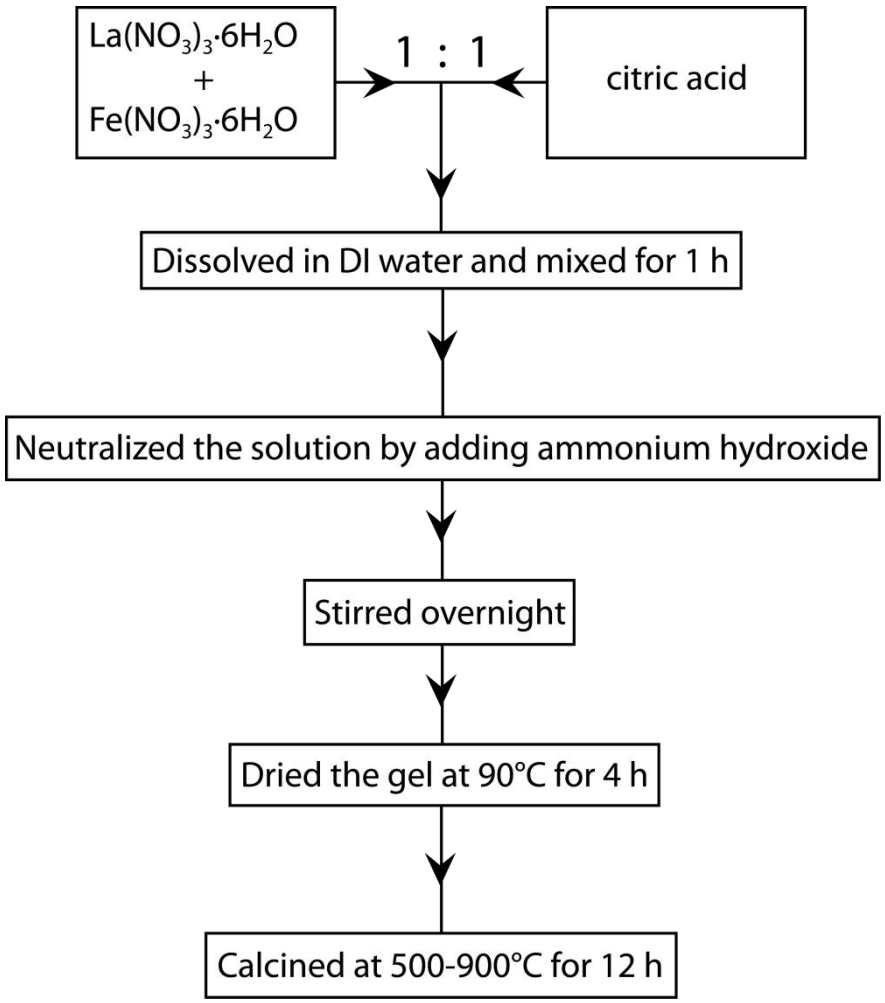

Figure 10. Schematic representation of LFO powder preparation by sol gel method.

3.1.2 Sensor fabrication

The obtained powders were used as sensitive layers by mixing each of them with a solvent (1,2-propanediol – Sigma Aldrich) to get a printable paste, which was deposited over platinum interdigitated electrodes by screen printing. The as obtained sensors were dried at 70°C overnight. Finally, they were calcined by applying a heating sequence at three steps (400°C, 500°C, and 400°C) for 10 mins each.

The standard substrate in my measurements is the one with platinum electrodes and heater. An alternative substrate, however, with different electrodes and heater material is also used in order to investigate the role of platinum electrodes in the gas sensing mechanism. The electrodes of the alternative substrate were made of gold (Au), while the heater was made of a mix of palladium and silver (Pd/Ag). The schematic layout and the cross section of the LFO sensor elements are represented in Figure 11.

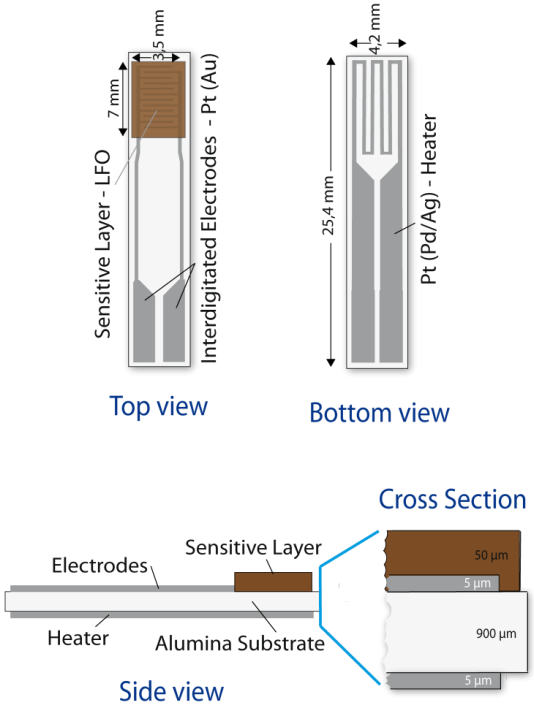

Figure 11. A sensor element consists of sensitive layer (brown), interdigitated electrodes (grey on front side), heater (grey on back side) and substrate (white).

3.2 Experimental Techniques

In this section, all experimental techniques that have been used in my investigations are briefly explained.

3.2.1 Structural and Morphological Characterizations

The powder X-ray diffraction (XRD) patterns of All LFO samples were measured using an X'Pert PRO MRD PANalytical diffractometer from Philips, which is equipped with a monochromatic Cu Kα radiation source (λ=0.1544 nm). The range is measured from 20 to 80° with a scanning speed of 1°/min.

The morphology of the samples was also examined by scanning electron microscopy (SEM) using an A JEOL JSM-6500F. The acceleration voltage is 15 kV, with a probe current of 74 μA, and a stage height of 10 mm. All SEM images were taken from thick film gas sensors.

3.2.2 DC Resistance Measurements

Measuring the DC resistance changes of the sensing layer is the main output to evaluate the gas sensing performance of metal oxide based gas sensors. The schematic diagram of the experimental set-up of the DC resistance measurement is shown in Figure 12. A computer controlled gas mixing system equipped with data acquisition cards and mass flow controllers delivers a continuous gas flow (150 mL/min) to a measurement chamber where a sensor is fixed in. A digital multimeter, which is also controlled by a computer, is used to read out the DC resistance of the sensing layer. To adjust the operating temperature of the sensor, a power supply is used to do that by applying a certain voltage to the heater according to calibration data. This allows us to measure the gas sensing performance of the LFO sensor in

application relevant conditions by controlling the test gas concentrations, different humidity backgrounds, and operating temperatures.

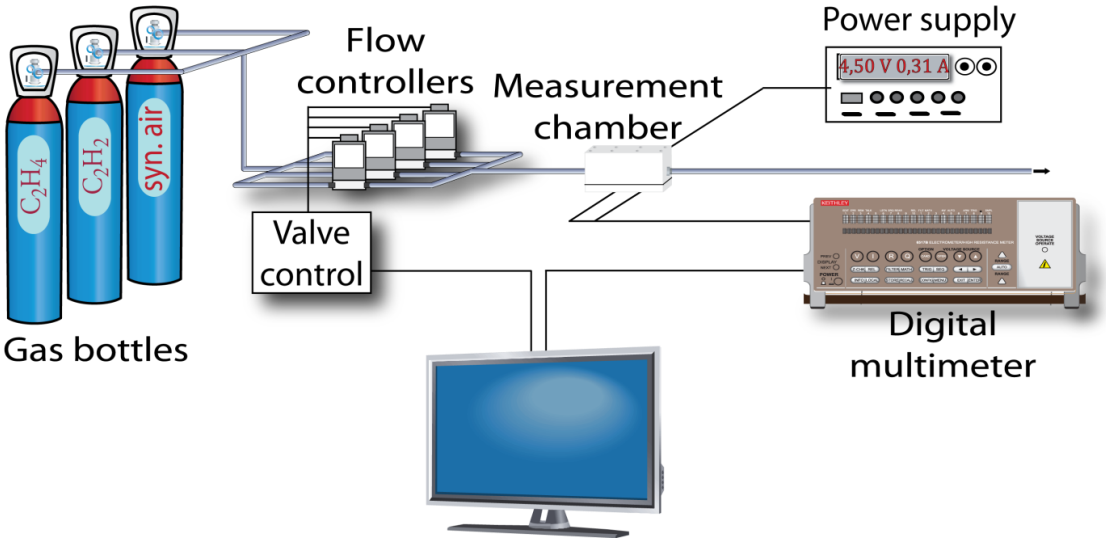

Figure 12. Setup for the resistance measurements of the sensor.

3.2.3 Operando DRIFT Spectroscopy

I recorded DRIFT spectra using a Fourier transform-infrared spectrometer (Bruker VERTEX70v). This spectrometer acted as a narrow-band MCT detector with a spectral resolution of 4 cm^{-1}. I also used a custom made chamber containing a KBr window to heat and record the resistance of the sensor as in its normal operation mode. This powerful technique allowed me to measure the resistance change of the sensor and its IR spectrum simultaneously under working conditions [60,61]. The operando DRIFT spectroscopy setup is depicted schematically in Figure 13.

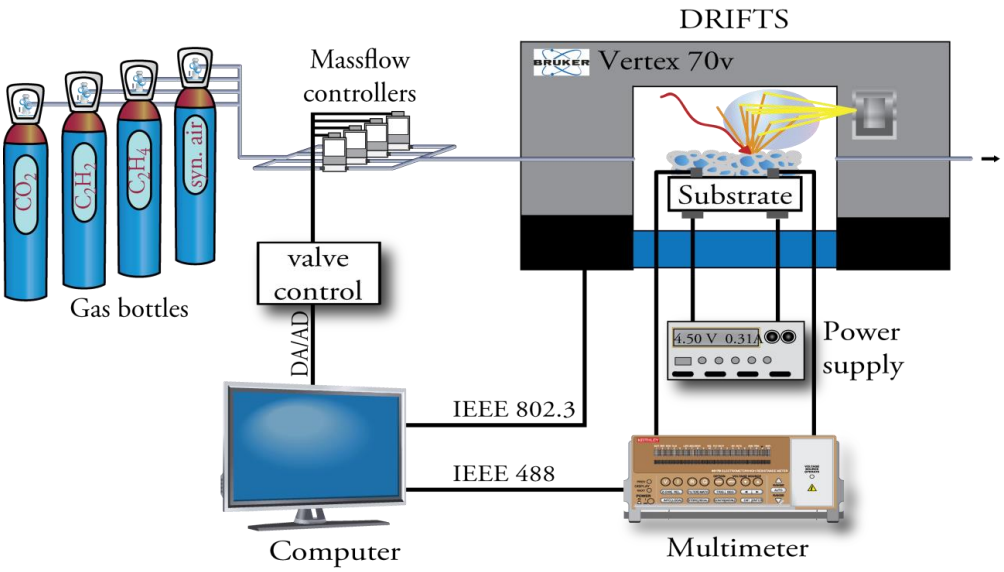

Figure 13. Experimental setup for simultaneous DRIFTS and resistance measurement.

The absorbance spectra were calculated from the single channel spectra using the following equation:

$$\text{Absorbance (A)} = -\log\left(\frac{\text{single channel test gas}}{\text{single channel reference}}\right) \qquad (8)$$

A single channel spectrum was recorded every 15 min during test gas exposure, except in some cases in which it was taken in shorter time intervals in order to follow the adsorption kinetics.

3.2.4 Catalytic Conversion Measurements

Perovskites have been used widely as catalysts. Therefore, considering the partial and complete oxidation of test gases on their surface is essential in order to understand the gas sensing mechanism. Moreover, the noble metals (such as Pt and Au), which are used to fabricate the sensor's parts (electrode and heater), can have a considerable contribution in the consumption of some gases. Oxidation of ethylene is a good example of the importance of catalyst selectivity. Completely different products are obtained by changing the catalysts. When ethylene is oxidized over platinum, as platinum basically breaks C-H bonds, full combustion of the gas takes place, and the major products are CO_2 and H_2O. In contrast to platinum, palladium leads to the partial oxidation product (such as acetaldehyde). Silver, however, uniquely yields ethylene oxide [62]. Therefore, to consider such influences on the sensing mechanism, the measurements were performed on the sensitive material and the remaining parts of the sensor separately.

The test sample (sensitive material or the remaining parts of the sensor) was placed between two layers of quartz wool in a quartz tube and fixed in a tube furnace (catalytic reactor). The gas flow was controlled by gas mixing system as described above. The concentration of exhaust gas (CO_2) was measured by a photo-acoustic IR gas analyser (INNOVA 1312 LumaSense Technologies). The setup of the experiment is illustrated in Figure 14.

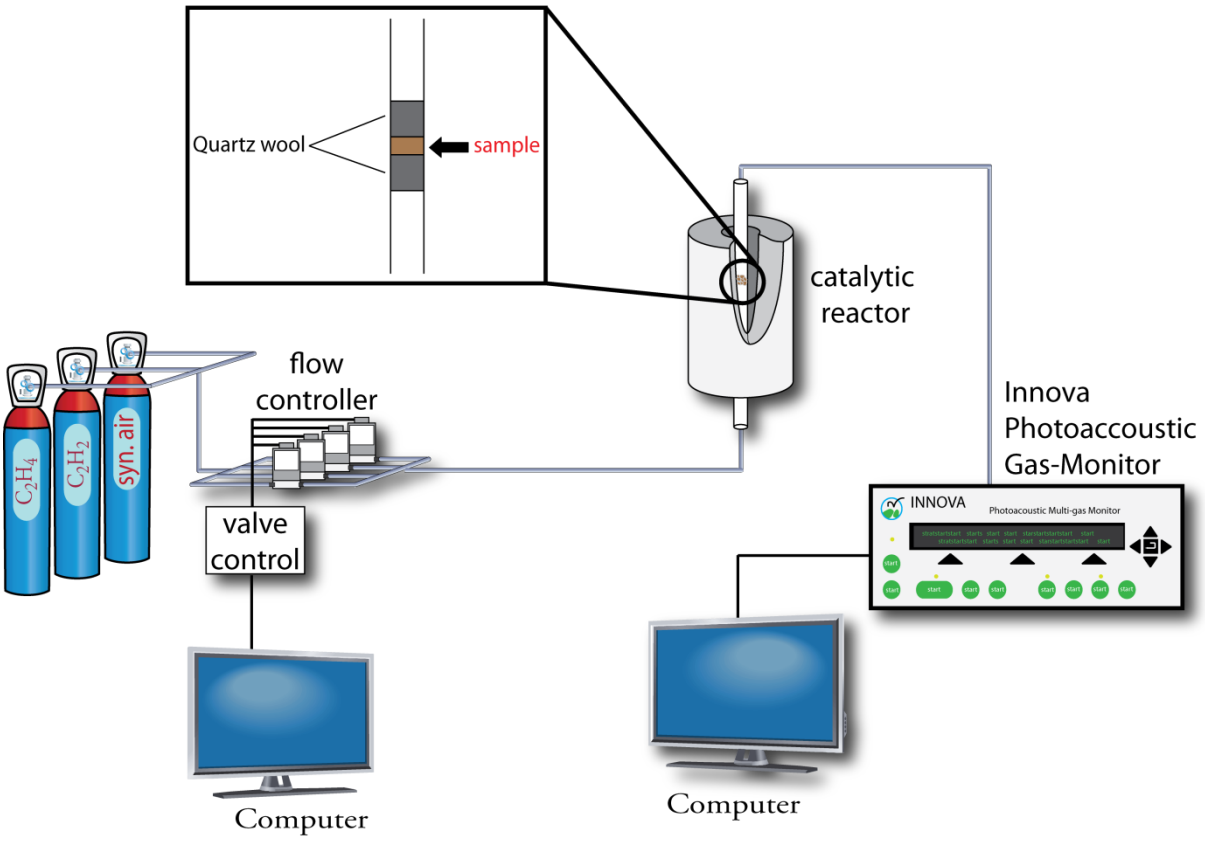

Figure 14. Experimental setup for catalytic conversion measurements.

4. Gas Sensing Properties

In this chapter, I investigate the structure of different LFO materials that are obtained by different routes (solid state reaction and sol gel methods). The materials, which have perovskite structure, are used as sensitive layers to investigate their gas sensing performance to the different target gases. Moreover, I will provide an overview of the gas sensing performance of the different sensors in order to select a sensor that has the best gas sensing performance. The selected sensor will be used for further sensing investigations and also for exploring the origin of the gas sensing mechanism.

4.1 Material characterization

The structure of resulted powders is examined by XRD to prove their perovskite phase.

4.1.1 Solid state reaction

The XRD patterns of all samples are shown in Figure 15. The LFO(500) and LFO(600) show the amorphous phase and the typical peaks of perovskite structure are not visible. This means that calcination temperatures of 500 and 600°C are not sufficient enough to produce a perovskite structure. The single phase perovskite crystal structure, however, is obtained at temperatures of 700, 800 and 900°C. The materials with perovskite structure have the orthorhombic crystal system according to Joint Committee on Powder Diffraction Standards (JCPDS). The reference number of the matched pattern, which is indicated as red bars in Figure 15, is (37-1493).

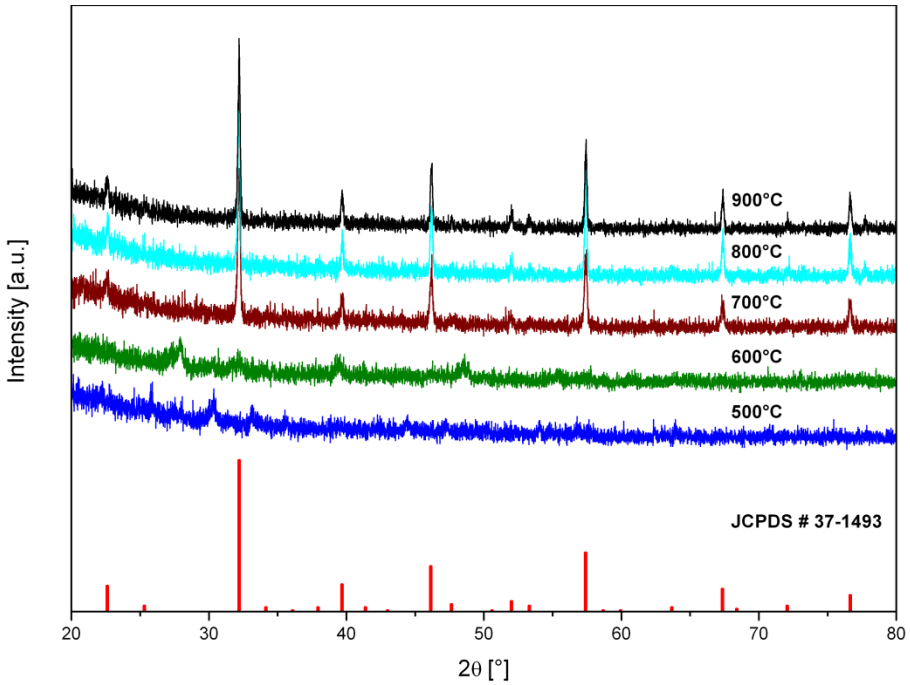

Figure 15. The XRD patterns of LFO powders at different calcined temperatures. The referenced peaks are shown as red bars.

4.1.2 Sol gel

The XRD patterns of LFO materials are shown in Figure 16. The black curve corresponds to the dried gel before calcination and indicates an amorphous structure. The other colored curves show the effect of calcination at different temperatures. As can be seen, the spectral peaks match perfectly to the well-known perovskite structure. This means that all of my sensing materials, which were calcined at 500°C and higher, had perovskite crystal structures, and appeared as orthorhombic phases according to Joint Committee on Powder Diffraction Standards (JCPDS). The same referenced XRD pattern is used (as mentioned in pervious section) and shown as red bars in Figure 16.

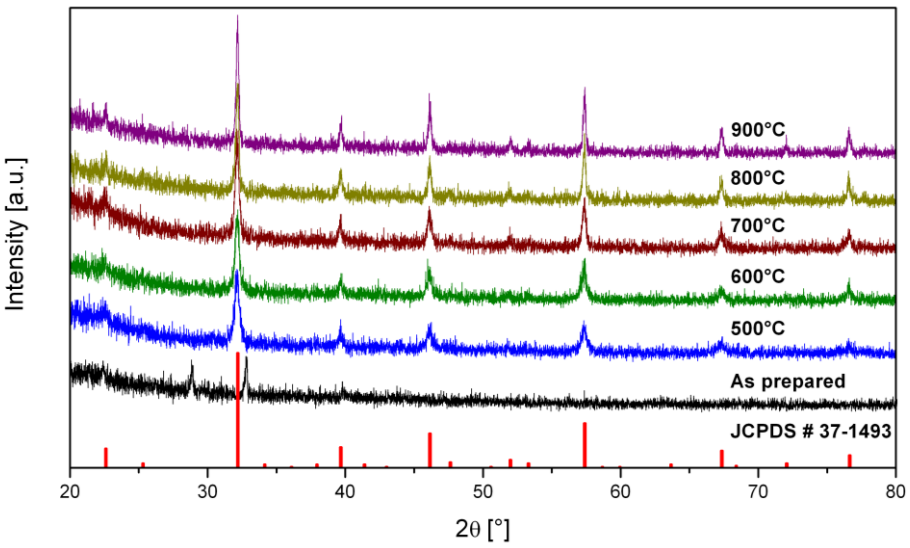

Figure 16. The XRD patterns of LFO powders as prepared and at different calcined temperatures. The referenced peaks are shown as red bars.

4.2 Gas sensing performance

Based on the XRD results, I have three LFO powders with perovskite structure that were obtained through solid state reaction and five materials that were achieved by the sol gel method. In this section, I will use the above mentioned powders as sensitive layers for sensing dissolved gases (CH_4, C_2H_6, C_2H_2, C_2H_4, CO_2, CO, and H_2), at various operating temperatures between 150°C and 300°C.

4.2.1 Sensors based on solid state reaction

Three different sensors namely, LFO(700), LFO(800) and LFO(900) were used in my gas sensing measurements because they had perovskite structures. The sensors were exposed to all dissolved gases separately at different operation temperatures including 150, 200, 250, and 300°C. Table 3 indicates the sensor signals of the different sensors to 500 ppm of each gas of the dissolved gases at 150°C. This concentration was selected to allow a relevant comparison between the gases. It is clear that the sensors only showed responses to acetylene and ethylene, among other gases.

The sensor signal is defined as:

$$\text{Sensor signal } (S.S) = \frac{R_g}{R_{air}} \qquad (9)$$

Where R_g is the measured resistance in the presence of analyte and R_{air} is the measured resistance in reference condition (dry or humid). It is important to note that a sensor signal of 1 corresponds to the absence of any sensor response.

Table 3. Sensor signals of LFO(700), LFO(800) and LFO(900) sensors for 500 ppm of different dissolved gases in power transformer oil.

	Sensor Signal						
Gas / Sensor	C_2H_2	C_2H_4	C_2H_6	CH_4	CO_2	CO	H_2
LFO(700)	4	2.5	1	1	1	1	1
LFO(800)	5.2	2.1	1	1	1	1	1
LFO(900)	4.9	2	1	1	1	1	1

Because the sensors showed a good selectivity to ethylene and acetylene, I will focus in the following on the sensing performance of all of my sensors to only these two gases. The sensor signals of all sensors, obtained as an average of two measurements to 5000 ppm acetylene and ethylene at different operating temperatures (150°C, 200°C, 250°C and 300°C), are shown in Figure 17. The error bars indicate the full variation of the sensor signals.

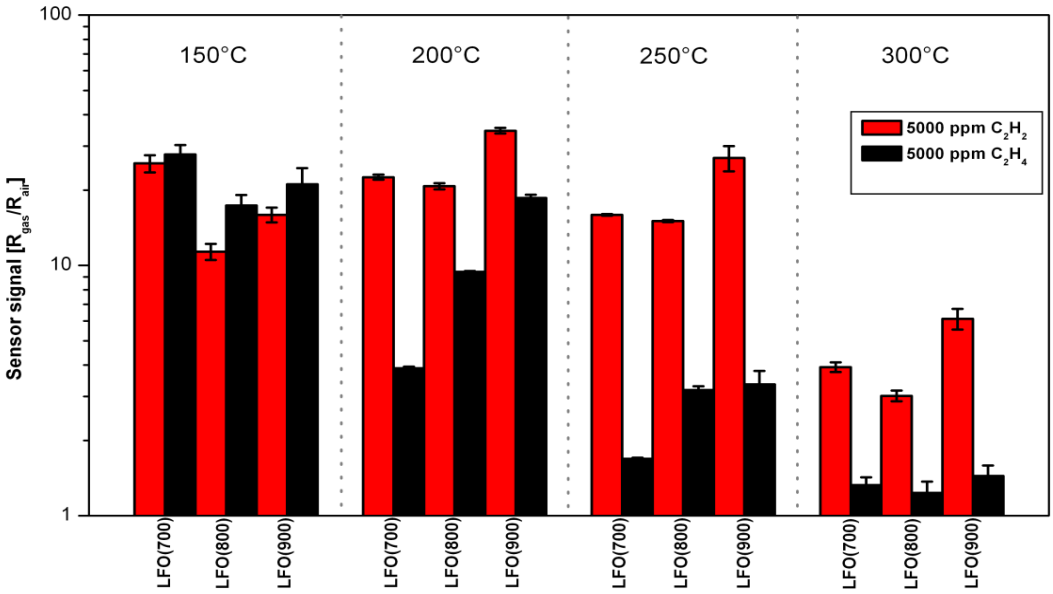

Figure 17. Sensor signals of LFO(700), LFO(800), and LFO(900) sensors on a logarithmic scale for 5000 ppm acetylene and ethylene in dry condition at operation temperatures 150, 200, 250 and 300°C.

It is clear that the sensors almost showed the same responses to both gases at 150°C. However, at higher temperature, they showed a more pronounced selectivity to acetylene. It is interesting that there was no significant change of the sensor signals to acetylene at all operating temperatures for all sensors except at 300°C where the sensor signals lost more than half of their values at lower temperatures. On the other hand, the ethylene response was changeable with changing the operating temperature. Increasing operating temperatures led to a reduction in the sensor signals to ethylene significantly. Moreover, the LFO(700) showed better selectivity to acetylene at 200°C than other sensors, suggesting a correlation between the calcination temperature and the selectivity to acetylene. At higher operating temperatures, a similar selectivity to acetylene was observed for all sensors.

4.2.2 Sensors based on sol gel

I applied the same approach of gas sensing investigation to the sensitive materials that were obtained by the sol gel method. In this case, I had five different sensors, namely LFO(500), LFO(600), LFO(700), LFO(800) and LFO(900). Table 4 shows the sensor signals of the five different sensors under exposure to 500 ppm of each target gase (C_2H_2, C_2H_4, CH_4, C_2H_6, CO, CO_2, and H_2) in dry conditions at 150°C. As can be seen, the sensor signals toward C_2H_2 and C_2H_4 were predominant compared to all other gases.

Table 4. Sensor signals of LFO(500), LFO(600), LFO(700), LFO(800) and LFO(900) sensors for 500 ppm of different dissolved gases in power transformer oil.

	Sensor Signal						
Gas / Sensor	C_2H_2	C_2H_4	C_2H_6	CH_4	CO_2	CO	H_2
LFO(500)	22.1	5.5	1.3	1.2	1.1	1.2	1.3
LFO(600)	28.8	6.4	1.7	1.2	1.1	1.2	1.3
LFO(700)	21.7	5.9	1.3	1.2	1.1	1.2	1.3
LFO(800)	18.7	4.4	1.2	1.2	1.1	1.2	1.2
LFO(900)	21.7	3.4	1.4	1.2	1.1	1.2	1.2

Because my sensors only showed significant responses to ethylene and acetylene, I will focus in the following on the sensing performance of all of my sensors to only these two gases. The sensor signals of the sensors at four different temperatures (150°C, 200°C, 250°C and 300°C) at 5000 ppm concentration of C_2H_2 and C_2H_4 are

shown in Figure 18. The measurements have been done on two different groups of sensors from the same materials to prove the reproducibility.

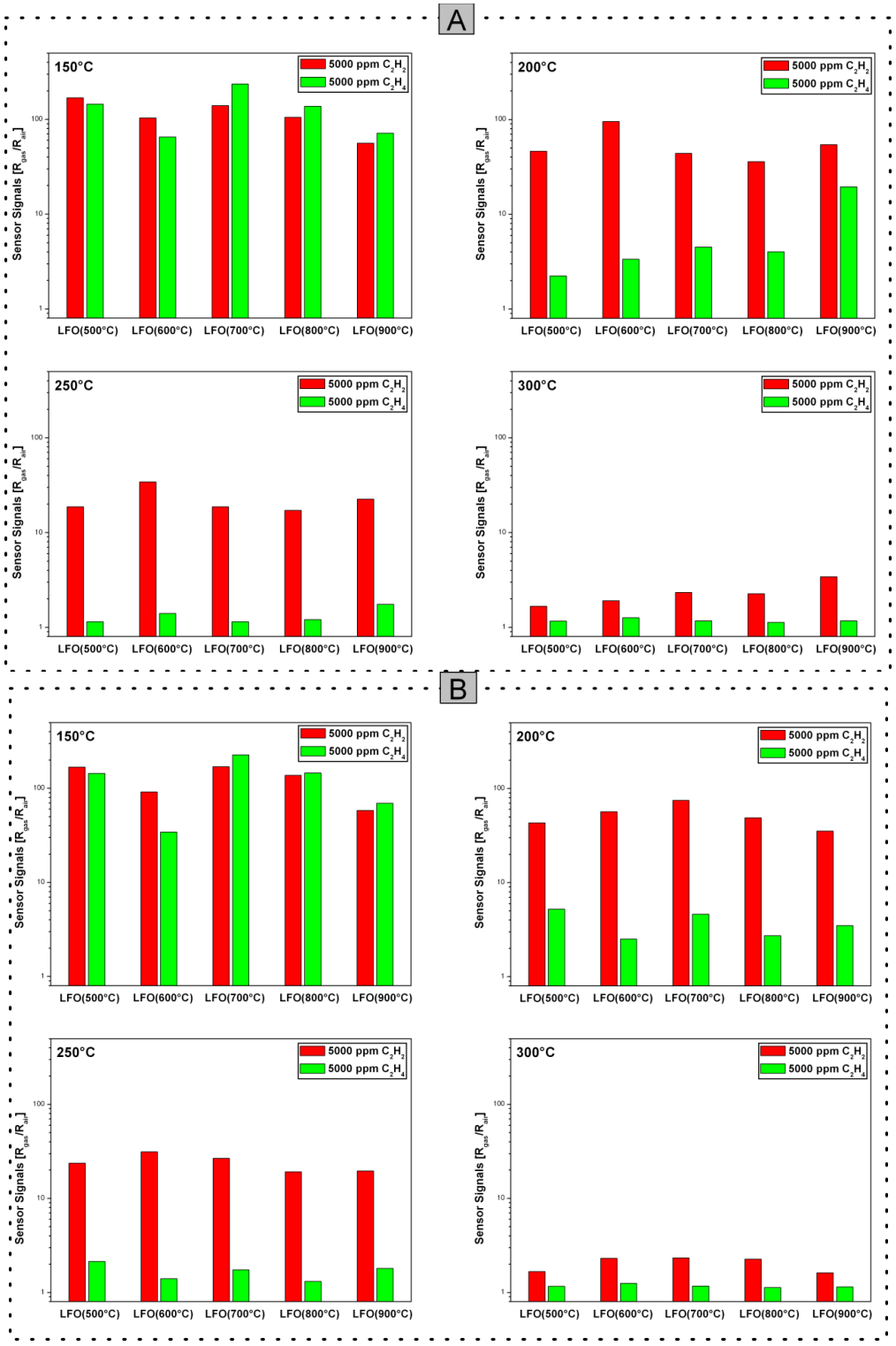

Figure 18. Sensor signals of LFO(500), LFO(600), LFO(700), LFO(800) and LFO(900) on a logarithmic scale for 5000 ppm C_2H_2 and C_2H_4 at 150°C, 200°C, 250°C and 300°C in dry condition, A) group sensors 1 and B) group sensors 2.

The operating temperature plays a key role in controlling the selectivity of LFO sensors to acetylene and ethylene. At 150°C, all sensors showed almost the same responses to both gases at 5000 ppm. By elevating the temperature to 200°C, a clear trend towards acetylene selectivity could be observed, which peaked at 250°C. It is worth observing that the calcination temperature had little influence on the gas sensing properties. All different sensors showed a similar trend of sensing behavior to both gases. Moreover, the patterns of the two groups of sensors were quite similar, demonstrating the reproducibility of my sensors signals.

4.3 Solid state vs Sol gel synthesis of the LFO based gas sensor

In this section, I briefly show a comparison between the two different groups of sensors that were obtained by different synthesis methods. A possible explanation of the variability of their sensing performance will be discussed.

The common characteristic of these two groups is that they showed a significant selectivity to acetylene and ethylene among other dissolved gases. This selectivity could be further improved to only detect acetylene by controlling the operating temperature. However, the sensitive materials, which were synthesized by sol gel, showed much higher responses than their solid state reaction counterparts. The enhancement of the sensor signals could be attributed to the morphology and the particle size of the materials. In the sol gel method, the particle size of the sensitive material was much smaller (around 50 nm) than its counterpart with size of about 1 to 2 µm, as shown in Figure 19. The shape of the resulting powders form sol gel was rod-like mesoporous, whereas the particles had a cubic shape in the solid state method. As a result, the presence of a porous layer and small particle size had higher likelihood of contact with the gases, leading to enhance the interaction between the

gases and the sensitive materials. The shown SEM images of LFO(900) in Figure 19 are representative examples of the images obtained from other samples using the two different synthesis routes that I explored.

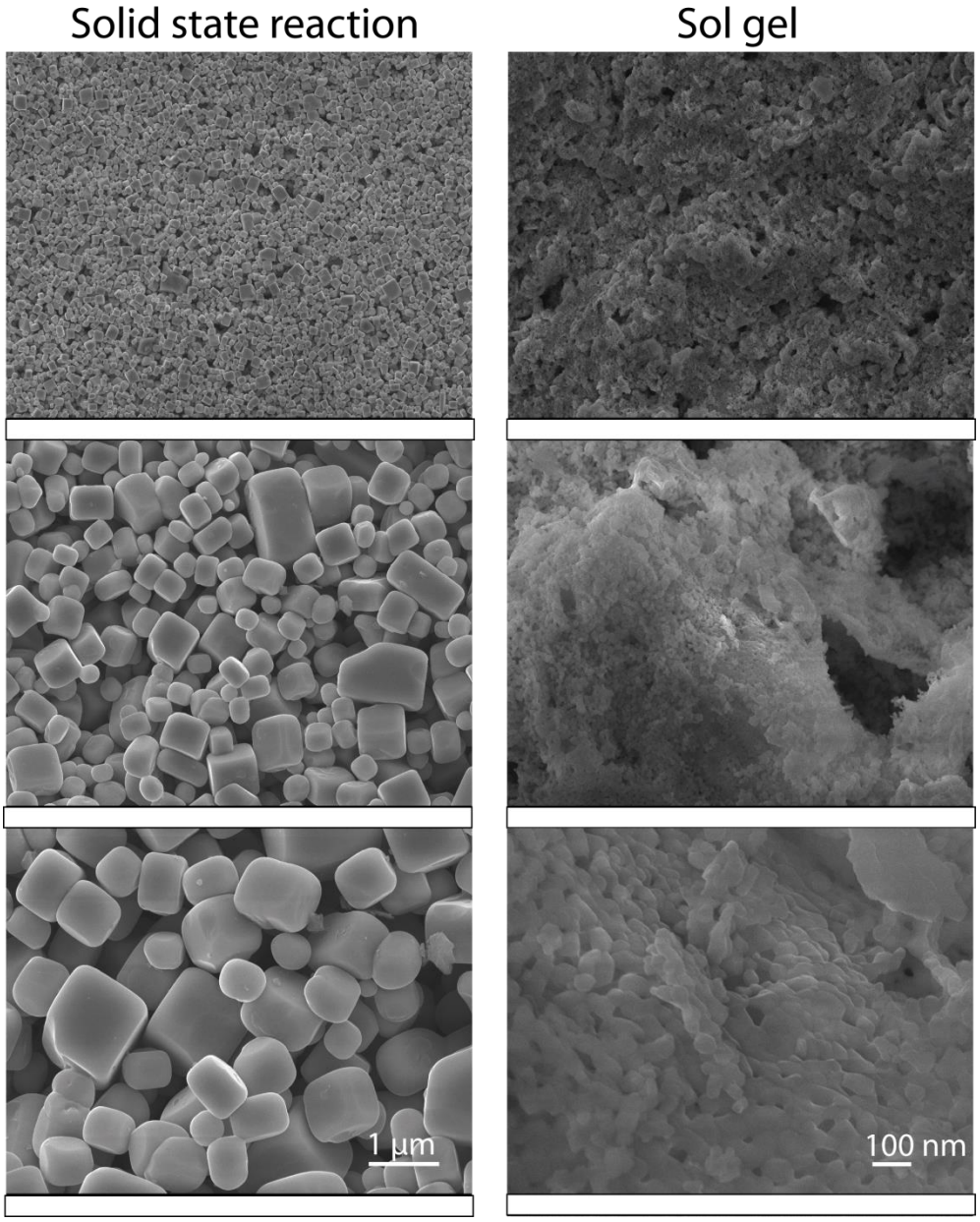

Figure 19. SEM images of LFO(900), which were prepared by solid state reaction (left side) and sol gel method (right side).

4.4 Gas sensing properties of LFO(600)

Based on the above comparison, the sensitive materials that were prepared by sol gel showed better responses to acetylene and ethylene than the ones obtained by solid state reaction. Moreover, even though there was no significant difference of the sensing performance of all sensitive materials synthesized by sol gel, the sensor based on LFO(600) still seemed to perform better at 200°C and 250°C (Figure 18). Therefore, I decided to use LFO(600) as a selected sensor for my next investigations.

4.4.1 Selectivity

I achieved highly selective discrimination of acetylene and ethylene using resistive metal oxide sensors based on LFO perovskite structure. Figures 20, 21, and 22 provide DC resistance data of the LFO(600) sensor to demonstrate the selectivity to acetylene and ethylene at 150°C and only to acetylene at 200°C, among other test gases. The sensor has been measured for each gas twice in dry conditions to confirm the reproducibility, and once in two different relative humidity conditions, namely 25% and 50% at 25°C (25% and 50% r.h. @ 25°C).

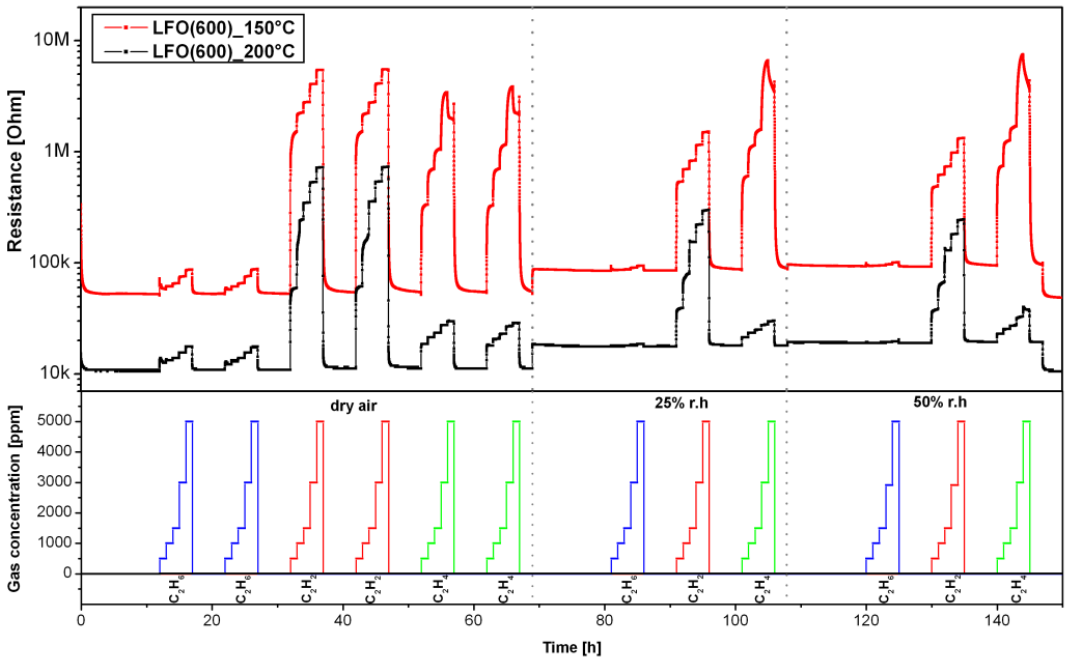

Figure 20. DC resistance measurements of LFO(600) sensor in 0%, 25%, and 50% r.h.@25°C conditions for 500, 1000, 1500, 3000 and 5000 ppm of C_2H_6, C_2H_2, and C_2H_4 at 150 and 200°C.

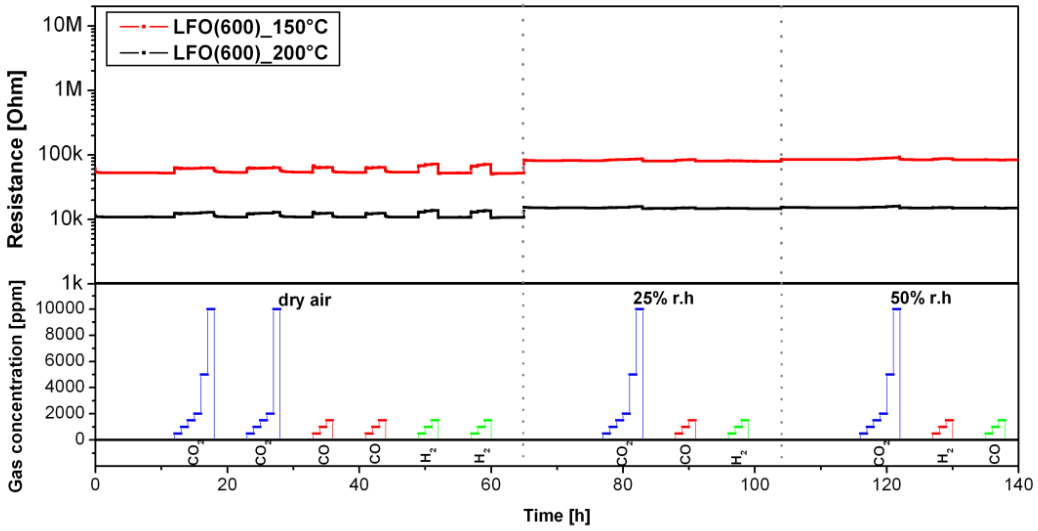

Figure 21. DC resistance measurements of LFO(600) sensor in 0%, 25%, and 50% r.h.@25°C conditions at 150°C and 200°C for 500, 1000, 1500, 2000, 5000, and 10000 ppm of CO_2 and 500, 1000 and 1500 ppm of CO and H_2.

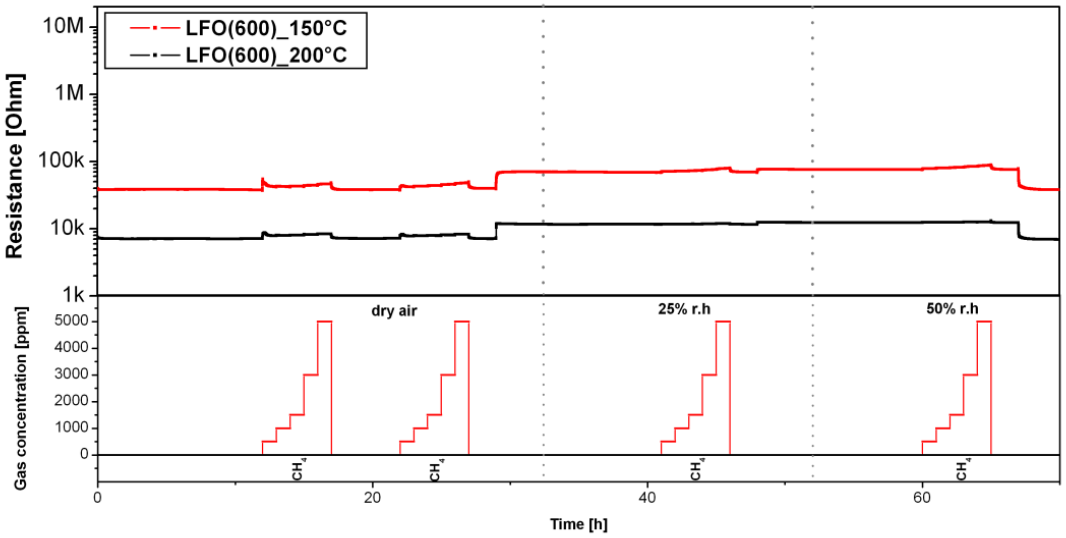

Figure 22. DC resistance measurements of LFO(600) sensor in 0%, 25%, and 50% r.h.@25°C conditions for 500, 1000, 1500, 3000, and 5000 ppm of CH_4 at 150 and 200°C.

The selectivity of the LFO sensors was valid over a range of gas concentrations and operating temperatures. To demonstrate this, Figure 23 shows the gas sensing performance for an exemplary sensor LFO(600) to acetylene and ethylene at various gas concentrations over a large range, and also at different temperatures.

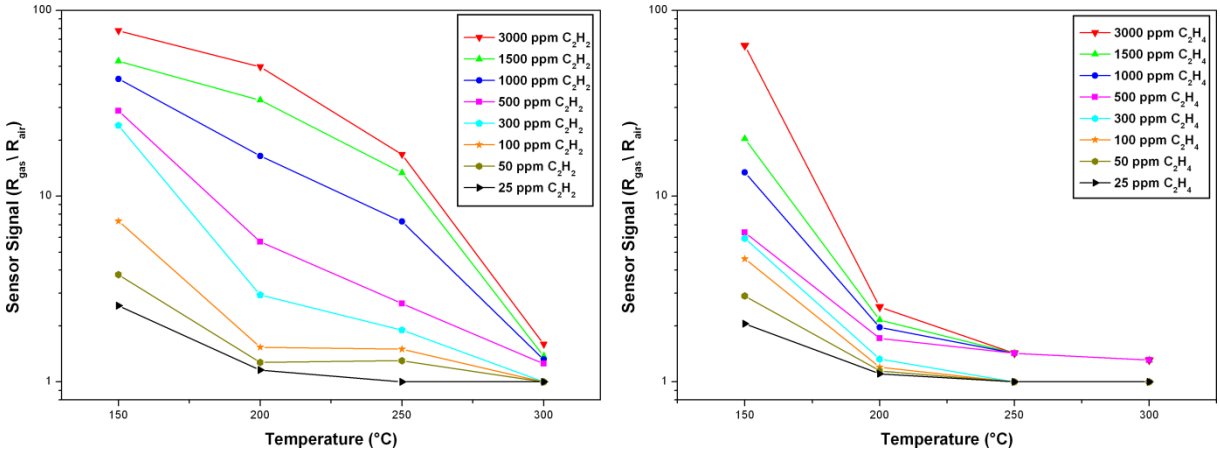

Figure 23. Sensor signals of LFO(600) on a logarithmic scale for different concentrations of C_2H_2 and C_2H_4 at 150°C, 200°C, 250°C and 300°C in dry condition.

As can be seen, the sensor exhibited similar behavioral responses to different concentrations of acetylene and ethylene at 150°C. The sensor signals were rising as a function of gas concentration. The sensor showed higher sensor signals to C_2H_2 than C_2H_4. The responses to ethylene were greater at 150°C than at any of the higher temperatures. The temperature of maximum response to this gas was evidently below 200°C. A weak response to ethylene was observed at 200°C and then has disappeared completely at 250°C and higher. On the other hand, good responses to acetylene were still observed at higher temperatures. Therefore, my sensors were robust over a large dynamic range.

4.4.2 Humidity effect

I tested the response characteristics of the LFO(600) sensor, which was exposed to 3000 ppm C_2H_2 and C_2H_4 at different temperatures, under different humidity conditions, including 0%, 25% and 50% r.h. @ 25°C. The results are shown in Figure 24.

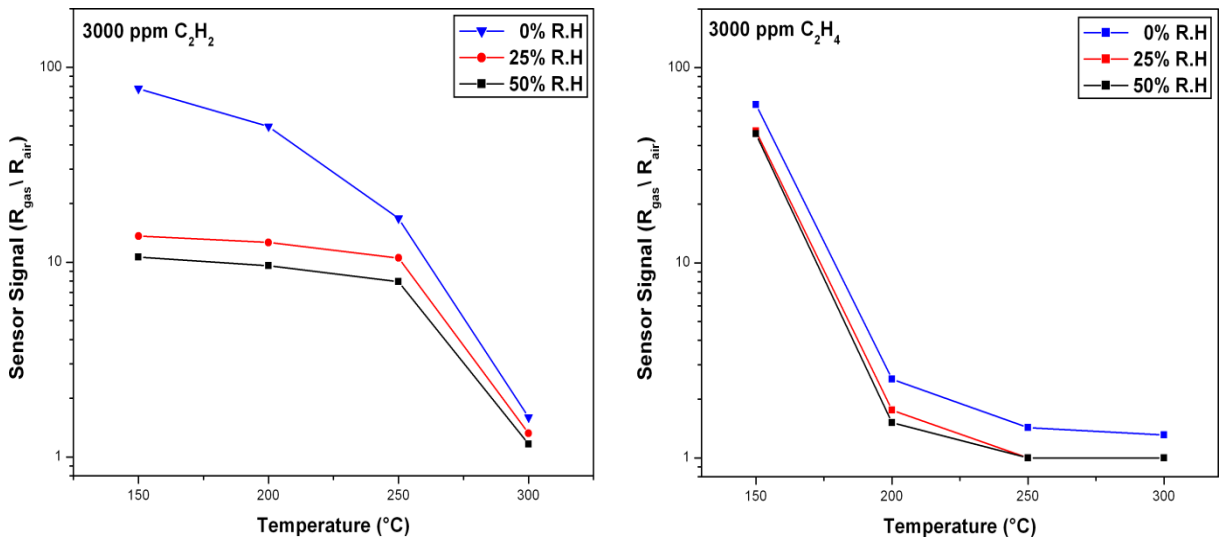

Figure 24. Sensor signals of LFO(600) on a logarithmic scale for 3000 ppm C_2H_2 and C_2H_4 at 150°C, 200°C, 250°C and 300°C in 0%, 25% and 50% r.h.@25°C.

Humidity had a stronger impact on the sensor response to acetylene compared to ethylene. In 25% r.h.@25°C, the sensor signals to acetylene were reduced from around 75 to 15 at 150°C, while the response to ethylene was only decreased from about 65 to 50 at the same temperature. It is clear that the sensor tends to be saturated faster in humid conditions than in dry condition during acetylene exposure. Moreover, the humidity effect on the response to acetylene was decreasing with increasing operating temperature. In 50% r.h.@25°C, the responses were not greatly different from those at 25% r.h.@25°C for both gases at all temperatures.

4.4.3 CO_2 background

Due to the presence of CO_2 in most application environments, it is necessary to investigate the sensor performance in its presence. Figure 25 shows the sensor signals of LFO(600) sensor for varying concentrations of acetylene and ethylene in a background of 1000 ppm CO_2 and in clean air at 250°C. The data reveals that the sensor responses to acetylene and ethylene remained unchanged by the presence of CO_2 gas. This enables my sensor to work well in real world atmospheres.

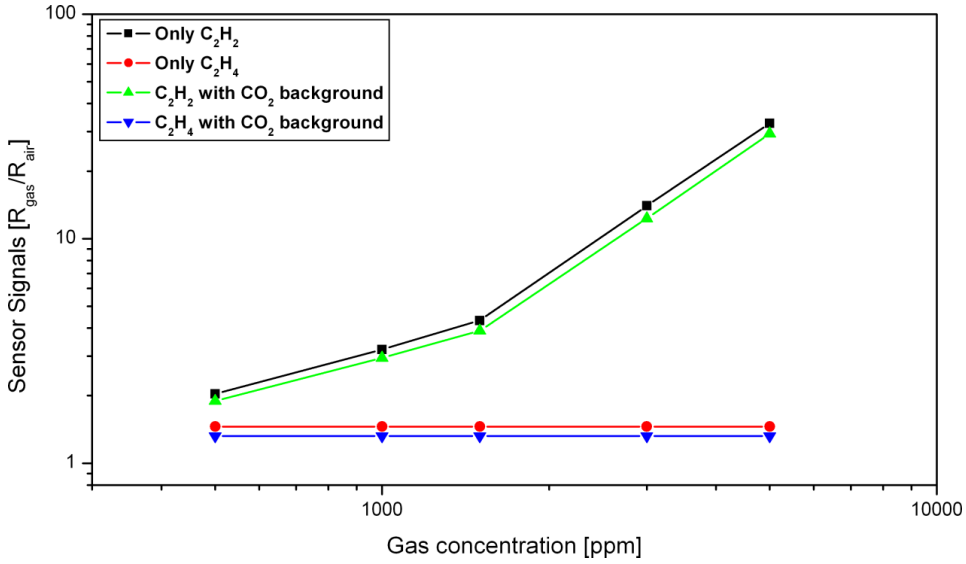

Figure 25. Sensor signals of LFO(600) sensor for 500, 1000, 1500, 3000, 5000 ppm C_2H_2 and C_2H_4 in a clean air and 1000 ppm CO_2 background at 250°C.

4.4.4 Cross Sensitivity

The cross sensitivity of the LFO(600) sensors to different combinations of acetylene and ethylene in dry conditions, measured at 250°C, is shown in Figure 26(A). The sensors have been exposed to both gases individually and simultaneously at different concentrations as shown in Table 5. The same measurement conditions have been used also in 25% r.h.@25°C for all different gas concentrations except 5000 ppm, which is not reachable for our gas mixing system without changing the total flow.

Table 5. Gas flow protocol of the cross sensitivity measurements and the sensor signals of the sensor in dry and 25% r.h.@25°C.

First cycle (only ethylene)			Second cycle (only acetylene)			Third cycle (both gases)		
Gas concentration (ppm)	Sensor Signal		Gas concentration (ppm)	Sensor Signal		Gas concentration (ppm)	Sensor Signal	
	0% r.h.	25% r.h.		0% r.h.	25% r.h.		0% r.h.	25% r.h.
500	1.4	1.1	500	2.6	1.4	500 C_2H_2 + 500 C_2H_4	2.9	1.4
1000	1.4	1.1	1000	4.2	2	1000 C_2H_2 + 1000 C_2H_4	4.3	2.2
1500	1.4	1.1	1500	5.9	3	1500 C_2H_2 + 1500 C_2H_4	6.3	3.3
3000	1.4	1.1	3000	24.1	8.4	3000 C_2H_2 + 3000 C_2H_4	24.8	8.5
5000	1.3	N/A	5000	34.5	N/A	5000 C_2H_2 + 5000 C_2H_4	34.5	N/A

The sensors showed almost the same response patterns to acetylene with and without ethylene in dry and 25% r.h.@25°C conditions, indicating good selectivity of my sensor. Two sensors have been used for each measurement to confirm the reproducibility of my findings.

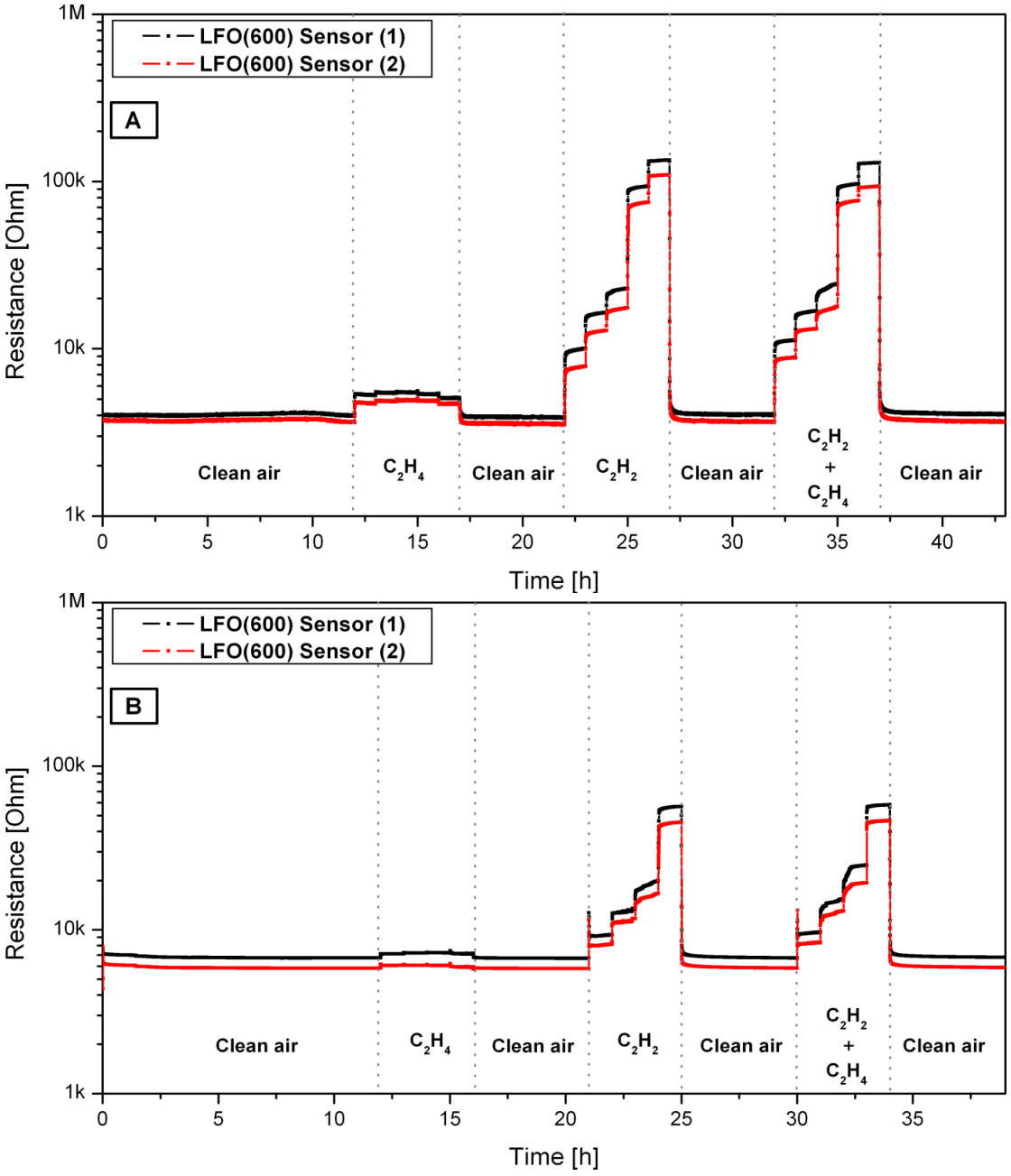

Figure 26. The cross sensitivity of C_2H_2 to C_2H_4 for different concentrations at 250°C in A) dry condition and B) 25% r.h.@25°C.

4.4.5 Non-Stoichiometric Compound

Because the B-site in perovskites is most probably responsible for the catalytic and gas sensing properties (as mentioned in section 3.2), different non-stoichiometric compounds of LFO have been prepared through the sol gel method at calcined

temperature 600°C. Five different sensitive materials of LF_xO (x = 0.0, 0.95, 0.90, 0.85 and 0.80) were prepared in order to investigate the role of non-stoichiometry compounds (or decreasing the amount of iron) on the gas sensing properties of LFO. Figure 27 shows the sensor signals of the five different sensors that were exposed to 3000 ppm of acetylene and ethylene in dry conditions at different operating temperatures (150, 200, 250, and 300°C).

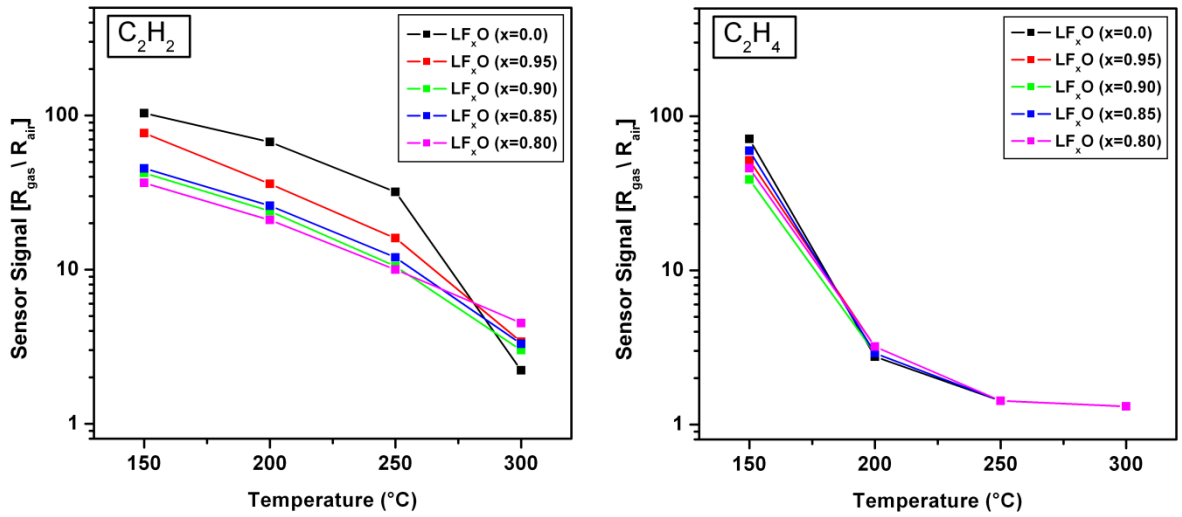

Figure 27. Sensor signals of $LF_xO(600)$ sensors for 3000 ppm C_2H_2 (left side) and C_2H_4 (right side) in dry air condition at 150, 200, 250 and 300°C.

The general trend of sensing behavior of all sensors to acetylene and ethylene was quite similar. The stoichiometric LFO sensor demonstrated the best sensing performance compared to non-stoichiometric LFO sensors. This was true for both gases at all operating temperatures, except for acetylene at 300°C. Moreover, it seems that the sensor response to acetylene was much more influenced by the change in the B-site composition than ethylene. In the case of acetylene, the sensor signals of the stoichiometric LFO sensor decreased to approximately half the maximum value in the non-stoichiometric sensors for x = 0.90 and lower. This

suggests that iron plays a key role in the sensing to acetylene. The sensor response decreased with decreasing iron content. No further influence could be seen on the sensor response by decreasing the amount of iron more than 10%.

4.5 Conclusion

I demonstrated a novel use of the LFO compound as a highly selective sensing material towards only acetylene and ethylene among all other dissolved gases that may be present in transformer oils. Moreover, I also showed that distinguishing between these two gases could additionally be achieved by controlling the operating temperatures. Two synthesis methods have been used to produce LFO powders, namely solid state reaction and sol gel. The sensitive materials, which were obtained by both routes, showed the same trend of selectivity. However, the sensitive materials that were prepared by sol gel indicated much higher responses than the ones that were synthesized by solid state reaction. In addition, the LFO(600) was selected to be used for further investigation due to its superior sensing performance. The sensor has shown very stable responses to acetylene during cross sensitivity with ethylene and carbon dioxide. Even though the sensor performance was influenced by the relative humidity backgrounds, still quite good sensor signals could be achieved.

5. Investigations of the ethylene and acetylene sensing mechanism

Based on the gas sensing results, I found that the LFO sensors show an exceptional selectivity to acetylene and ethylene. It is important to understand the underlying mechanism for future development of selective gas sensing materials. The possibility of understanding the sensing mechanism strongly depends on the chances of isolating intermediated species in the study of each step in the gas sensing cycle, as explained earlier (see section 2.5). In order to achieve this, my investigation plan was dedicated to the following key concepts:

- Operando diffuse reflectance infrared Fourier transform spectroscopy (DRIFTS) experiments under different conditions to provide very valuable information about surface change by taking IR spectra during gas exposure. Isotope labelling exchange experiments have been used effectively for interpreting the spectra associated with:

  I. H_2O/D_2O exchange
  II. $^{12}CO_2/^{13}CO_2$ exchange
  III. C_2H_4/C_2D_4 exchange

- Investigating the catalytic activity of the sensitive material and the remaining parts of the sensor as a necessary prerequisite to understanding their contributions in the gas sensing mechanism.

5.1 Investigation of Ethylene and Acetylene Surface Reactions

Even though my investigations were mainly focused on ethylene and acetylene to explore how LFO sensors react only to these two gases among all other dissolved gases, I also examined CO_2 as an additional gas for reference. I chose this gas because it can be a final product of a hydrocarbon reaction, and it may therefore re-adsorb at the surface. Moreover, perovskites are reactive to CO_2 in ambient air, which might lead to forming carbonates at their surface [59,63,64]. Considering the chemisorption mechanisms of CO_2 on LFO surfaces is therefore essential in order to achieve reliable information about resulting species, such as carbonates and bicarbonates. This can in turn help to interpret the DRIFT spectra of hydrocarbons.

Figure 28 shows LFO sensor DRIFT absorbance spectra recorded at two operating temperatures (150°C and 250°C) under exposure to 500 ppm CO_2, C_2H_4, and C_2H_2. The spectra were taken after 1 hour of the gas exposure and then referenced to the spectrum that was recorded in clean air. The sensor signals, which were calculated from simultaneous resistance measurements, are shown in the right side of Figure 28.

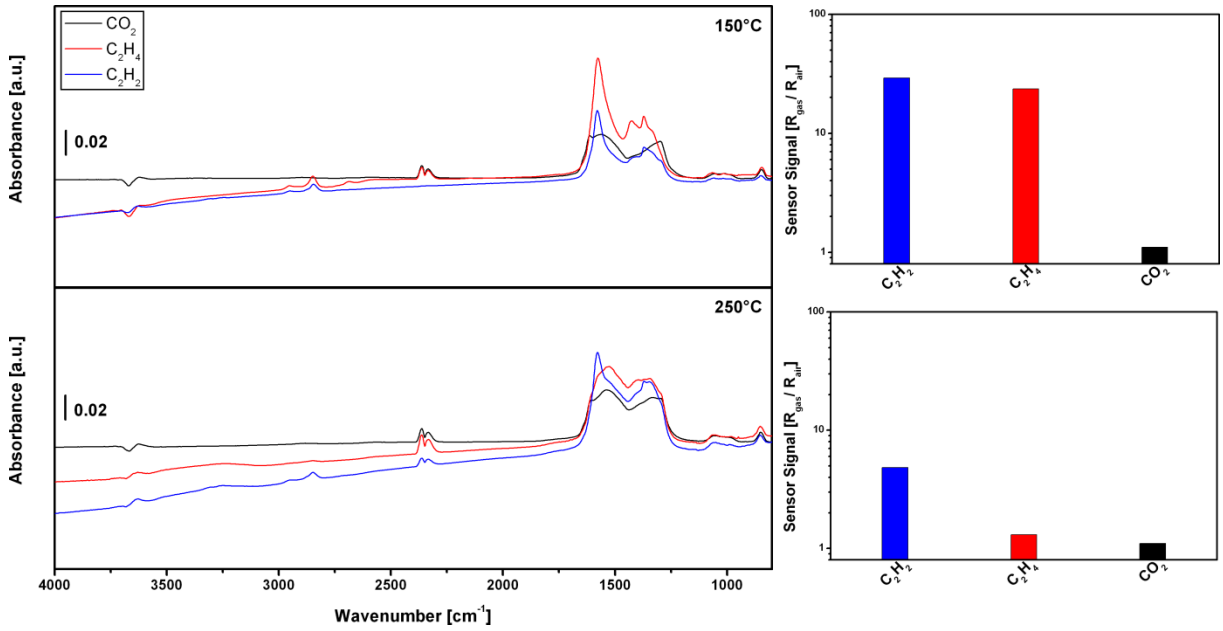

Figure 28. DRIFT spectra (left side) and the sensor signals (right side) of the LFO sensor exposed to 500 ppm CO_2, C_2H_4, and C_2H_2 in dry conditions at 150°C and 250°C. The spectra were referenced to the spectrum that was measured in clean air.

At first glance, one gets the impression that there is a correlation between some IR bands and the gas responses; as an example, the presence of the bands just below 3000 cm^{-1} is accompanied by a good sensor response. Not that clear, because of the overlap between many bands between 1200 and 1600 cm^{-1}, the presence of the sharp peak around 1580 cm^{-1} seems to also be correlated to large sensor signals. This makes the identification of such species very important in order to know the origin of the resistance change. Moreover, if the reaction of a hydrocarbon leads to a spectrum that is quite similar to the one of CO_2, then no response from the sensor was recorded. The formation of CO_2 at the LFO surface during hydrocarbon reactions except for acetylene at 150°C has been observed. In the following sections, I describe the results of extensive experiments dissecting the above observations and allowing a better understanding of the adsorption and desorption mechanisms of CO_2, C_2H_4, and C_2H_2 on LFO.

5.1.1 CO_2 reactivity on LFO surface

The DRIFT spectra and the resistance measurements of LFO exposed to 500, 1000, 1500, and 2000 ppm CO_2 at 150°C in dry and 10% r.h.@25°C conditions are shown in Figure 29. The spectra were referenced to the spectrum that was recorded in clean air. Despite no significant change in the resistance measurements of the sensor under CO_2 exposure in general, a sharp decrease in the resistance of the sensor in the first few minutes of the exposure was observed, followed by a slow recovery. The reversibility of the behavior can be seen at the end of exposure, with the resistance value jumping back in the opposite direction from the jump when gas exposure took place. Moreover, the effect was present when increasing the gas concentration, but with lower impact. The presence of humidity reduced the resistance change. These results indicate that the small variation in the resistance could be attributed to the presence of different type of species that have different electrical effects.

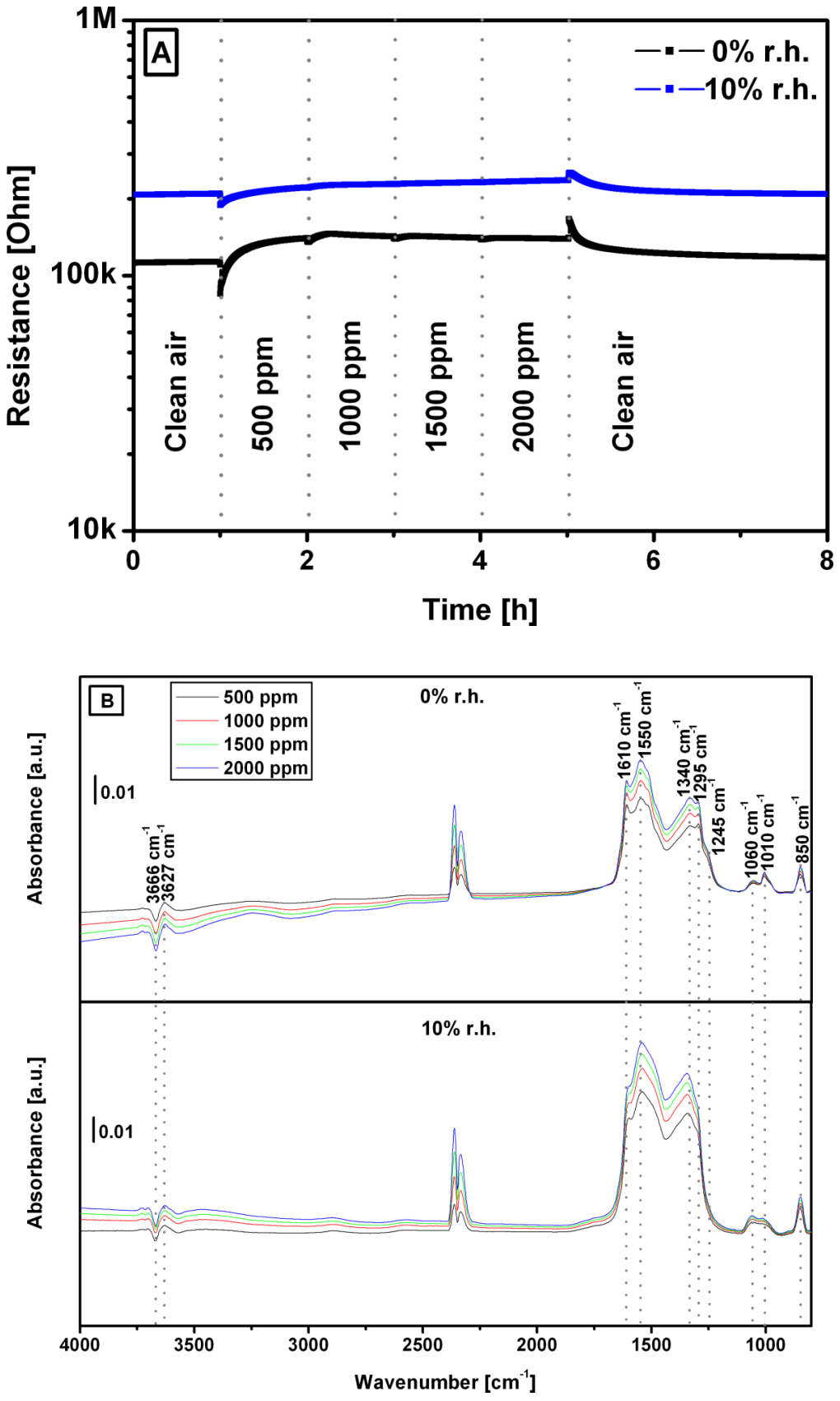

Figure 29. The resistance measurements (A) and DRIFT spectra (B) of LFO sensors under different concentrations of CO_2 exposures (500, 1000, 1500, and 2000 ppm) at 150°C in dry and 10% r.h.@25°C conditions. The spectra were referenced to the spectrum which was recorded in clean air condition.

All IR spectra showed a systematic change in all bands with increasing gas concentrations. The bands at 3666 and 3627 cm^{-1} can be attributed to OH groups. It seems that the hydroxyls were consumed to form new species that were most probably bicarbonates. The bands at 2363 and 2343 cm^{-1} are well known as vibrations of CO_2 in the gaseous phase. Finally, the bands around and below 1500 cm^{-1}, in the so-called fingerprint region, were quite complex.

The well-known information about adsorption of CO_2 on metal oxides (as explained in section 2.4.1) and other effective experiments such as the adsorption kinetics at the surface and isotopic labelling will be used to make my assignments of IR peaks.

I start with the most common isotopic labelling experiment based on H_2O and D_2O. The LFO sensor exposed to 500 ppm CO_2 at 10% r.h. @25°C of two different backgrounds namely H_2O and D_2O for an operation temperature of 150°C as shown in Figure 30. The spectra were referenced to the spectrum that was recorded in the respective clean air condition.

The two obvious bands centered at 3666 and 3627 cm^{-1} in OH groups are shifted to OD region at 2690 and 2658 cm^{-1}, respectively. The remaining peaks are not shifted, which means no significant contribution of the hydrogen in these vibrations. Therefore, I expect that they belong to the carbon related species. At around 1600 cm^{-1}, however, a very small shift can be observed, which could be attributed to the small contribution of the hydrogen in OCO vibration of the bicarbonate species. This also gives an indication of bicarbonate formation.

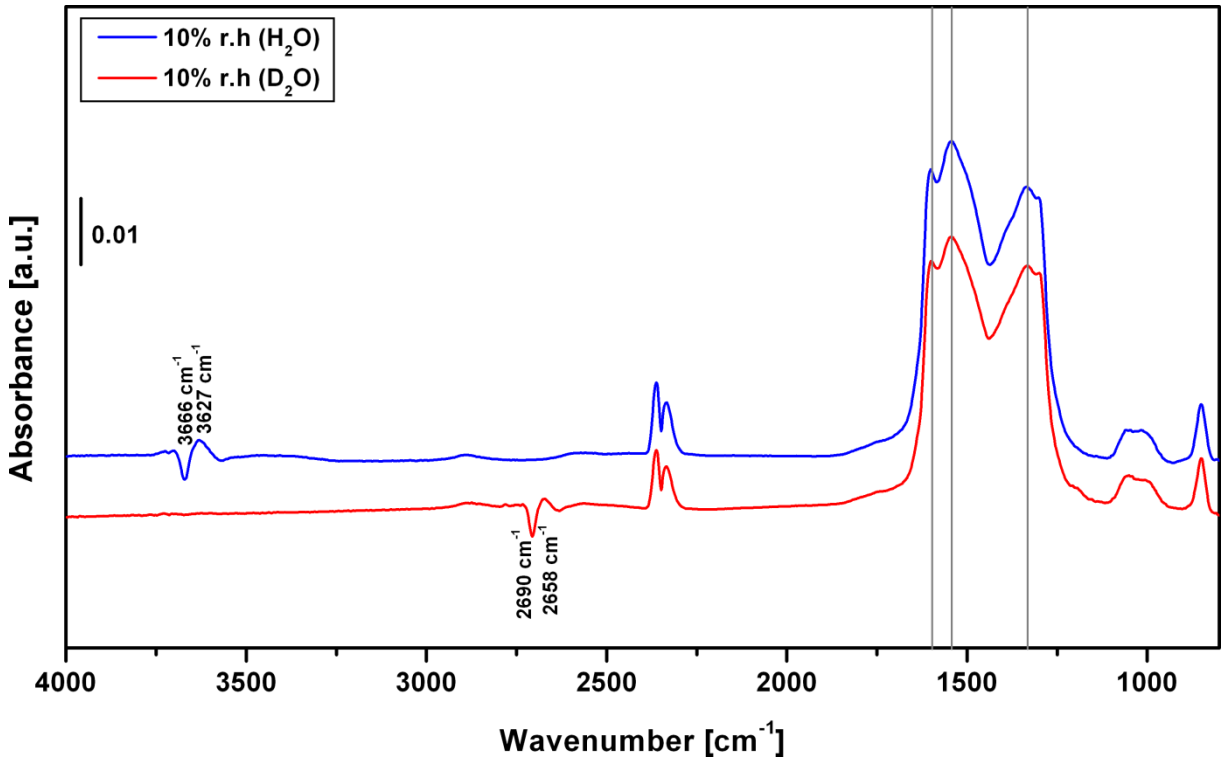

Figure 30. DRIFT spectra of LFO sensor exposed to 500 ppm CO_2 in H_2O (blue color) and D_2O (red color) backgrounds in dry condition at 150°C. The spectra were referenced to the spectrum that was measured in respective clean air condition.

To gain a deeper insight into the reaction kinetics at the surface, I performed time-resolved experiments for observing and predicting the nature and the adsorption kinetics of the surface's species. Figure 31 shows the DRIFT spectra of the LFO sensor, which were recorded every minute, under exposure to clean air or 500 ppm CO_2 in dry conditions at 150°C. In each panel, the reference spectrum was different: clean air (Figure 31A), first minute of CO_2 exposure (Figure 31B), and its previous measurement (Figure 31C).

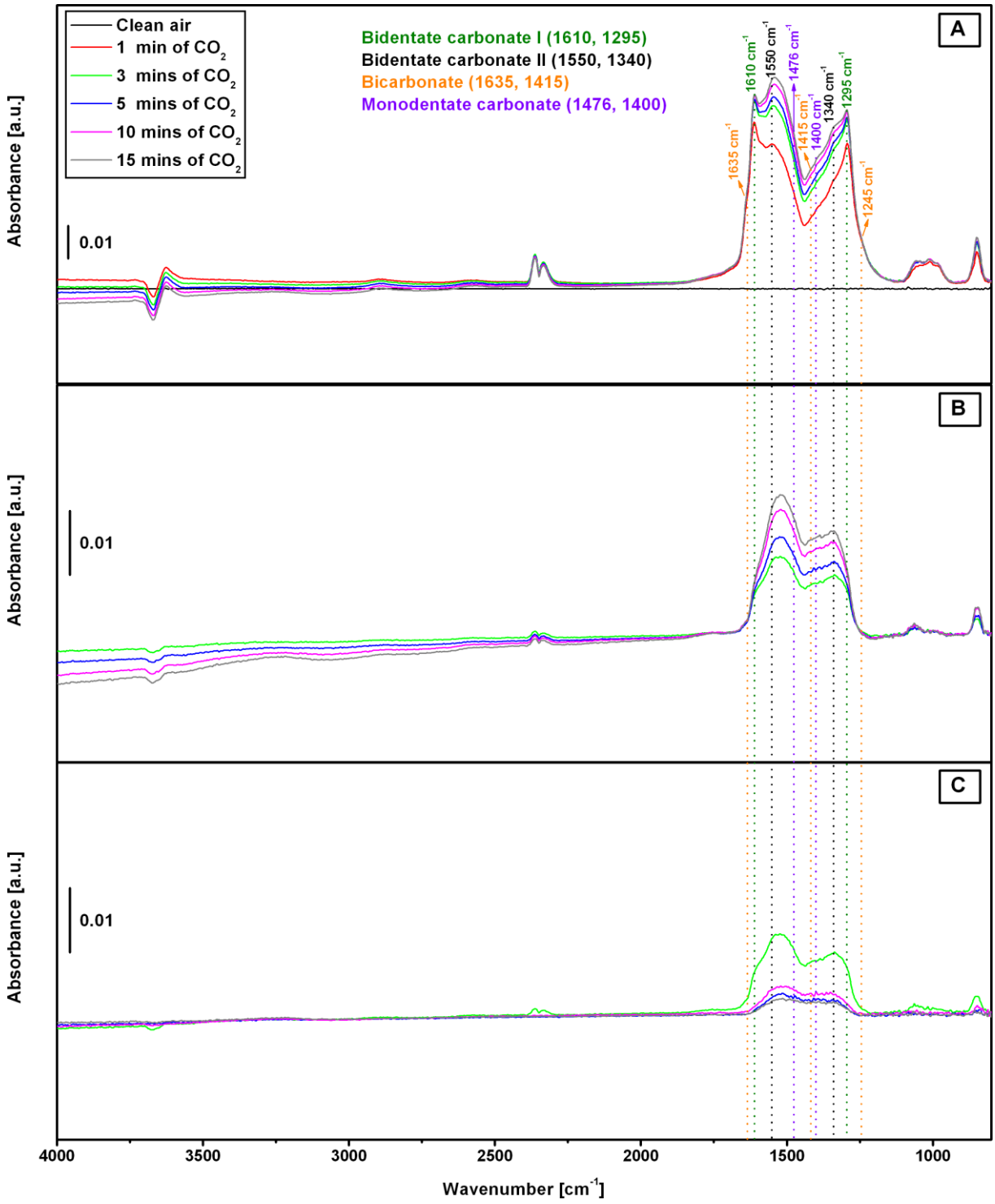

Figure 31. DRIFT spectra of LFO sensors exposed to 500 ppm CO_2 and measured at 1, 3, 5, 10, and 15 mins. The spectra were referenced to spectra measured under: A) clean air, B) the first min of CO_2 exposure C) its previous measurement.

Under gas exposure, I observed the following spectral features:

- Two pronounced peaks centered at 1610 and 1295 cm^{-1} and two centered at 1550 and 1340 cm^{-1}. Both groups can be assigned to bidentate carbonates due to a Δv_3 value higher than 200. I will name them in the following bidentate carbonate (I) and bidentate carbonate (II), respectively.
- The presence of the bands centered at 1635 and 1245 cm^{-1} together with an increase in hydroxyl group at 3627 cm^{-1} are the characteristic IR signature of bicarbonates.

The valley centered at 1430 cm^{-1} is an indication of overlapped peaks. Therefore, using isotopic exchange experiments is a possible way to distinguish between such peaks. The DRIFT spectra of LFO sensor exposed to 500 ppm $^{12}CO_2$ and $^{13}CO_2$ in dry condition at 150°C as shown in Figure 32.

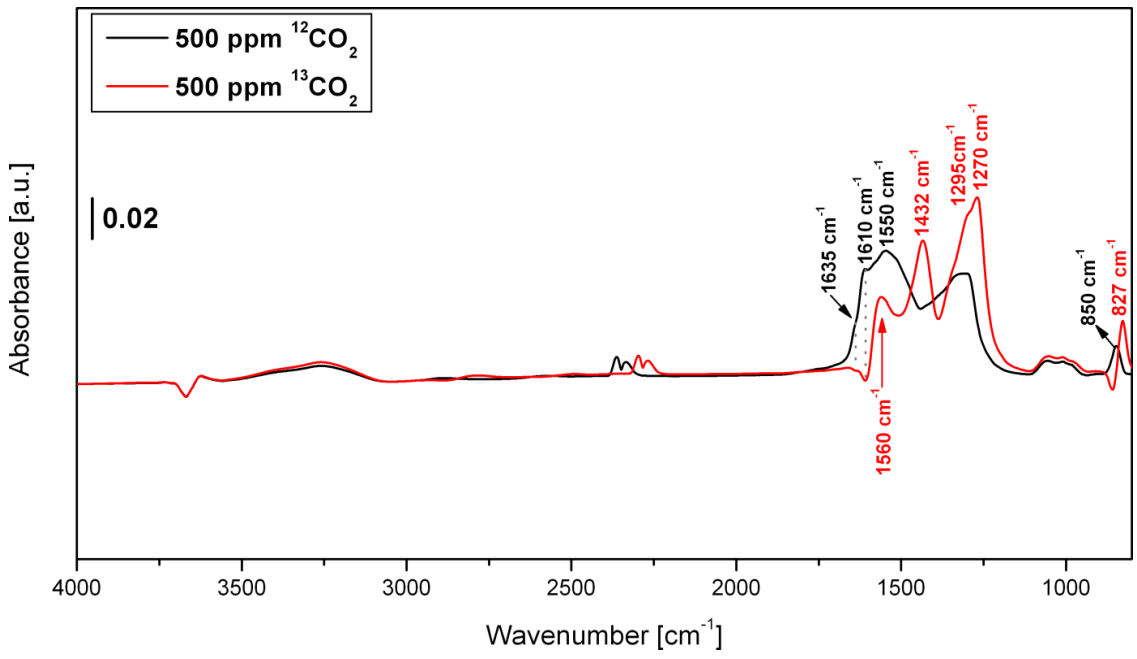

Figure 32. DRIFT spectra of LFO exposed to 500 ppm $^{12}CO_2$ (black color) and $^{13}CO_2$ (red color) in dry condition. The spectra were referenced to the spectrum that was measured in clean air condition.

Even though I expect to see the shifts in all carbon related species, the bands centered at around 1050 cm^{-1} do not show significant shifts. This can be attributed to the weak contribution of the carbon in the v_1 vibration mode as reported in a previous paper [65]. The peak centered at 1432 cm^{-1} is clearly observed under $^{13}CO_2$ exposure, which is most probably a result of the band shift at 1476 cm^{-1}. This peak and the one at 1400 cm^{-1} can be associated with monodentate carbonates. The summary of carbon-like compounds and their characteristic IR bands based on my time-resolved and isotopic labelling experiments is illustrated in table 6.

Table 6. The assignment of IR bands of carbon related species based on time-resolved and isotopic labelling ($^{12}CO_2$ /$^{13}CO_2$) experiments. The theoretical isotopic shift is (0.972).

Surface species	**$^{12}CO_2$ (cm^{-1})**	**$^{13}CO_2$ (cm^{-1})**	**Shift**
Bicarbonate	1635	Hidden	
Bidentate (I)	1610	1560	0.969
Bidentate (II)	1550	Hidden	
Monodentate	1476	1432	0.970
Monodentate	1400	Hidden	
Bidentate (II)	1340	1295	0.966
Bidentate (I)	1295	1270	0.980

Even though I mainly use the v_3 vibration mode in my assignments, it is worth noting that the vibration band centered at 850 cm^{-1}, which is related to the v_2 vibration mode, is shifted to 827 cm^{-1} under $^{13}CO_2$ exposure. The isotopic shift of this vibrational frequency is quite similar to a calculated factor of (0.972).

The dynamics of species formation can be followed using the different evaluation strategies presented in Figure 31. The use of different references allows for a step by step time analysis. I found that the formation of all species starts immediately after the introduction of CO_2. The bicarbonate and bidentate (I) species show the fastest buildup and also saturation after 3 and 10 minutes, respectively. The buildup of the bidentate (II) and of the monodentate carbonates seems to be somehow delayed; the former becomes the dominant process after the first minute of the gas exposure and reaches saturation after 15 minutes. The latter is more difficult to observe because it is masked by the former; it is, however, possible to clearly identify it under $^{13}CO_2$ exposure (see Figure 32). This seems to be correlated with the CO_2 sensor response (see Figure 29A). Also, there I observed first a decrease of the sensor resistance followed by an increase and response saturation.

The results obtained at 250°C are shown in Figure 33 where the LFO exposed to 500, 1000, 1500, and 2000 ppm CO_2 at 250°C in dry and 10% r.h.@25°C conditions. The spectra were referenced to the spectrum that was recorded in clean air.

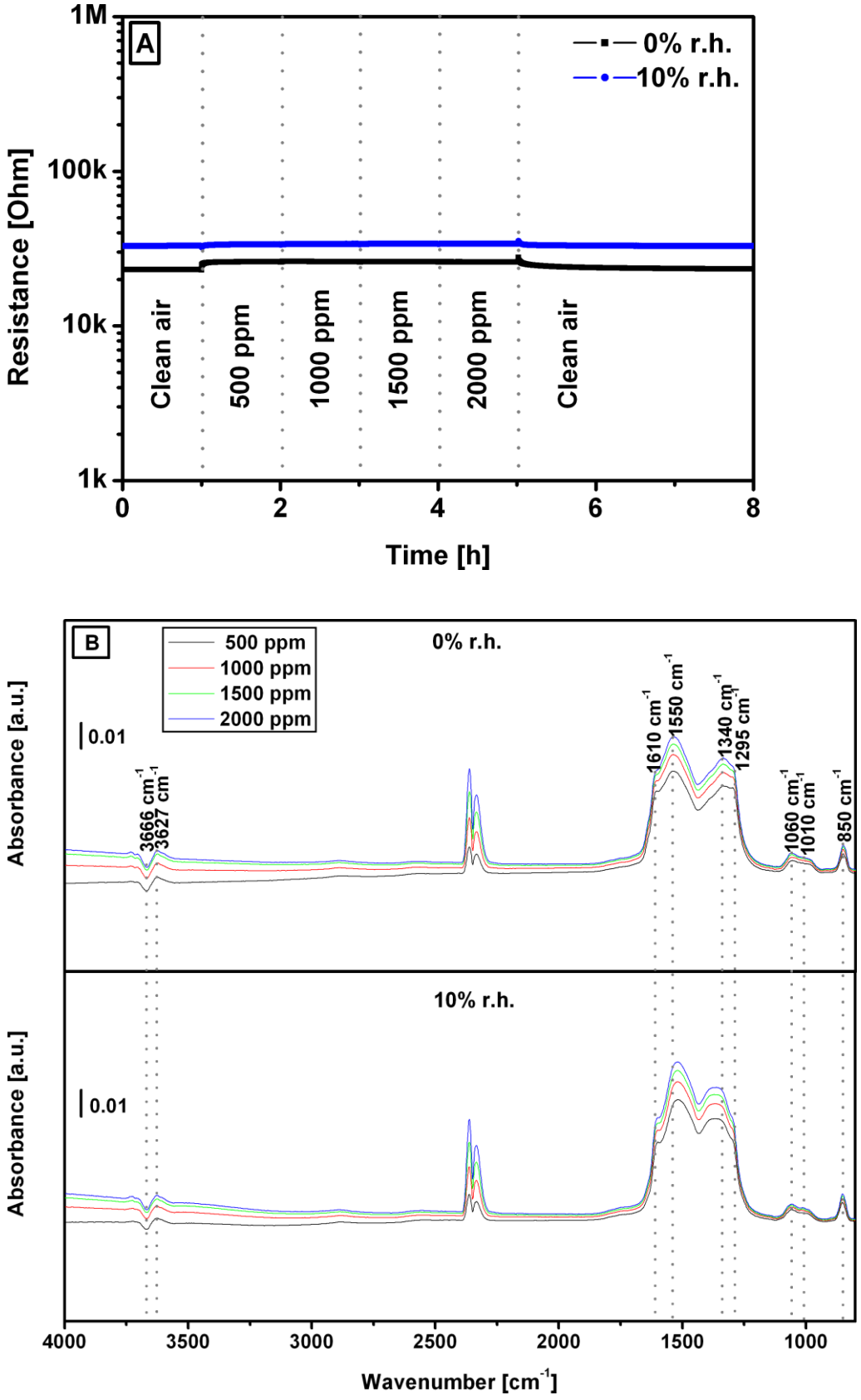

Figure 33. DRIFT spectra and resistance measurements of LFO sensors exposed to 500, 1000, 1500, and 2000 ppm CO_2 at 250°C in dry and 10% r.h.@25°C conditions. The spectra were referenced to the spectrum that was measured in clean air condition.

By comparing Figures 29 and 33, I found that the general trends are quite similar at all conditions (two different temperatures and two different humidity levels). However, the influence of humidity and operating temperature is visible. For example, the response and recovery times as well as the magnitude of the sensor signals are affected. The species identified in the DRIFTS spectra are the same but, as in the case of the sensor signals, their dynamics and relative weight are impacted by the change of the operation temperature and humidity level. The enhancement of CO_2 adsorption in the presence of humidity on some materials, such as iron oxides, has been reported in the literature [66,67]. These effects are illustrated in the following figure where the changes that take place immediately after the gas exposure was stopped are shown (Figure 34). All spectra were referenced to the spectrum that was taken at the end of the gas exposure.

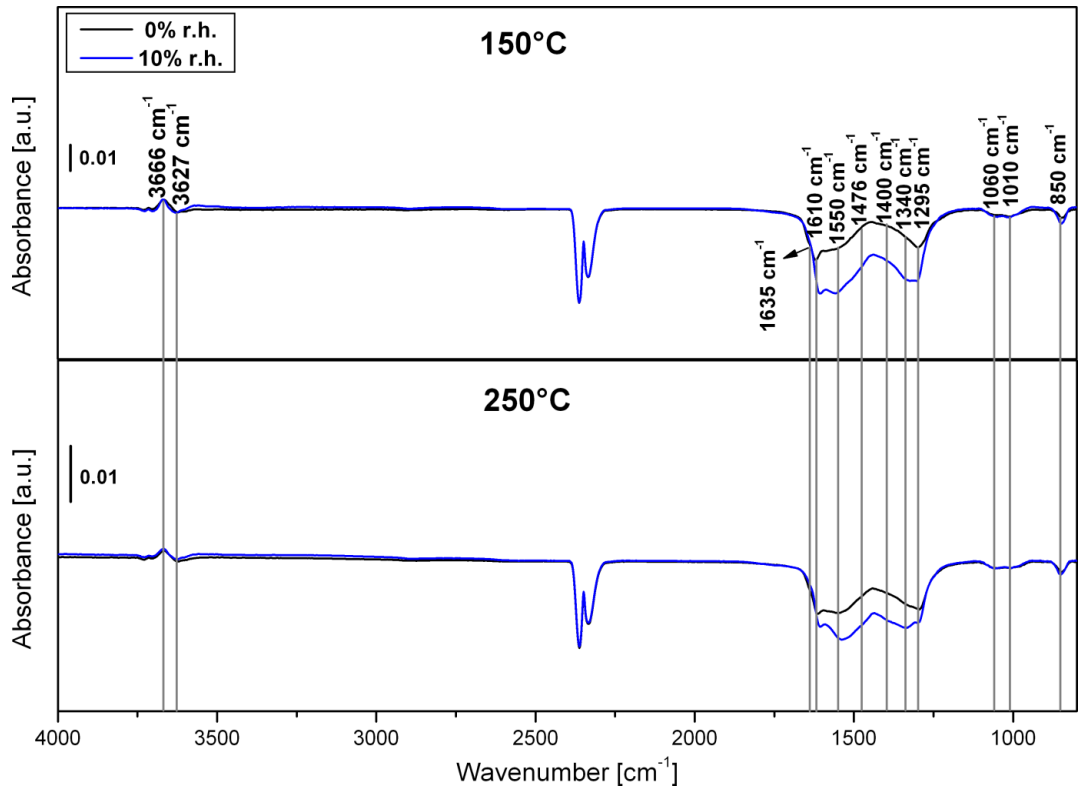

Figure 34. DRIFT spectra of the LFO sensor recorded after 15 mins of the CO2 exposure at 150°C and 250°C in dry and 10% r.h.@25°C conditions. All spectra were referenced to the spectrum that was measured at the end of CO2 exposure.

A significant decrease in the bicarbonate and bidentate (I) and monodentate carbonates is taking place in all four conditions with a kinetic that is mirroring the one recorded under exposure. The bidentate (II) carbonates are an exception, probably because of their stronger bond to the surface [68].

Overall, my DRIFT results revealed that carbonates in different configurations – monodentate and bidentate – and bidentate bicarbonates were formed on the LFO surface in dry and humid conditions at both temperatures during CO_2 exposure. It is important to note that the kinetic of their formation is different: firstly, the bidentate carbonates (I) and bicarbonates are formed followed by the monodentate carbonates and bidentate carbonates (II).

Moreover, the absorption bands of LFO under CO_2 exposure are quite similar to the ones which are reported for iron oxides [68], suggesting that the surface Fe ions are the main active sites in the gas adsorption process at the LFO surface. My finding is in agreement with a previous density function theory (DFT) study reporting that surface Fe ions dominate the oxygen adsorption mechanism on LFO (010) surface [46].

5.1.2 Hydrocarbons reactivity on LFO surface

Good understanding of bicarbonates and different configurations of carbonate species will help me to identify the nature of other species that will arise during hydrocarbon adsorption on the surface of LFO sensor. In particular, the CO_2 formation was clearly seen during their surface reaction mechanisms.

5.1.2.2 Surface reaction of C_2H_4

Adsorption of hydrocarbons on metal oxide surfaces can yield to different types of surface species. Carboxylate-like compounds, however, are the most frequent surface species during alkene adsorption on metal oxides surface at temperatures below 200°C [69].

It is worth showing the IR spectra of ethylene in gaseous phase before going through its surface reaction mechanism on LFO surface. Figure 35 indicates the absorbance IR bands of ethylene as taken from National Institute of Standards and Technology (NIST) chemistry webbook [70].

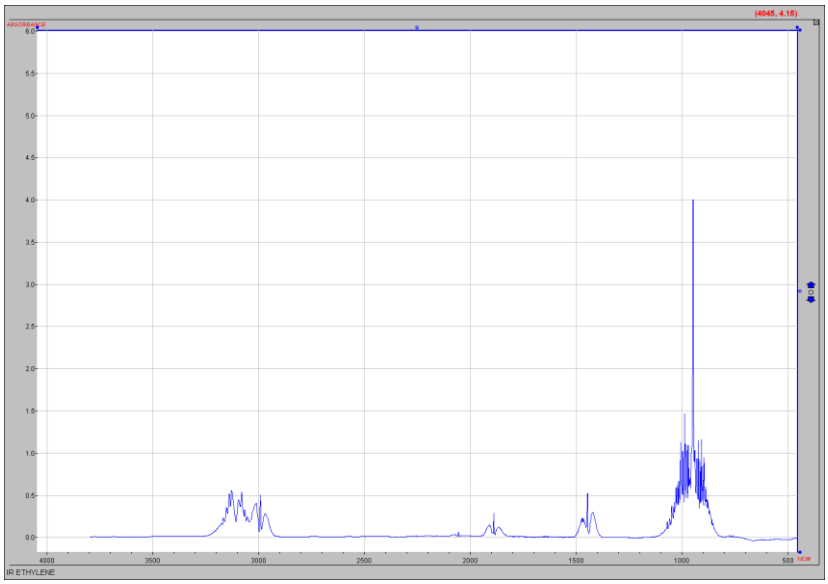

Figure 35. IR spectrum of ethylene in gaseous phase (150 mmHg diluted to a total pressure of 600 mmHg with N_2). The figure is adapted from [70].

Some of these bands can be seen in my following investigations when ethylene is not completely oxidized on the surface of the material, in particular at low operating temperatures.

DRIFT spectra combined with results of resistance measurements, in the presence of different concentrations of C_2H_4 (500, 1000, 1500 and 3000 ppm) in dry and 10% r.h.@25°C for an operation temperature of 150°C, are shown in Figure 36. The resistance of the sensor changed from just few tens of kOhms in clean air to about 10 MOhms under exposure to 3000 ppm C_2H_4. The large resistance change is mirrored by a significant change in the intensity of IR absorption bands, which were proportional to the gas concentration. No significant difference was observed between dry and humid conditions for both IR spectra and resistance data.

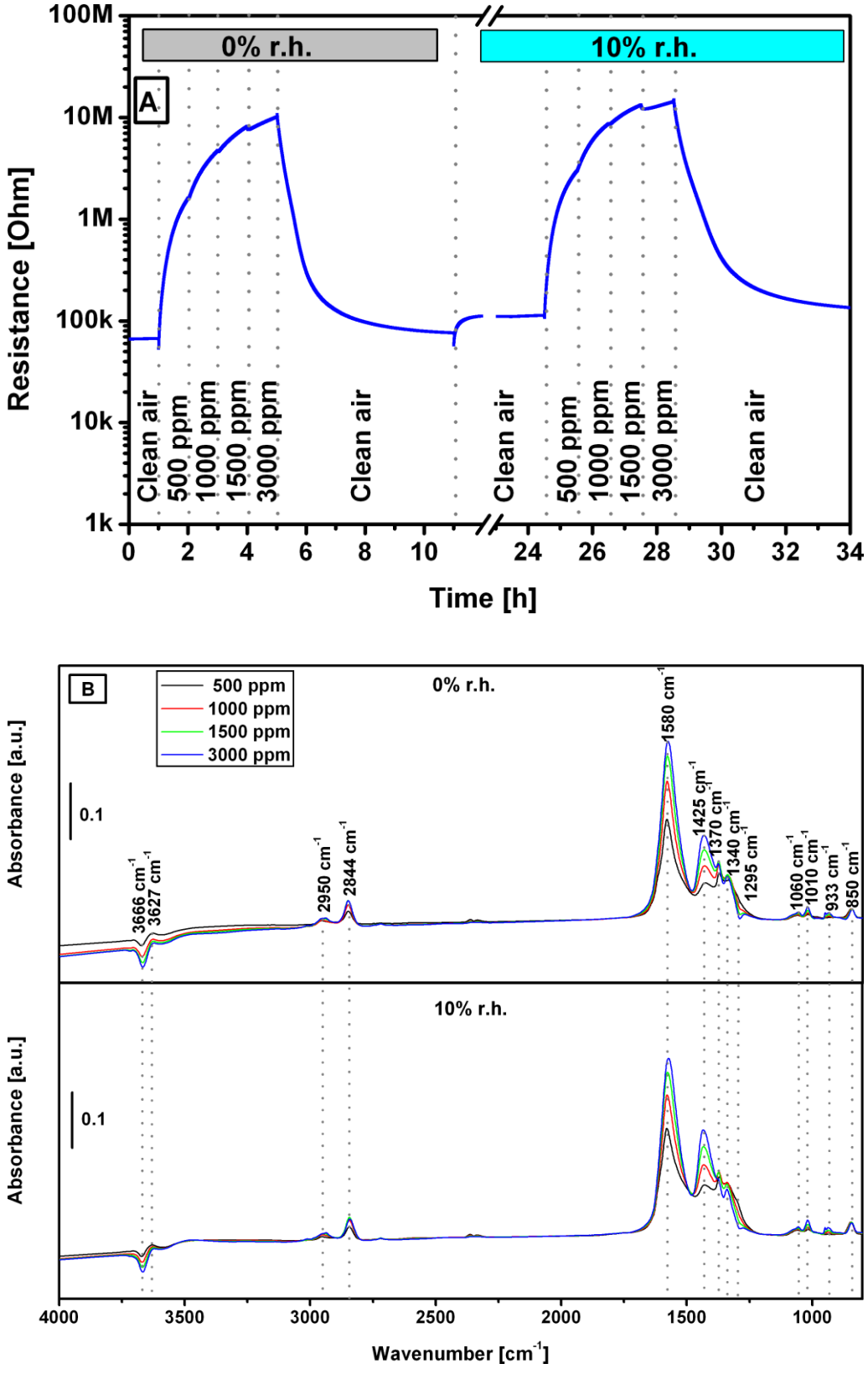

Figure 36. The resistance measurements (A) and DRIFT spectra (B) of LFO sensors exposed to various concentrations of C_2H_4 (500, 1000, 1500 and 3000 ppm) at 150°C in dry and 10% r.h.@25°C conditions. The spectra were referenced to the spectrum that was measured in clean air conditions.

The bands at 2950, 2844, 1580, 1425, and 1370 cm^{-1}, which are present under ethylene exposure did not exist under CO_2 exposure. This adds a new complexity to the spectral profile in the fingerprint region. One possibility to interpret the spectra and distinguish between overlapped vibrations is to perform an isotopic exchange experiment. Figure 37 illustrates the DRIFT spectra of LFO exposed to 500 ppm C_2H_4 and C_2D_4 in dry conditions at 150°C.

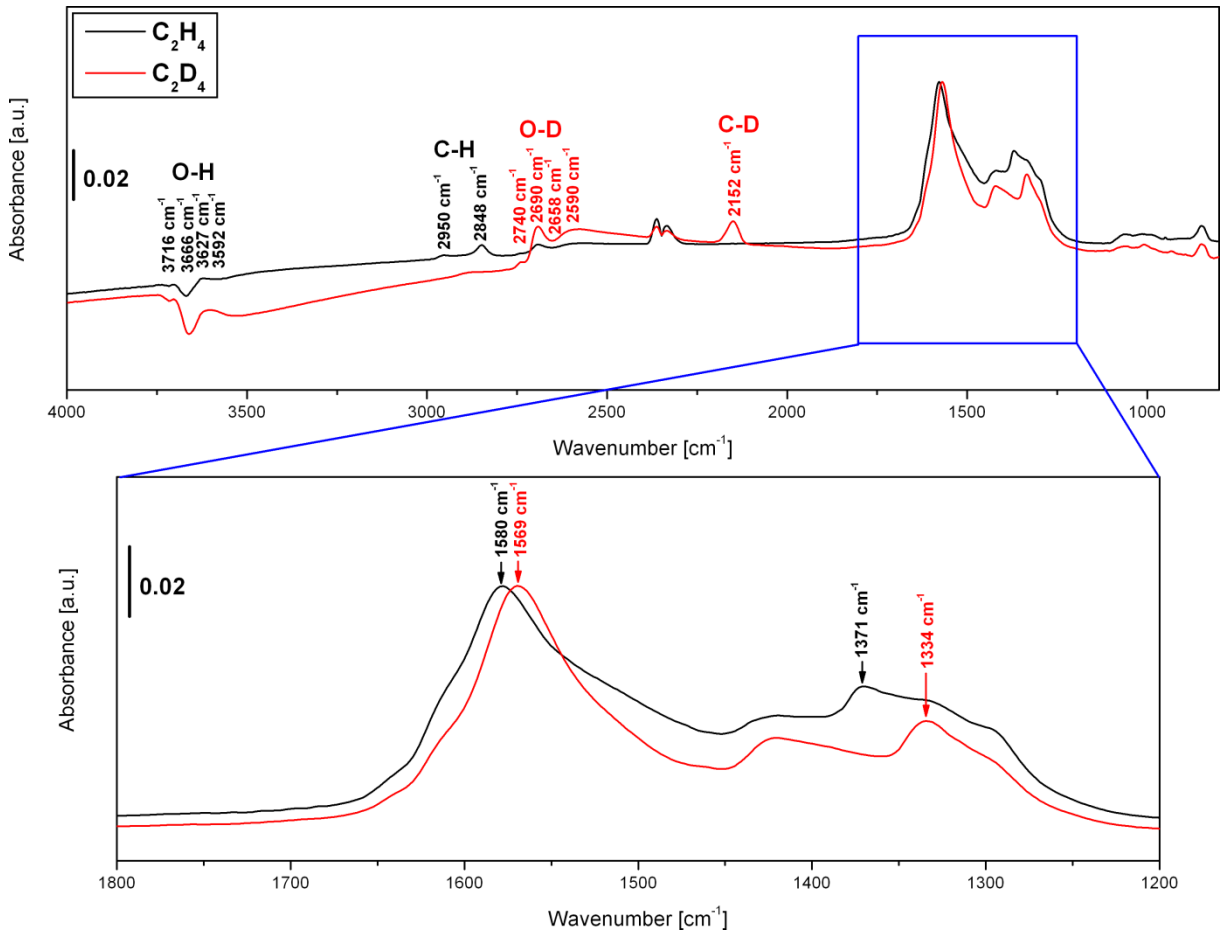

Figure 37. DRIFT spectra of LFO sensors exposed to 500 ppm C_2H_4 (black line) and C_2D_4 (red line) in dry condition at 150°C. The spectra were referenced to a spectrum that was recorded in dry condition.

The isotopic shifts of the hydroxyl group vibrational frequencies are very close to the expected, calculated factor, 0.728. The bands at 3716, 3666, 3627, and 3592 cm^{-1} in the OH region were shifted to the OD region with the bands at 2740, 2690, 2658, and

2590 cm^{-1}, respectively. The first two bands (3716 and 3666 cm^{-1}) and the band at 3592 cm^{-1} are attributed to terminal and rooted hydroxyl groups, respectively [71], whereas the peak at 3627 cm^{-1} is already assigned to the OH vibration of the bicarbonate. The two C-H bands at 2950 and 2848 cm^{-1} were shifted to the C-D region; the corresponding C-D bands were centered at a broad band at around 2152 cm^{-1}. Moreover, small shifts can also be seen in the bands at 1580 and 1371 cm^{-1} with around 10 and 40 cm^{-1}, respectively. These two peaks are attributed to OCO asymmetric (1580 cm^{-1}) and symmetric (1371 cm^{-1}) stretching vibrations [69]. The symmetric vibration showed higher shift in the isotopic experiment than the asymmetric one because of a considerable contribution from δCH to this vibration [69]. As a result, the bands at 2950 and 2848 cm^{-1} together with 1580, and 1373 cm^{-1} are assigned to bidentate formate species. The band at 1425 cm^{-1} can be attributed to the δCH vibration of hydrocarbon fragments [72] and probably indicates adsorbed but unreacted/not completely reacted hydrocarbon, in this case ethylene. The highest intensity band at 1580 cm^{-1} is considered to have two components, one refers to formates and another to carbonates [73] because of the presence of the accompanying bands at 1340 and 1295 cm^{-1}.

Increasing the temperature to 250°C causes a loss of sensor response to ethylene. Figure 38 shows the IR spectra and the resistance measurement results for different concentrations of C_2H_4 (500, 1000, 1500, and 3000 ppm) at 250°C in dry and 10% r.h.@25°C.

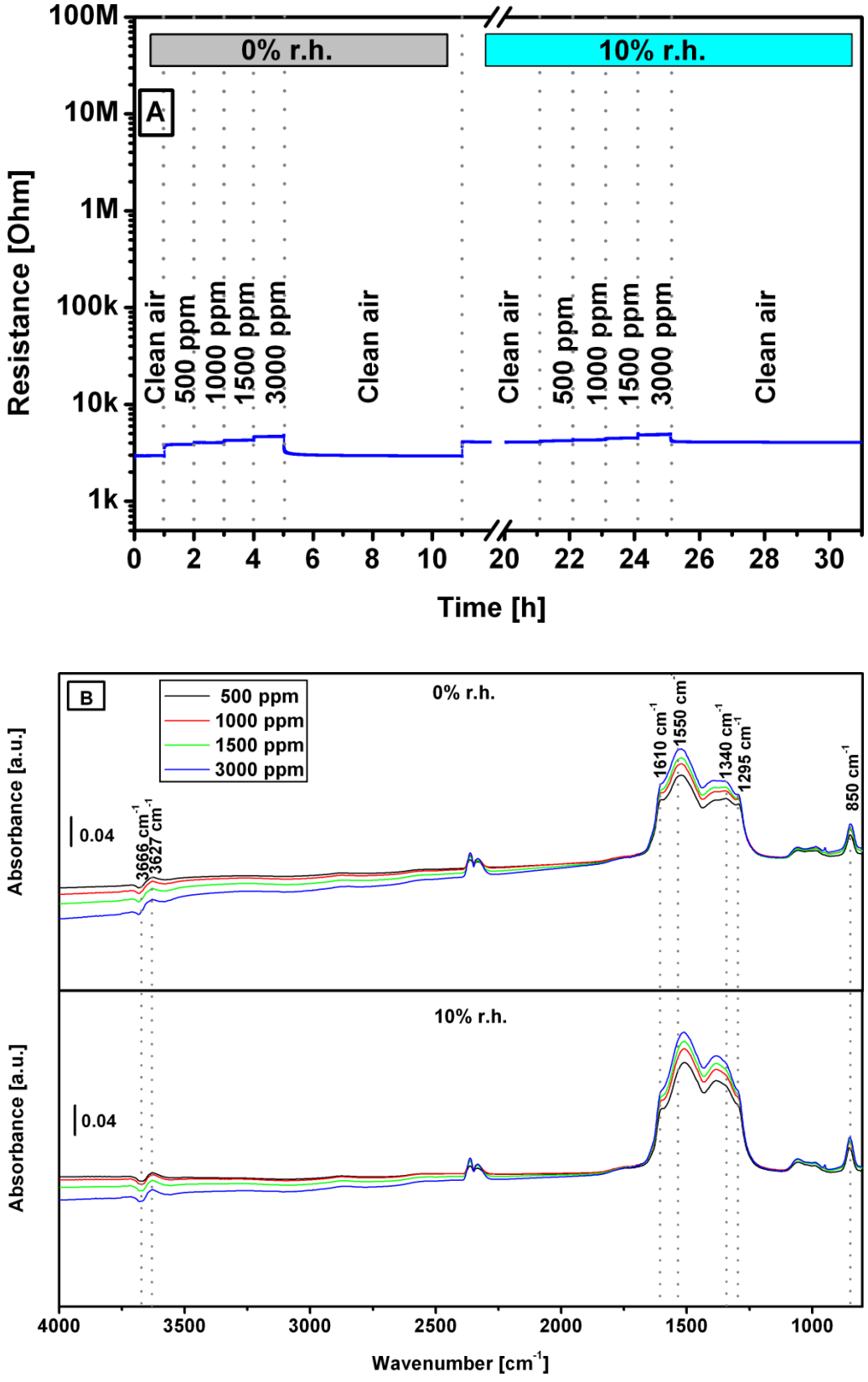

Figure 38. The resistance measurements (A) and DRIFT spectra (B) of LFO sensor exposed to various concentrations of C_2H_4 (500, 1000, 1500 and 3000 ppm) at 250°C in dry and 10% r.h.@25°C. The spectra were referenced to spectrum that was measured in clean air conditions.

The analysis of the IR data reveals the disappearance of the formates, whereas the carbonates and bicarbonates are still present. In fact, at this temperature, the DRIFT spectra corresponding to C_2H_4 and CO_2 are qualitatively identical. The fact that the generation of CO_2 is increasing with increasing ethylene concentrations suggests that the carbonates and bicarbonates are the result of the reaction between the CO_2 formed by the oxidation of ethylene/reduction of LFO and the surface of LFO and by oxidation on the electrodes of the substrate. However, even if the sensitive material is reduced, the electrical effect is quite low – see Figure 38A. The presence of humidity leads to a further decrease in the electrical effect, which can be correlated to bidentate carbonates (II) becoming the dominant species in DRIFT spectra – this is similar to what I observed under CO_2 exposure in the same conditions (see Figure 33). Possibly, the accumulation of the bidentate carbonates (II) passivates the surface by that hindering alternative reactions that may have an electrical effect.

To know what is exactly happening at the surface of the sensitive material during the first 15 minutes of ethylene exposure and the first 15 minutes after the gas exposure was stopped, I recorded the IR spectra of the sensor directly after the onset and offset of gas flow, as shown in Figures 39 and 40, respectively. In Figure 39, all spectra were referenced to the spectrum that was taken in clean air. However, in Figure 40, all spectra were referenced to the spectrum that was taken at the end of the test gas exposure. This is an effective way to track the adsorption/desorption processes of the species on/from the surface in order to follow the surface species formation which are responsible about the resistance change.

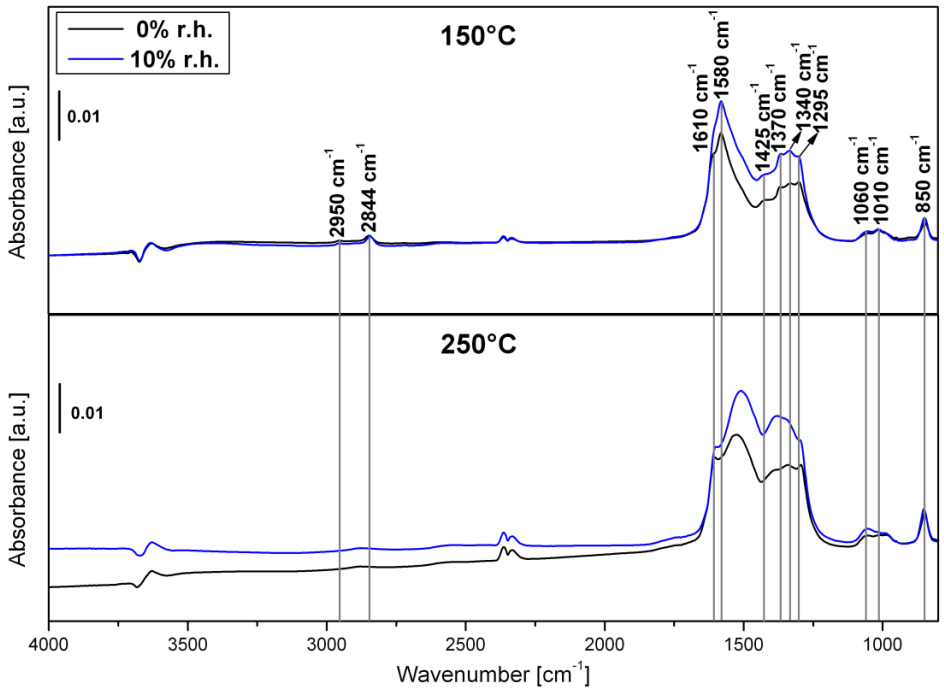

Figure 39. DRIFT spectra of the LFO sensor recorded after 15 mins of the C_2H_4 exposure at 150°C and 250°C in dry and 10% r.h.@25°C conditions. All spectra were referenced to the spectrum that was measured in clean air.

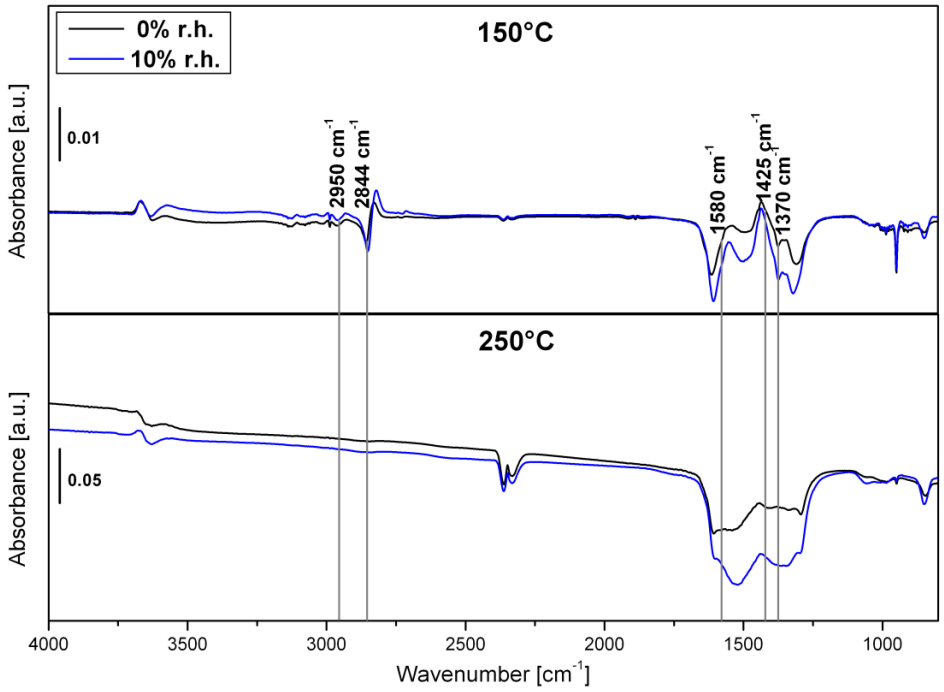

Figure 40. DRIFT spectra of the LFO sensor recorded after 15 mins of the C_2H_4 exposure stopped at 150°C and 250°C in dry and 10% r.h.@25°C conditions. All spectra were referenced to the spectrum that was measured at the end of C_2H_4 exposure.

At the beginning of ethylene exposure at 150°C, the formation of the surface species (carbon related compounds and formates) is observed clearly – see the upper panel of Figure 39. At this temperature, the formates and the hydrocarbon fragments are the dominant surface species in both conditions dry and humid. When the gas stopped at 150°C (the upper panel of Figure 40), a significant decrease in all species types, except hydrocarbon fragments, takes place in dry and humid conditions, suggesting that the hydrocarbon fragments need more time than others to be removed. At 250°C, the kinetic of adsorption and desorption mechanisms are quite identical to the ones under CO_2 exposure (see Figure 34). The DRIFT results revealed that the presence and disappearance of formates is correlated with the electrical change of the sensor under ethylene exposure.

5.1.2.3 Surface reaction of C_2H_2

As is well known, acetylene is much more stable than ethylene. In acetylene, the two carbon atoms are connected by triple bond (one sigma (σ) bond and two pi (π) bonds). In ethylene, however, only two bonds are attaching the two carbon atoms, namely sigma and pi bonds.

A similar way of surface chemistry investigations will be also used in acetylene case. The IR spectrum of acetylene in gaseous phase is shown in Figure 41.

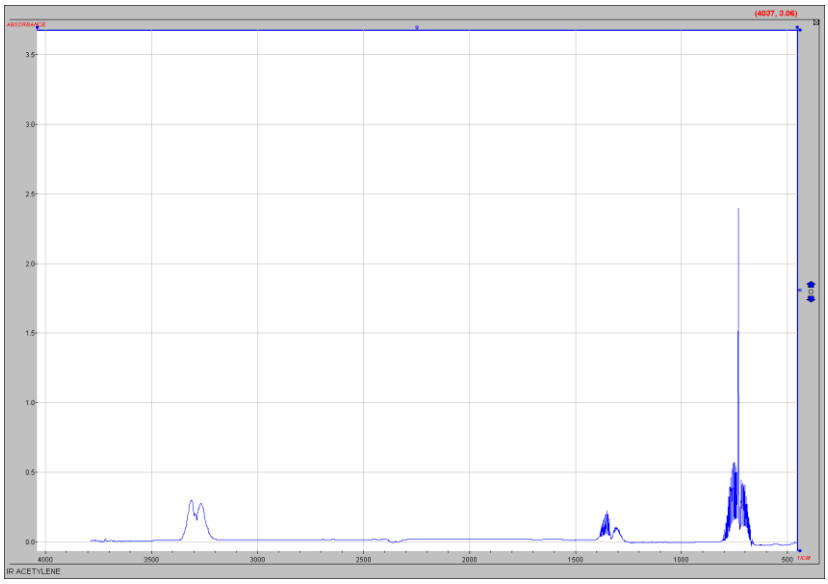

Figure 41. IR spectrum of ethylene in gaseous phase (50 mmHg diluted to a total pressure of 600 mmHg with N_2). The figure is adapted from [45].

Among all IR bands, the two peaks centered at 3300 cm^{-1} are a signature of the presence of acetylene in the porous of the sensitive material without adsorbing. The remaining IR peaks of acetylene spectrum are most probably overlapped with other vibrations (carbonate and metal - oxide vibrations).

The reaction of acetylene on the LFO sensor is of special interest since the sensor shows a good response to acetylene at both temperatures (150°C and 250°C), which is in contrast to the case of ethylene. To follow such a reaction, I performed two sets of experiments similar to the ones that I did for ethylene, where the sensor exposed to different concentration of C_2H_2 in dry and 10% r.h.@25°C for an operation temperature of 150°C and 250°C. The results are shown in Figures 42 and 43, respectively.

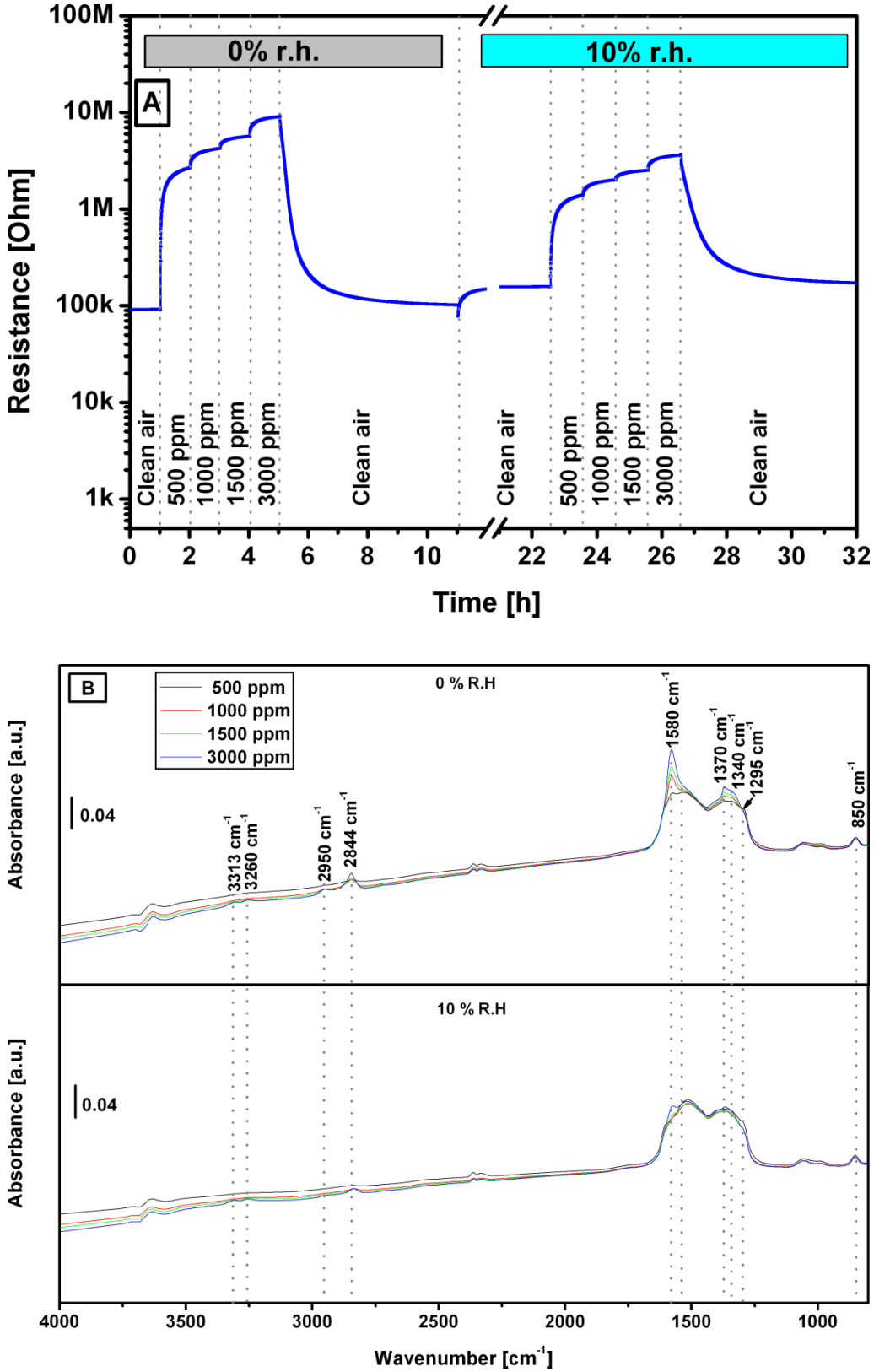

Figure 42. The resistance measurements (A) and DRIFT spectra (B) of LFO sensor exposed to various concentrations of C_2H_2 (500, 1000, 1500, and 3000 ppm) at 150°C in dry and 10% r.h.@25°C. The spectra were referenced to spectrum that was measured in clean air.

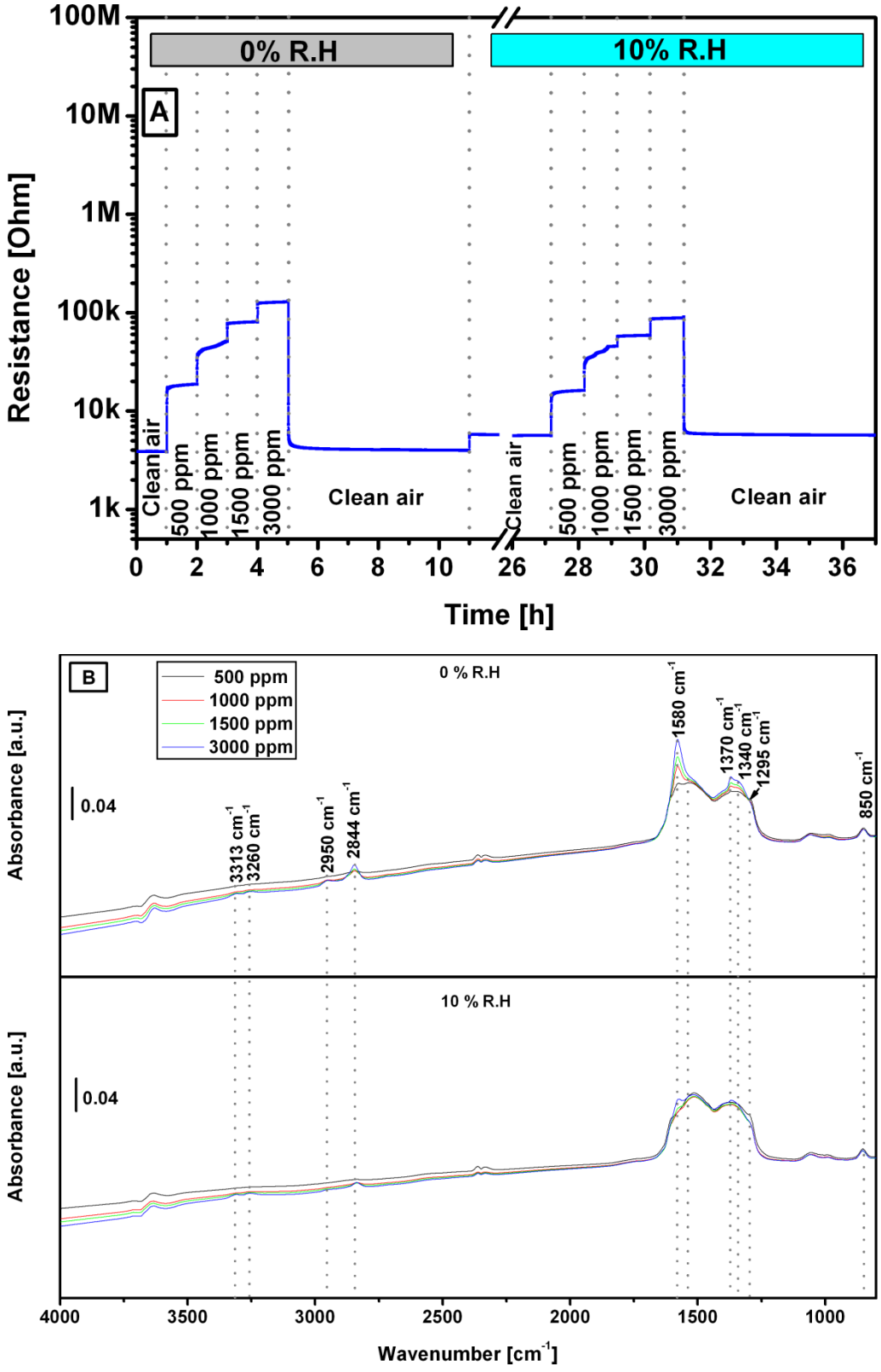

Figure 43. The resistance measurements (A) and DRIFT spectra (B) of LFO sensor exposed to various concentrations of C_2H_4 (500, 1000, 1500 and 3000 ppm) at 250°C in dry and 10% r.h.@25°C. The spectra were referenced to spectrum that was measured in clean air.

As can be clearly seen, the reaction of acetylene at the LFO surface leads to the formation of formate, carbonate, and bicarbonate species at both temperatures. The hydrocarbon fragment at 1425 cm^{-1} was only observed at 150°C, which is quite reasonable because increasing the temperature usually accelerates the chemical reactions. The two new bands at 3313 and 3260 cm^{-1} are associated to acetylene in the gaseous phase [70]. The formate was the main adsorbate at 150°C and, in dry condition, I recorded a very large sensor signal, quite similar to the one corresponding to ethylene exposure at the same temperature. At 250°C one records a significant reduction of the sensor signal and a significant decrease of the magnitude of the formate bands. The contribution of the carbonates increases in line with the reduction of the material indicated by the gaseous CO_2 bands.

The sensor response was reduced at both temperatures by the presence of humidity. A possible explanation is provided by DRIFT: in Figure 42, at 150°C, one can very clearly see that the intensity of the gas phase acetylene bands is much higher in humid conditions than in dry ones. The same tendency is also observed at 250°C; see Figure 43. This may indicate that the dissociation of acetylene is inhibited by the additional coverage with OH groups – the result is the decrease of the concentration of formates.

To gain better insights about the surface reaction mechanism during the first 15 minutes of acetylene exposure, the DRIFT spectra of the sensor were recorded at the first contact between the gas and the sensor and once it was stopped, as shown in Figure 44 and 45, respectively. In Figure 44, all spectra were referenced to the spectrum that was taken in clean air. However, in Figure 45, all spectra were referenced to the spectrum that was taken at the end of the acetylene exposure.

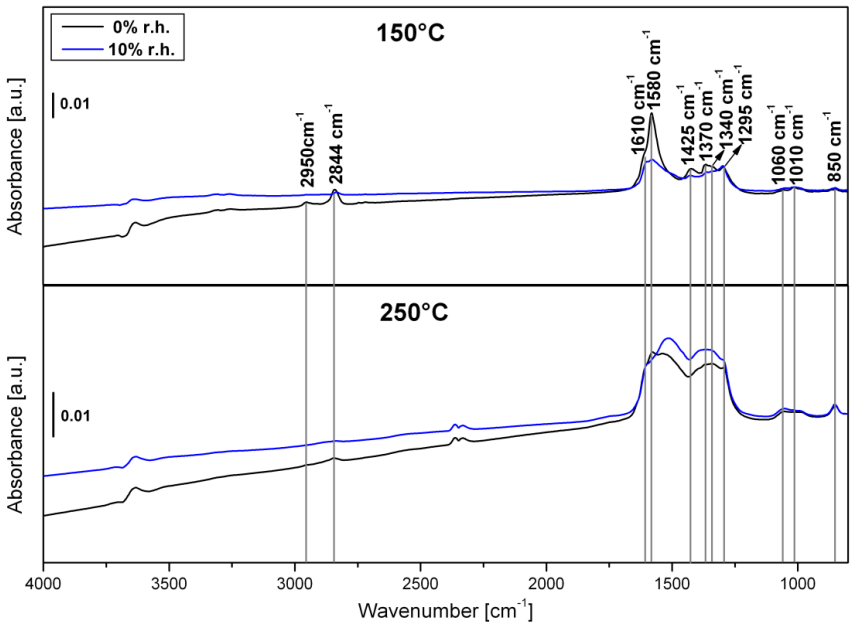

Figure 44. DRIFT spectra of the LFO sensor recorded after 15 mins of the C_2H_2 exposure at 150°C and 250°C in dry and 10% r.h.@25°C conditions. All spectra were referenced to the spectrum that was measured in clean air.

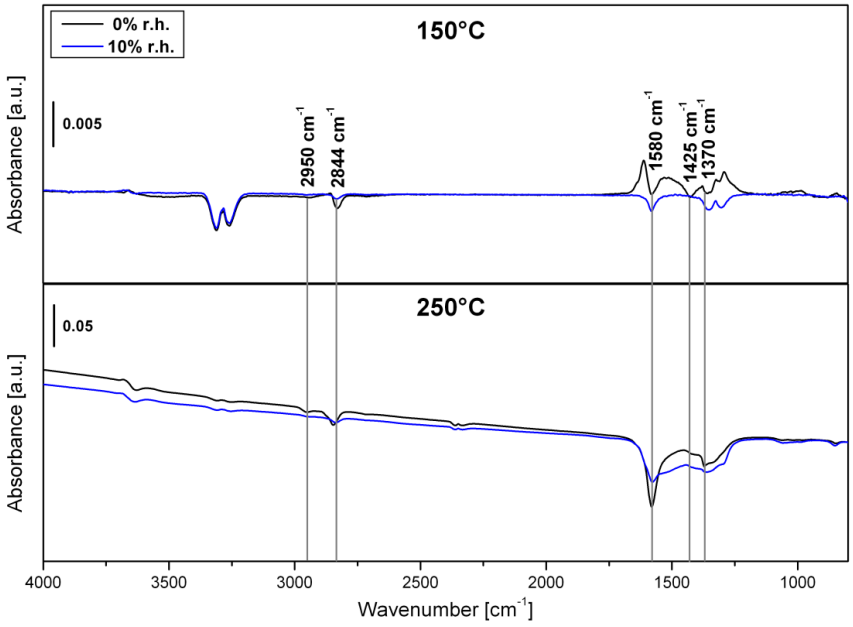

Figure 45. DRIFT spectra of the LFO sensor recorded after 15 mins of the C_2H_4 exposure stopped at 150°C and 250°C in dry and 10% r.h.@25°C conditions. All spectra were referenced to the spectrum that was measured at the end of C_2H_4 exposure.

The formates formation on LFO surface and their desorption processes at both temperatures in dry and 10% r.h.@25°C conditions are taking place in all four

conditions with a kinetic that is correlating the one recorded the electrical measurements under acetylene exposure and once it is stopped. The DRIFT spectrum of LFO, which was taken after 15 minutes from the end of gas exposure in dry condition at 150°C (see the black line in the upper panel of Figure 45), shows a clear decrease in formate species while the carbonates still can be observed at the surface. Consequently, without doubt, the formates are the surface species that are responsible for the electrical effects. From the same spectrum, the peak centered at 1580 cm^{-1}, which is associated to formate vibrations, can be distinguished from the one centered at 1610 cm^{-1}, which is related to the bidentate carbonate. Normally, it is difficult to distinguish between such peaks because they are close to each other and overlapped. Moreover, the combustion of acetylene at 150°C is much lower than at 250°C - this is indicated by the absence of CO_2 formation and the high intensity of IR bands of acetylene in gaseous phase at 150°C.

5.2. The role of platinum in the gas sensing mechanism

The above results have all focused on different aspects related to the sensitive material of SMOX sensors and how selectivity in gas sensing can be achieved. However, the type of electrode used can itself influence gas sensing performance, as explained in the Introduction (Section 2.2). To investigate this issue, I next used two LFO sensors that were deposited on two different electrode materials, namely platinum (LFO @ Pt – electrode) and gold (LFO @ Au – electrode). All other experiment conditions were the same. The resistance measurements and the operando DRIFT spectroscopy characterizations of the two sensors will be investigated in the following sections.

5.2.1 DC resistance measurements

The DC resistance results of the two sensors to various concentrations of ethylene and acetylene (500, 1000, 1500 and 3000 ppm) at 0%, 25% and 50% r.h.@25°C, and also at four different sensor operating temperatures (150, 200, 250 and 300°C) as shown in Figure 46 and 47.

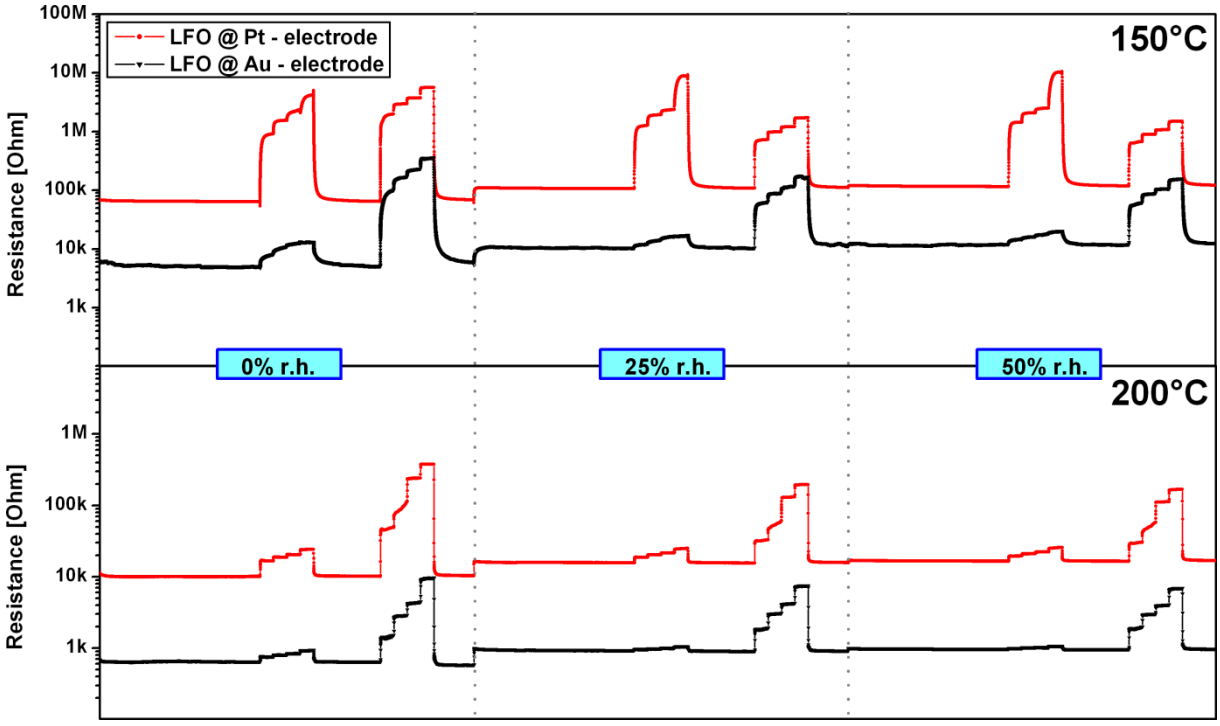

Figure 46. DC resistance measurements of LFO @ Pt – electrode and LFO @ Au – electrode sensors at 0%, 25% and 50% r.h.@25°C for 500, 1000, 1500 and 3000 ppm of C_2H_4 and C_2H_2 at 150 and 200°C.

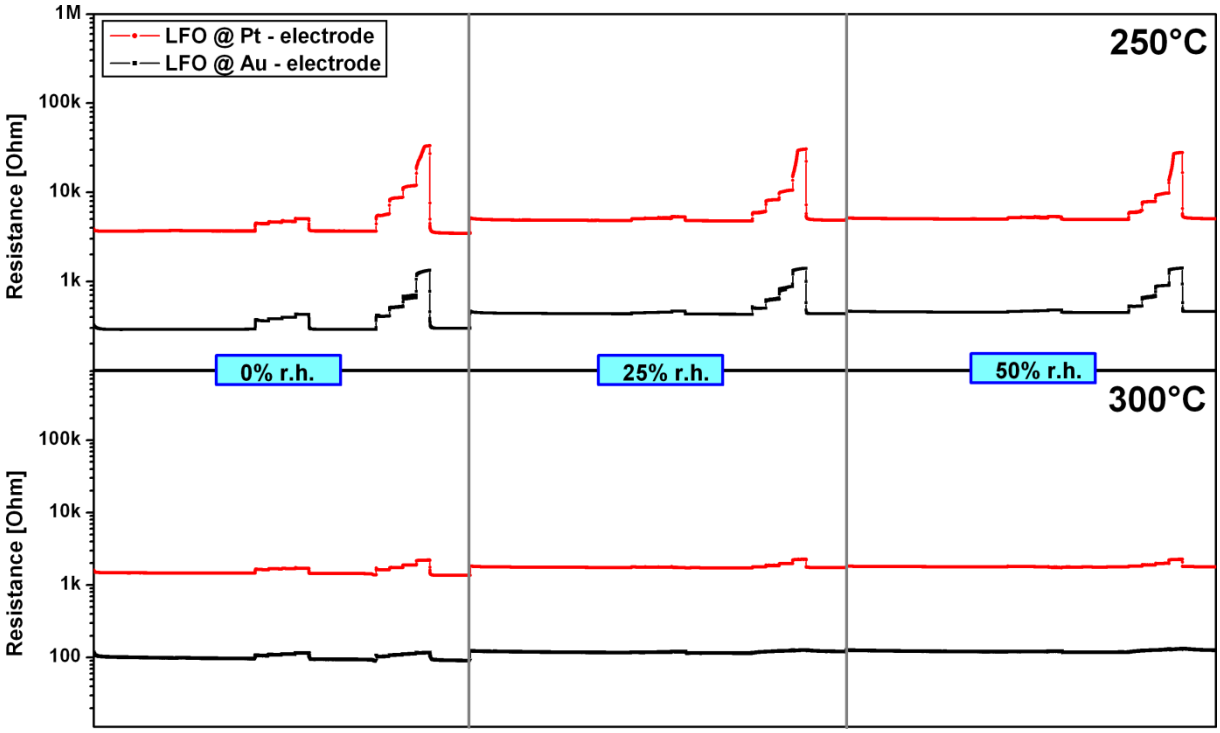

Figure 47. DC resistance measurements of LFO @ Pt – electrode and LFO @ Au – electrode sensors at 0%, 25% and 50% r.h.@25°C for 500, 1000, 1500 and 3000 ppm of C_2H_4 and C_2H_2 at 250 and 300°C.

It is quite striking to see that the change of the electrode material has a much stronger impact on the ethylene sensing than acetylene. In the case of ethylene, the sensor signal of the LFO @ Au – electrode sensor decreases more than 30 times compared to the LFO @ Pt – electrode sensor at 150°C. In the case of acetylene, however, both sensors indicate a similar sensing behaviour over all different operating temperatures. From a practical perspective, these findings suggest that remarkable selectivity for only acetylene can be achieved, if necessary, by careful selection of electrode material.

These findings also suggest, from a more theoretical perspective, that the reactivity of acetylene and ethylene are very different mechanistically and that the activation of the reaction with ethylene in particular takes place on the Pt electrodes. To verify this, I will perform further DRIFT investigations on both different sensors (LFO @ Pt – electrode and LFO @ Au – electrode). This allows me to follow the surface change when the electrode material is changed and therefore its role in the reaction mechanism.

5.2.2 DRIFT investigations

To have a good comparison between the two sensors (LFO @ Pt – electrode and LFO @ Au – electrode), I plotted the DRIFT spectra and the sensor signals of both sensors at two different temperatures (150°C and 250°C) in dry condition for ethylene and acetylene as in the following sections.

5.2.2.1 C_2H_4

Figure 48 shows the DRIFT spectra and the sensor signals of both sensors in dry condition during ethylene exposure at 150°C. The reaction of ethylene on the LFO

sensor is of special interest at this temperature since the sensor shows a good response to ethylene when the sensitive material was deposited on alumina substrates, provided with Pt electrodes, which is in contrast to the one provided with Au electrodes .

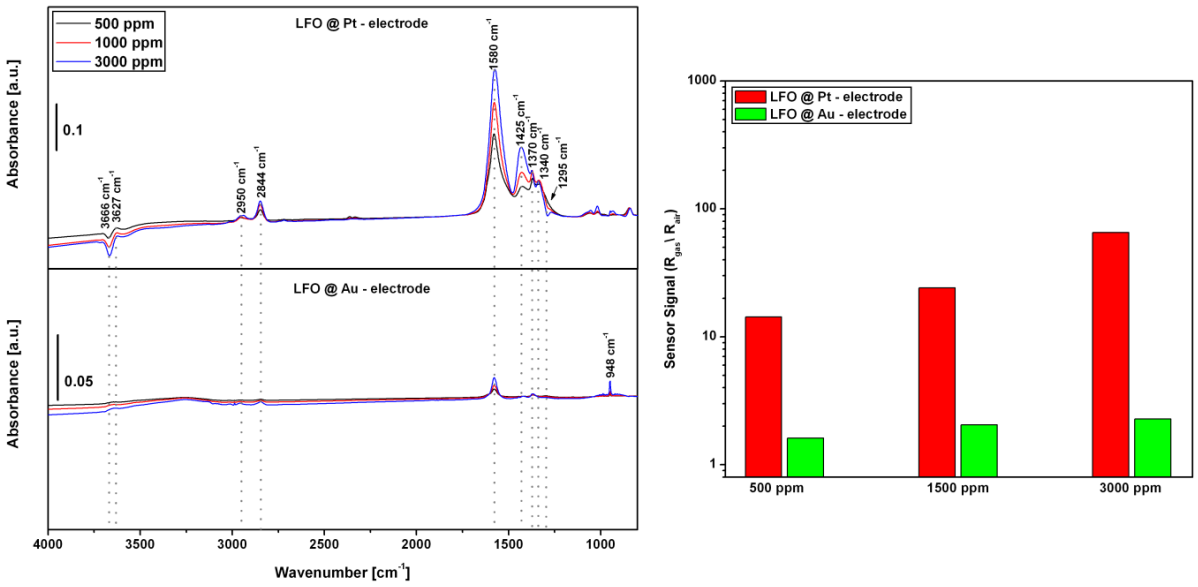

Figure 48. DRIFT spectra and the sensor signals of LFO @ Pt – electrode and LFO @ Au – electrode sensors exposed to various concentrations of C_2H_4 (500, 1000 and 3000 ppm) at 150°C in dry conditions. The spectra were referenced to the spectrum that was measured in clean air condition.

The DRIFT spectra revealed that the presence of platinum is required for ethylene reactivity - this is indicated by the absence of most IR bands (no formation of surface species) when the substrate with Au electrode is used. Even though the magnification in the figure is doubled, only few weak bands of LFO @ Au – electrode sensor can be observed (see the lower panel of Figure 48). This group of bands, except the one centered at 948 is cm^{-1}), related to formate species that are also correlated with the sensor signals at different gas concentrations. The band at around 948 cm^{-1} is associated to ethylene in the gaseous phase.

Increasing the operating temperature to 250°C, no significant difference of the sensor response is recorded between the two sensors under the gas exposure.

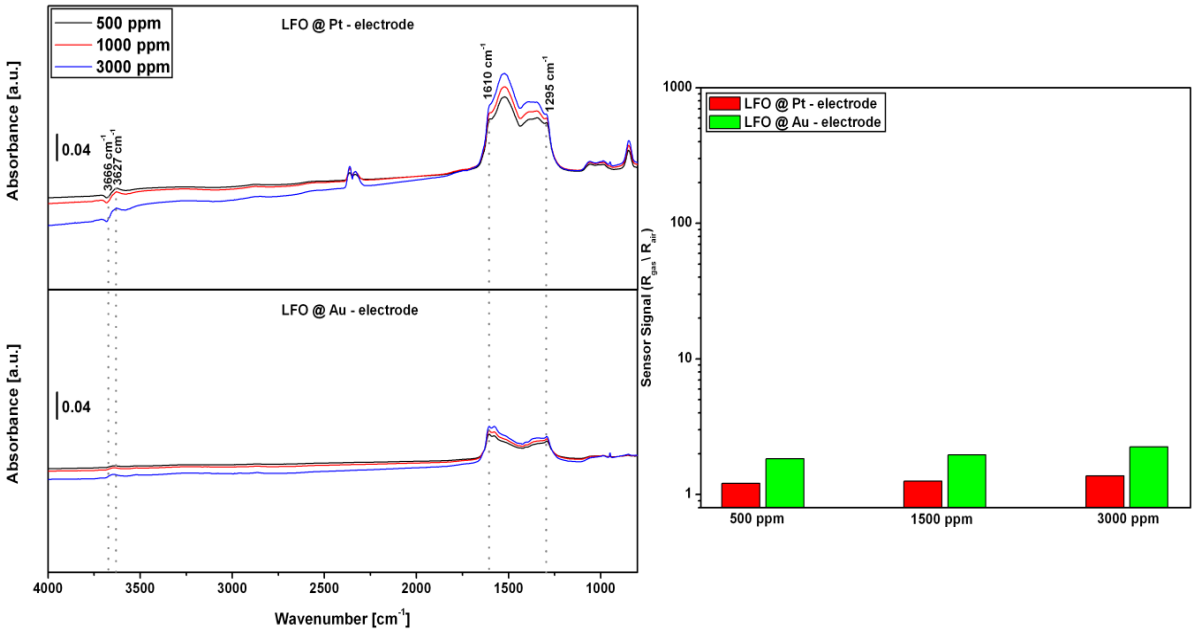

Figure 49. DRIFT spectra and the sensor signals of LFO @ Pt – electrode and LFO @ Au – electrode sensors exposed to various concentrations of C_2H_4 (500, 1000 and 3000 ppm) at 250°C in dry conditions. The spectra were referenced to the spectrum that was measured in clean air condition.

The DRIFT spectra provided that the carbonates formation on LFO @ Au – electrode sensor is much less than its counterpart. This gives an indication that the amount of CO_2 formation is dependent on the electrode material than the sensitive material. It seems that the generation of CO_2 is more likely in the case of Pt electrode than the Au one.

5.2.2.2 C_2H_2

Figures 50 and 51 show the DRIFT spectra and the sensor signals of both sensors in dry condition during acetylene exposure at 150°C and 250°C, respectively.

The gas sensing performance of LFO based on Pt and Au electrodes to acetylene at the two operating temperatures is quite similar (see the right sides of Figure 50 and 51). This is also reflected by IR spectra where both sensors indicate almost identical IR spectra at both temperatures (see the left sides of the same figures).

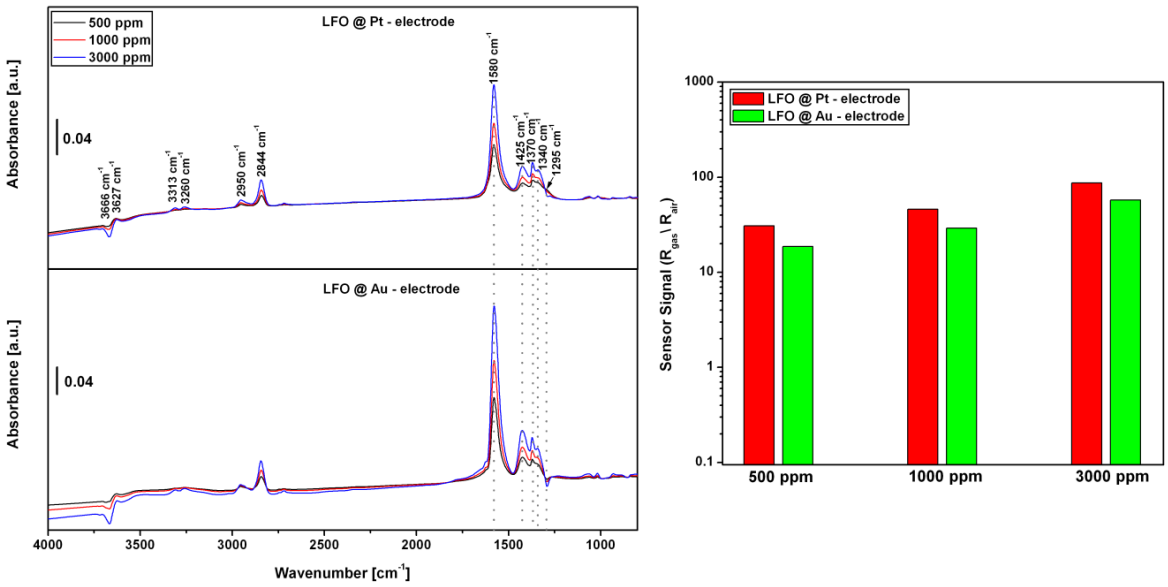

Figure 50. DRIFT spectra and the sensor signals of LFO @ Pt – electrode and LFO @ Au – electrode sensors exposed to various concentrations of C_2H_2 (500, 1000 and 3000 ppm) at 150°C in dry conditions. The spectra were referenced to the spectrum that was measured in clean air condition.

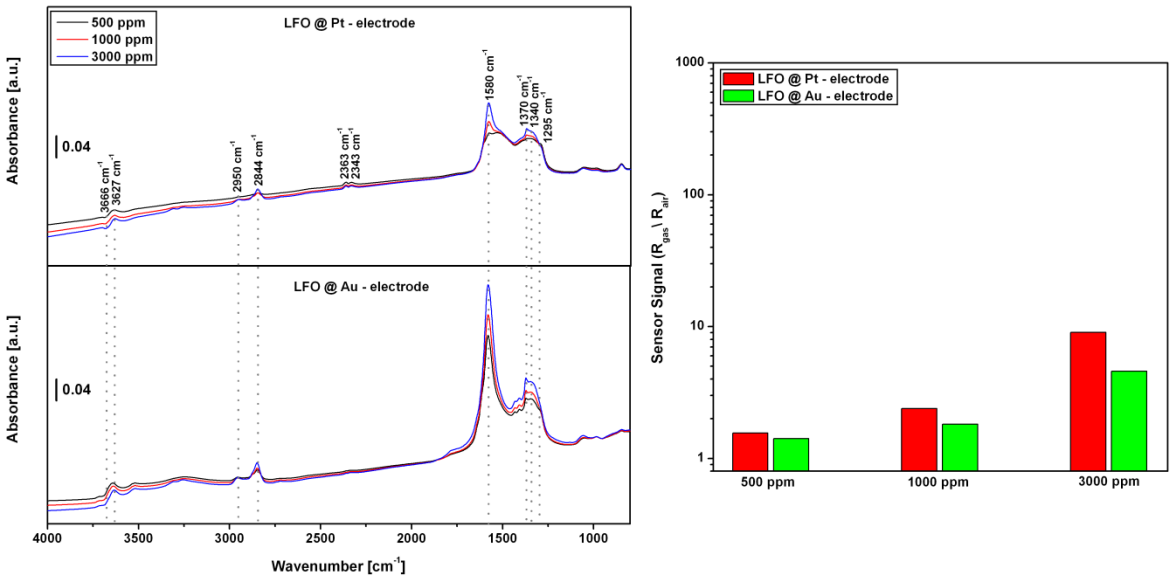

Figure 51. DRIFT spectra and the sensor signals of LFO @ Pt – electrode and LFO @ Au – electrode sensors exposed to various concentrations of C_2H_2 (500, 1000 and 3000 ppm) at 250°C in dry conditions. The spectra were referenced to the spectrum that was measured in clean air condition.

Based on the above results, I can see that the ethylene reaction is more influenced by the change of the electrode material than acetylene. However, the source of the CO_2 formation still is unclear even though such information is so essential to understand the gas sensing mechanism of LFO. In the following section, I will use the catalytic conversion measurement to investigate the origin of CO_2 formation. The net result of the whole investigation is that I end up with a very deep mechanistic insight on a novel discovery of gas sensing selectivity by SMOX sensors.

5.2.3 The origin of CO_2

To propose an accurate reaction mechanism of LFO, it is quite necessary to know the origin of CO_2 formation. This is especially important because on most oxides, which show chemoresistive effects, the latter are related to the reduction/oxidation of the surface. If the CO_2 is produced by the reduction of the surface under hydrocarbons exposure, it would be surprising that such a surface chemistry would not produce electrical effects/sensor signals.

Many studies have reported that the decomposition of ethylene and acetylene on different materials can happen over a wide range of temperatures [74–78]. At low temperatures, different types of hydrocarbon fragments can be produced due to incomplete combustion process of the gases. The type of these species depends mainly on the temperature and the surface activity. However, at high temperatures, ethylene and acetylene are fully oxidized and end up with CO_2 and H_2O as final products of the reactions, as shown in Eqs. (10-11).

$$C_2H_4 + 3O_2 \rightarrow 2CO_2 + 2H_2O \qquad (10)$$

$$C_2H_2 + {}^{5}/_{2}\, O_2 \rightarrow 2CO_2 + H_2O \qquad (11)$$

Besides the sensitive material, other sensor parts (electrodes), made of platinum or gold, can have a considerable contribution to the combustion of some gases such as ethylene [62,79]. For example, C_xH_x is combusted to CO_2 and water on Pt catalyst [62]. Moreover, acetylene is much more stable than ethylene as I mentioned above. Therefore, the full combustion of ethylene on Pt should take place at lower temperature than acetylene. To examine that, catalytic conversion measurements have been performed on the LFO powder, Pt electrodes and Au electrodes, separately, in order to measure the formation of CO_2 during C_2H_2 and C_2H_4

exposures at different operating temperatures (25, 150, 200, 250 and 300°C) as shown in Figure 52.

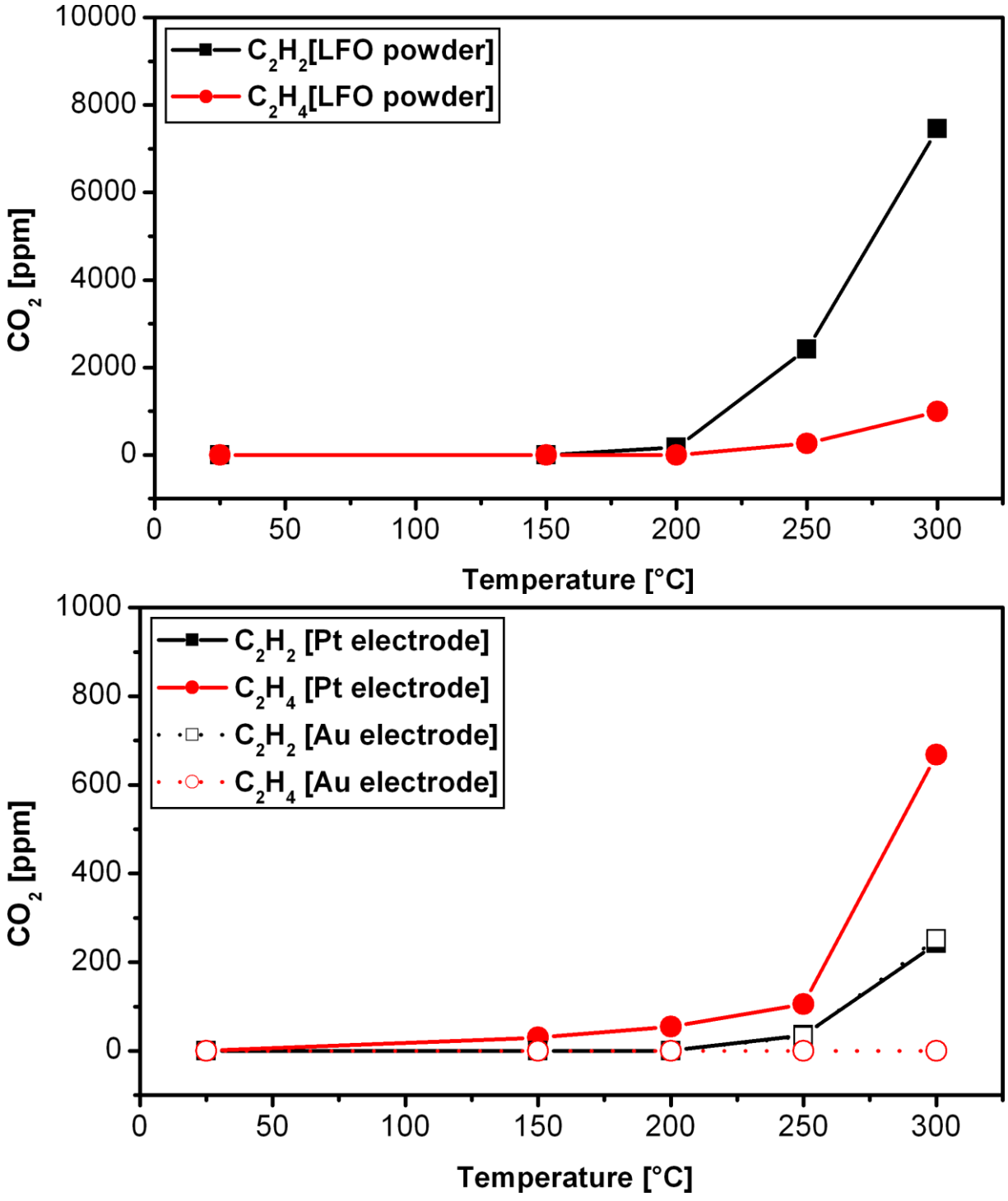

Figure 52. The catalytic conversion of 3000 ppm C_2H_2 and C_2H_4 on LFO powder (upper panel) and the substrate electrodes (lower panel) at different temperatures (25, 150, 200, 250 and 300°C) in dry condition.

It is clear that at 150°C acetylene and ethylene do not fully combust by reacting with the sensitive material and Au electrodes – this is indicated by the lack of CO_2 formation, see Figure 52. Ethylene, however, is combusted by reacting with Pt electrodes. This implies that there is no reaction between the LFO surface oxygen and the gases, so sensitive material's surface is not reduced could only result in the breaking of the gases and the generation of different hydrocarbon fragments.

At 250°C, the experimental results indicate that both gases can reduce the sensitive material because for both I observe the generation of CO_2. In the case of acetylene, the main source of CO_2 is the sensitive material while for ethylene the reaction with the platinum electrodes clearly dominates. For a valid comparison of the quantities generated by the different sensor parts, one has to keep in mind that the amount of sensitive material used in the catalytic conversion measurements is much higher than the actual one on the sensors. I have used 150 mg of LFO powder; the typical weight of the sensing layers is around 20 mg. Moreover, it is very interesting that the reactivity of acetylene on both electrodes (Pt and Au) is identical over all operating temperatures; see the black solid and dotted lines in the lower panel of Figure 52. On the other hand, ethylene is so reactive with Pt and does not show any kind of reactivity to Au electrodes, see the red solid and dotted lines in the same Figure.

These findings are also in line with my DRIFT spectra (see Figure 28) where CO_2 was not detected at 150°C in the case of acetylene and it was observed at both temperatures (150 and 250°C) under ethylene exposure; the origin of the CO_2 generation in the case of ethylene at 150°C is the combustion taking place on the Pt electrodes.

All of the above highlights an intriguing feature of sensing hydrocarbons with LFO, namely that the sensor response is larger, at 150°C, in the absence of surface reduction (as proven by the lack of CO_2 formation). This indicates that the sensing mechanism, contrary to the normally expected reduction/oxidation mechanism, is likely mediated by the reactions responsible for formate formation. To explain this, in the following section, I will examine how formate reactions can determine the electrical properties of LFO sensors.

5.3. Gas sensing mechanism

The most common mechanism, which explains gas sensing behavior in oxide semiconductors, is the equilibrium between surface reduction and oxidation that depends on the composition of the ambient atmosphere [33,34]. For example, in the case of oxidation, which means the healing of surface oxygen vacancies, the concentration of holes increases, as electrons are captured at the surface, leading to a reduction in the resistance of the sensor. By exposing the sensor to a reducing gas, oxygen ions are removed from the surface, and trapped electrons return to the bulk of the solid. The resistance then increases due to a reduction in the number of holes, which are the main free charge carriers in p-type semiconductors. This does not seem to be the main cause of sensor signal for LFO. In this case, I saw electrical effects associated with formates, bicarbonates, and carbonates.

Figure 53 illustrates the schematic representation of the proposed reaction mechanism for CO_2 that ends up with the three different species observed in my IR study. These are formed during the time in which the resistance of the sensor changes; they are bidentate bicarbonate and bidentate and monodentate carbonates.

To form the bidentate carbonate two surface sites are required, namely an oxygen vacancy and a surface oxygen. The healing of the oxygen vacancy involves the capturing of an electron from the bulk, which is equivalent to the injection of a hole in the valence band. The formation of the bond between the carbon atom and the surface oxygen is giving back the electron to the LFO. All in all, this process does not have an electrical effect.

To form a bidentate bicarbonate, the oxygen vacancy needs to be in the vicinity of a hydroxyl group. Also here, an oxygen vacancy is healed, through a process that injects a hole in the valence band. In this case, the transfer of the electron to the LFO does not take place because in the reaction with the hydroxyl group, no net charge is transferred.

For the monodentate carbonate, one only needs a surface oxygen. Here, an electron is given back to the LFO because of the formation of the bond between the carbon atom and the surface oxygen.

Based on the surface reaction kinetics of CO_2 on LFO (see Figure 31), the pronounced and fast formation of the bicarbonate, which was observed in the first minute of the gas exposure, can explain the sharp decrease in the resistance of LFO under CO_2 exposure at 150°C (see Figure 29). Later, when the monodentate started to be formed, an increase in the resistance was measured. The two reactions, which are forming bidentate bicarbonates and monodentate carbonates, reached equilibrium after a few minutes of the gas exposure; afterwards, under CO_2 exposure, no significant resistance change can be observed. When the gas is removed, a mirrored behavior is observed. The same is also happening at 250°C albeit with a lower intensity.

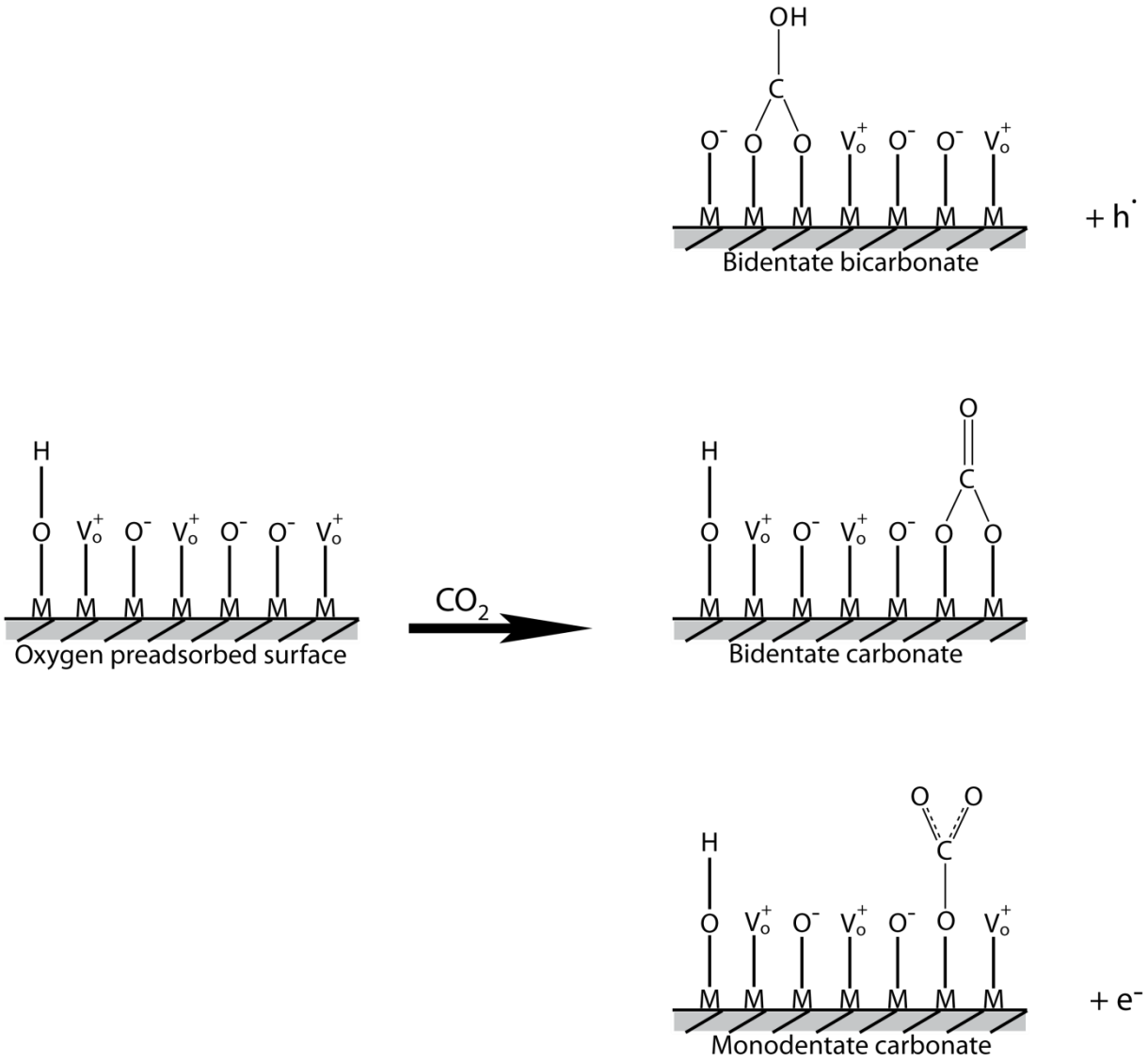

Figure 53. Schematic representation of the surface reaction with CO_2.

The reactions of ethylene and acetylene on LFO surface result in formates in addition to the other carbonate-like compounds. Their – formates – formation at the surface is shown schematically in Figure 53. Because of the formate structure, two surface oxygen sites are required for the reaction. The associated bonds – between the carbon atom and the surface oxygen – are releasing two electrons back to the LFO. In the case of ethylene two formates and a water molecule can be produced during the surface reaction; only two formates can result under acetylene exposure.

Based on my DRIFT observations and resistance measurements, the formation of formate species at the surface of LFO was seen during the exposure of both gases at 150°C and only under acetylene exposure at 250°C; the recorded resistance increase (see Figure 36, 42 and 43) can be explained by the increase in the number of electrons, which is determining a decrease of the holes in the valence band.

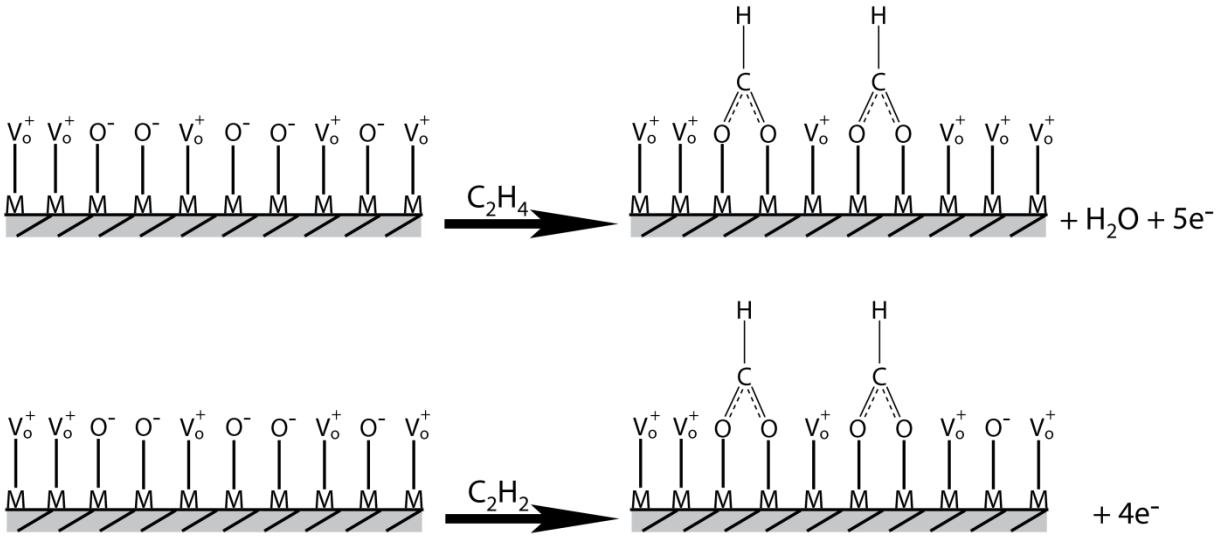

Figure 54. Schematic representation of the surface reaction with ethylene and acetylene.

The results of the catalytic combustion experiments (shown in Figure 52) and the comparison between the sensing performance of the sensors provided with Pt and Au electrodes (see Section 5.2) suggest that in the case of acetylene, at 150°C, the generation of hydrocarbon fragments and the subsequent buildup of formates takes place because of the reaction with the sensitive material; the temperature is not high enough to fully combust the acetylene. In the case of ethylene, at 150°C, the initial reaction – breaking of ethylene – takes place on the Pt electrodes; part of ethylene is fully combusted, the non-combusted hydrocarbon fragments react with the sensitive material to buildup formates. When the temperature increases to 250°C, the very efficient reaction between ethylene and Pt probably results in full combustion.

Consequently, the sensor signals almost fully disappear. In the case of acetylene, the combustion on the Pt electrode is not as effective as for ethylene; because of that the reaction paths resulting in the buildup of formates is still present and so is the gas sensitivity.

5.4 Conclusion

I combined operando DRIFT spectroscopy with DC resistance measurements to investigate the surface chemistry change of LFO simultaneously with its resistance measurements under CO_2, C_2H_4 and C_2H_2 exposure. Several types of carbonates and bidentate bicarbonates were detected during the CO_2 exposure. However, the reactivity of C_2H_4 and C_2H_2 on the LFO surface showed that the formation of formates was much more favorable than other species at 150°C, whereas only acetylene was able to form formates at 250°C. The presence of the formate species at the sensor surface is a crucial factor of detecting a significant resistance change (i.e. a sensor response). The change of electrode materials has a much stronger impact on the ethylene sensing than acetylene. The activation of the reaction with ethylene needs platinum electrodes to break its bonds first by forming hydrocarbon fragments at 150°C or CO_2 at 250°C, leading to two different groups of surface species namely, formates or carbonates respectively. My experimental findings combined with the postulation of the reaction mechanisms indicate that the formation of formates at the sensitive material surface during gas exposure plays a key role in the gas sensing mechanism of LFO sensor. This is a very significant alteration of the well-accepted mechanism for gas detection semiconducting metal oxides, namely the reduction/oxidation of their surface.

6. Summary

In this work, I developed a perovskite structure material (LFO) for a novel use in detecting ethylene and acetylene selectively in the presence of other dissolved gases in transformers. I also explained the underlying gas sensing mechanism of such behaviors.

In the first part, the LFO materials have been prepared by the solid state reaction and the sol gel methods. I was able to obtain the perovskite crystal structure of the resulted powders at calcined temperature from 700°C in the case of solid state method while the perovskite phase could be achieved starting from 500°C in the sol gel method. The materials, which have perovskite structure, are used as a sensitive layer during exposure to various test gases, including C_2H_2, C_2H_4, CH_4, C_2H_6, CO, CO_2 and H_2 at different operating temperatures (150°C, 200°C, 250°C and 300°C). All of my sensors show a significant response to unsaturated hydrocarbons, namely acetylene and ethylene, but not to the other gases. I further improve this high selectivity of my sensors, to only detect acetylene and not ethylene, by controlling the operating temperature. The sensitive materials, which are obtained by sol gel, show much higher sensor signals compared to those synthesized by solid state reaction. The effects of calcination temperatures on the sensing performance are insignificant where all different sensors show similar sensor responses. Moreover, the LFO sensor has shown very stable responses to acetylene during cross sensitivity with ethylene and carbon dioxide. However, the sensor performance is influenced by the relative humidity backgrounds under acetylene exposure while a similar sensing behavior is observed in dry and humid conditions for ethylene.

In the second part, I combined catalytic conversion measurements with simultaneously performed operando DRIFT spectroscopy and DC resistance measurements in order to understand the origin of the gas sensing mechanism. The surface reaction of CO_2, C_2H_4 and C_2H_2 on LFO are investigated systematically to identify the type and role of different adsorbates by applying different evaluation strategies and isotopic experiments. During CO_2 exposure, different types of carbonates and bicarbonate are detected by IR spectra which are responsible for opposing electrical effects that are not resulting in an equilibrium sensor signal. In the case of ethylene and acetylene, the temperature dependent formation of formates, which takes place under such gases exposure, is responsible for the recorded sensor signals. This is a very significant alteration of the well-accepted mechanism for gas detection semiconducting metal oxides, namely the reduction/oxidation of their surface. The results indicate that for both gases at an operation temperature of 150°C the buildup of formates takes place; however, only acetylene is able to form formates at 250°C and this explains the selectivity of LFO sensors. The way in which the formates are changing the LFO electrical resistance is explained. Moreover, it is demonstrated that for ethylene the presence of the Pt electrodes is essential while for acetylene the formates are the natural product of the reaction with the sensitive material. By identifying a novel sensing mechanism, these findings are opening up new avenues for the development of gas sensors.

7. Outlook

My work is highlighting the potential use of perovskites in the field of chemoresistive gas sensors and opening up a new way to improve our understanding of the gas sensing mechanism.

In the level of material, there is plenty of room to tailor different perovskite materials by changing the A and B site with different elements, whether fully or partially. Moreover, preparing perovskite materials by new synthesis route could improve the sensing performance as I saw in my study. At the same time, expanding the target gases beyond the dissolved gases may result in a different type of interesting application.

In the sensing mechanism, the significant alteration of the well-accepted mechanism for gas detection semiconducting metal oxides has been reported for the first time in this work. The validity of such mechanism for other materials can be examined.

8. References

[1] A. Gurlo, N. Barsan and U. Weimar., Metal Oxides - Chemistry and Applications, in: J.L.G. Fierro (Ed.), CRC Press, 2006: pp. 683–738.

[2] X. Liu, S. Cheng, H. Liu, S. Hu, D. Zhang, H. Ning, A survey on gas sensing technology, Sensors. 12 (2012) 9635–9665. doi:10.3390/s120709635.

[3] C. Sun, P.R. Ohodnicki, E.M. Stewart, S. Member, Chemical Sensing Strategies for Real-Time Monitoring of Transformer Oil : A Review, IEEE Sens. J. 17 (2017) 5786–5806.

[4] S.S.M. Ghoneim, I.B.M. Taha, A new approach of DGA interpretation technique for transformer fault diagnosis, Int. J. Electr. Power Energy Syst. 81 (2016) 265–274. doi:10.1016/j.ijepes.2016.02.018.

[5] M. Duval, J.J. Dukarm, Improving the reliability of transformer gas-in-oil diagnosis, IEEE Electr. Insul. Mag. 21 (2005) 21–27. doi:10.1109/MEI.2005.1489986.

[6] J.C. Dennison, J.M. Trout, Transformer oil DGA monitoring technology study 2015, Proc. IEEE Power Eng. Soc. Transm. Distrib. Conf. (2016) 1–5. doi:10.1109/TDC.2016.7519918.

[7] M. Duval, H. Ireq, Dissolved Gas Analysis: It Can Save Your Transformer, IEEE Electr. Insul. Mag. 5 (1989).

[8] Sadeq Yasoob Jasim & Jyoti Shrivastava, Dissolved Gas Analysis of Power Transformers, Int. J. Electr. Electron. Eng. Res. JEEER. 3 (2013) 1–10.

[9] Q. Zhang, Q. Zhou, Z. Lu, Z. Wei, L. Xu, Y. Gui, Recent Advances of SnO_2 - Based Sensors for Detecting Fault Characteristic Gases Extracted From Power Transformer Oil, Front. Chem. 6 (2018) 1–7. doi:10.3389/fchem.2018.00364.

[10] Z. Wei, Q. Zhou, Z. Lu, L. Xu, Y. Gui, C. Tang, Physica E : Low-dimensional Systems and Nanostructures Morphology controllable synthesis of hierarchical WO 3 nanostructures and C_2H_2 sensing properties, Phys. E Low-Dimensional Syst. Nanostructures. 109 (2019) 253–260. doi:10.1016/j.physe.2019.01.006.

[11] M.S. Park, R. Yoo, B. Jang, Y. Park, M.H. Kim, H. Lee, W. Lee, Highly Sensitive Acetylene Sensing Properties of Al- and In-doped ZnO Quantum Dots, 17th Int. Meet. Chem. Sensors - IMCS 2018. 1 (2018) 796–797. doi:10.1039/C5RA10327D.

[12] N. Tamaekong, C. Liewhiran, A. Wisitsoraat, S. Phanichphant, Sensors and Actuators B : Chemical Acetylene sensor based on Pt/ZnO thick films as prepared by flame spray pyrolysis, Sensors Actuators B. Chem. 152 (2011) 155–161. doi:10.1016/j.snb.2010.11.058.

[13] C. Balamurugan, S.J. Song, H.S. Kim, Enhancing gas response characteristics of mixed metal oxide gas sensors, J. Korean Ceram. Soc. 55 (2018) 1–20. doi:10.4191/kcers.2018.55.1.10.

[14] S. Palimar, S.D. Kaushik, V. Siruguri, D. Swain, A.E. Viegas, C. Narayana, N.G. Sundaram, Investigation of Ca substitution on the gas sensing potential of $LaFeO_3$ nanoparticles towards low concentration SO_2 gas, Dalt. Trans. 45 (2016) 13547–13555. doi:10.1039/C6DT01819J.

[15] X. Li, C. Tang, M. Ai, L. Dong, Z. Xu, Controllable synthesis of pure-phase rare-earth orthoferrites hollow spheres with a porous shell and their catalytic performance for the CO + NO reaction, Chem. Mater. 22 (2010) 4879–4889. doi:10.1021/cm101419w.

[16] J. Jalbert, R. Gilbert, Comparison between headspace and vacuum gas extraction techniques for the gas chromatographic determination of dissolved gases from transformer insulating oils, in: Conf. Rec. IEEE Int. Symp. Electr. Insul., Pittsburgh, 1994: pp. 123–129. doi:10.1109/elinsl.1994.401452.

[17] B. Kolb, Static ssss Headspace – Gas Chromatography : Theory and Practice, Second Edi, A JOHN WILEY & SONS, INC., 2006.

[18] A.C. Soria, M.J. García-Sarrió, M.L. Sanz, Volatile sampling by headspace techniques, TrAC - Trends Anal. Chem. 71 (2015) 85–99. doi:10.1016/j.trac.2015.04.015.

[19] S. Bustamante, M. Manana, A. Arroyo, P. Castro, A. Laso, R. Martinez, Dissolved gas analysis equipment for online monitoring of transformer oil: A review, Sensors. 19 (2019) 4–12. doi:10.3390/s19194057.

[20] N. Bakar, A. Abu-Siada, S. Islam, A review of dissolved gas analysis measurement and interpretation techniques, IEEE Electr. Insul. Mag. 30 (2014) 39–49. doi:10.1109/MEI.2014.6804740.

[21] S.X. and Ju Tang, Xiaoxing Zhang, Y. Gui, Experimental Analysis of Modified CNTs-Based Gas Sensor, in: Electrochem. Sensors Technol., 2017: pp. 85–118. doi:http://dx.doi.org/10.5772/intechopen.68590.

[22] T. Hübert, L. Boon-Brett, G. Black, U.B. Banach, Hydrogen sensors - A review, Sensors Actuators, B Chem. 157 (2011) 329–352. doi:10.1016/j.snb.2011.04.070.

[23] F.J. Ibañez, F.P. Zamborini, Chemiresistive sensing with chemically modified metal and alloy nanoparticles, Small. 8 (2012) 174–202. doi:10.1002/smll.201002232.

[24] M. Duval, A review of faults detectable by gas-in-oil analysis in transformers, IEEE Electr. Insul. Mag. 18 (2002) 8–17. doi:10.1109/MEI.2002.1014963.

[25] IEEE, IEEE Guide for the Interpretation of Gases Generated in Oil-Immersed Transformers, IEEE, 2009.

[26] I. 60599, Mineral Oil-Filled Electrical Equipment in Service Guidance on the Interpretation of Dissolved and Free Gases Analysis, IEC: Geneva, Switzerland, 2015.

[27] CIGRE, Advances in DGA Interpretation, CIGRE Paris, Fr. 771 (2019).

[28] W. Pattanadech, N.; Wattakapaiboon, Application of Duval Pentagon

Compared with Other DGA Interpretation Techniques: Case Studies for Actual Transformer Inspections Including Experience from Power Plants in Thailand, in: 5th Int. Conf. Eng. Appl. Sci. Technol., Luang Prabang, Laos, 2019: pp. 1–4.

[29] W. Pattanadech, N.; Sasomponsawatline, K.; Siriworachanyadee, J.; Angsusatra, The conformity of DGA interpretation techniques: Experience from transformer 132 units, in: IEEE 20th Int. Conf. Dielectr. Liq., Roma, Italy, 2019: pp. 1–4.

[30] C. Wagner, The mechanism of the decomposition of nitrous oxide on zinc oxide as catalyst, J. Chem. Phys. 18 (1950) 69–71. doi:10.1063/1.1747459.

[31] T. Seiyama, A. Kato, K. Fujiishi, M. Nagatani, A New Detector for Gaseous Components Using Semiconductive Thin Films, Anal. Chem. 34 (1962) 1502–1503. doi:10.1021/ac60191a001.

[32] N. Taguchi, Gas detecting device, 3695848, 1972. https://patents.google.com/patent/US3695848A/en.

[33] N. Barsan, U. Weimar, Conduction model of metal oxide gas sensors, J. Electroceramics. 7 (2001) 143–167. doi:10.1023/A:1014405811371.

[34] A. Hemeryck, J. Rebholz. A. Oprea, D. Degler, N. Barsan, Gas Sensors Based on Conducting Metal Oxides, in: N. Barsan and K. Schierbaum (Ed.), Gas Sensors Based Conduct. Met. Oxides, Elsevier Inc., 2019: pp. 13–166.

[35] Y. Wei, J. Liu, Z. Zhao, Y. Chen, C. Xu, A. Duan, G. Jiang, H. He, Highly active catalysts of gold nanoparticles supported on three-dimensionally ordered macroporous $LaFeO_3$ for soot oxidation, Angew. Chemie - Int. Ed. 50 (2011) 2326–2329. doi:10.1002/anie.201006014.

[36] Y. Zheng, K. Li, H. Wang, D. Tian, Y. Wang, X. Zhu, Y. Wei, M. Zheng, Y. Luo, Designed oxygen carriers from macroporous $LaFeO_3$ supported CeO_2 for chemical-looping reforming of methane, Appl. Catal. B Environ. 202 (2017) 51–63. doi:10.1016/j.apcatb.2016.08.024.

[37] E. Maguire, B. Gharbage, F.M.B. Marques, J.A. Labrincha, Cathode materials for intermediate temperature SOFCs, Solid State Ionics. 127 (2000) 329–335. doi:10.1016/S0167-2738(99)00286-6.

[38] S. Thirumalairajan, K. Girija, N.Y. Hebalkar, D. Mangalaraj, C. Viswanathan, N. Ponpandian, Shape evolution of perovskite $LaFeO_3$ nanostructures: A systematic investigation of growth mechanism, properties and morphology dependent photocatalytic activities, RSC Adv. 3 (2013) 7549–7561. doi:10.1039/c3ra00006k.

[39] K. Fan, H. Qin, L. Wang, L. Ju, J. Hu, CO_2 gas sensors based on $La_{1-x}Sr_xFeO_3$ nanocrystalline powders, Sensors Actuators B Chem. 177 (2013) 265–269. doi:10.1016/j.snb.2012.11.004.

[40] X. Wang, H. Qin, L. Sun, J. Hu, CO_2 sensing properties and mechanism of nanocrystalline $LaFeO_3$ sensor, Sensors Actuators B. Chem. 188 (2013) 965–971. doi:10.1016/j.snb.2013.07.100.

[41] H. Obayashi, Y. Sakurai, T. Gejo, Perovskite-type oxides as ethanol sensors, J. Solid State Chem. 17 (1976) 299–303. doi:10.1016/0022-4596(76)90135-3.

[42] M.A. Peña, J.L.G. Fierro, Chemical structures and performance of perovskite oxides, Chem. Rev. 101 (2001) 1981–2017. doi:10.1021/cr980129f.

[43] P.A. and J.D.E. Paula, Physical Chemistry, 8th ed., Oxford University Press, 2006.

[44] S. Wicker, Influence of humidity on the gas sensing characteristics of SnO_2 - DRIFTS investigation of different base materials and dopants, 2016.

[45] L. Vattuone, M. Rocca, U. Valbusa, Anharmonic shift in the stretching frequency of O_2 chemisorbed on Ag (110), Surf. Sci. 314 (1994). doi:10.1016/0039-6028(94)90225-9.

[46] X. Liu, J. Hu, B. Cheng, H. Qin, M. Zhao, C. Yang, First-principles study of O_2 adsorption on the $LaFeO_3$ (0 1 0) surface, Sensors Actuators, B Chem. 139 (2009) 520–526. doi:10.1016/j.snb.2009.03.052.

[47] S.M. and L.G.T. J. M. D. Tascón, Preparation, Characterization and Catalytic Properties of $LaMeO_3$ Oxides, Z. Phys. Chem. 124 (1981) 109.

[48] R. Lago, G. Bini, M.A. Peña, J.L.G. Fierro, Partial oxidation of methane to synthesis gas using $LnCoO_3$ perovskites as catalyst precursors, J. Catal. 167 (1997) 198–209. doi:10.1006/jcat.1997.1580.

[49] M. Alifanti, J. Kirchnerova, B. Delmon, Effect of substitution by cerium on the activity of $LaMnO_3$ perovskite in methane combustion, Appl. Catal. A Gen. 245 (2003) 231–244. doi:10.1016/S0926-860X(02)00644-0.

[50] M. Alifanti, R. Auer, J. Kirchnerova, F. Thyrion, P. Grange, B. Delmon, Activity in methane combustion and sensitivity to sulfur poisoning of $La_{1-x}Ce_x$ $Mn_{1-y}Co_yO_3$ perovskite oxides, Appl. Catal. B Environ. 41 (2003) 71–81.

[51] J. Faye, A. Baylet, M. Trentesaux, S. Royer, F. Dumeignil, D. Duprez, S. Valange, J.M. Tatibouët, Influence of lanthanum stoichiometry in $La_{1-x}FeO_{3-\delta}$ perovskites on their structure and catalytic performance in CH_4 total oxidation, Appl. Catal. B Environ. 126 (2012) 134–143. doi:10.1016/j.apcatb.2012.07.001.

[52] M. Markova-Velichkova, T. Lazarova, V. Tumbalev, G. Ivanov, D. Kovacheva, P. Stefanov, A. Naydenov, Complete oxidation of hydrocarbons on $YFeO_3$ and $LaFeO_3$ catalysts, Chem. Eng. J. 231 (2013) 236–244. doi:10.1016/j.cej.2013.07.029.

[53] O. Mihai, D. Chen, A. Holmen, Chemical looping methane partial oxidation: The effect of the crystal size and O content of $LaFeO_3$, J. Catal. 293 (2012) 175–185. doi:10.1016/j.jcat.2012.06.022.

[54] G. Busca, V. Lorenzelli, Infrared Spectroscopic Identification of Species arising from Reactive Adsorption of Carbon Oxides on Metal Oxide Surfaces, Mater. Chem. 7 (1982) 89–126. doi:10.1016/0390-6035(82)90059-1.

[55] W. Taifan, J. Boily, J. Baltrusaitis, Surface chemistry of carbon dioxide revisited, Surf. Sci. Rep. 71 (2016) 595–671. oi:10.1016/j.surfrep.2016.09.001.

[56] K. Nakamoto, J. Fujita, S. Tanaka, M. Kobayashi, Infrared Spectra of Metallic Complexes. IV. Comparison of the Infrared Spectra of Unidentate and Bidentate Metallic Complexes, J. Am. Chem. Soc. 79 (1957) 4904–4908. doi:10.1021/ja01575a020.

[57] A. Davó-Quiñonero, M. Navlani-García, D. Lozano-Castelló, A. Bueno-López, J.A. Anderson, Role of Hydroxyl Groups in the Preferential Oxidation of CO over Copper Oxide-Cerium Oxide Catalysts, ACS Catal. 6 (2016) 1723–1731. doi:10.1021/acscatal.5b02741.

[58] J. Hwang, R.R. Rao, Y. Katayama, D. Lee, X.R. Wang, E. Crumlin, T. Venkatesan, H.N. Lee, Y. Shao-Horn, CO2 Reactivity on Cobalt-Based Perovskites, J. Phys. Chem. C. 122 (2018) 20391–20401. doi:10.1021/acs.jpcc.8b06104.

[59] J.M. Polfus, B. Yildiz, H.L. Tuller, R. Bredesen, Adsorption of CO2 and Facile Carbonate Formation on BaZrO3 Surfaces, J. Phys. Chem. C. 122 (2018) 307–314. doi:10.1021/acs.jpcc.7b08223.

[60] S. Harbeck, A. Szatvanyi, N. Barsan, U. Weimar, V. Hoffmann, DRIFT studies of thick film un-doped and Pd-doped SnO_2 sensors: Temperature changes effect and CO detection mechanism in the presence of water vapour, Thin Solid Films. 436 (2003) 76–83. doi:10.1016/S0040-6090(03)00512-1.

[61] K. Großmann, S. Wicker, U. Weimar, N. Barsan, Impact of Pt additives on the surface reactions between SnO_2, water vapour, CO and H_2; An operando investigation, Phys. Chem. Chem. Phys. 15 (2013) 19151–19158. doi:10.1039/c3cp52782d.

[62] C.G. Freyschlag, R.J. Madix, Precious metal magic: Catalytic wizardry, Mater. Today. 14 (2011) 134–142. doi:10.1016/S1369-7021(11)70085-2.

[63] V.G. Milt, R. Spreiz, M.A. Ulla, E.A. Lombardo, J.L.G. Fierro, The nature of active sites for the oxidation of methane on La-based perovskites, Catal. Letters. 42 (1996) 57–63. doi:10.1007/BF00814467.

[64] E.A. Lombardo, K. Tanaka, I. Toyoshima, XPS Characterization of reduced $LaCoO_3$ perovskite, J. Catal. 80 (1983) 340–349. doi:10.1016/0021-9517(83)90259-2.

[65] B. Xu, A. Hirsch, L. Kronik, K.M. Poduska, Vibrational properties of isotopically enriched materials: the case of calcite, RSC Adv. 8 (2018) 33985–33992. doi:10.1039/C8RA06608F.

[66] J. Baltrusaitis, V.H. Grassian, Surface reactions of carbon dioxide at the adsorbed water-iron oxide interface, J. Phys. Chem. B. 109 (2005) 12227–12230. doi:10.1021/jp051868k.

[67] S.U. Rege, R.T. Yang, A novel FTIR method for studying mixed gas adsorption at low concentrations: H_2O and CO_2 on NaX zeolite and γ-alumina, Chem. Eng. Sci. 56 (2001) 3781–3796. doi:10.1016/S0009-2509(01)00095-1.

[68] G. Busca and V. Lorenzelli, Infrared Study of CO_2 Adsorption on Haematite, Mater. Chem. 5 (1980) 213–224.

[69] A. Davydov, Molecular Spectroscopy of Oxide Catalyst Surfaces, John Wiley and Sons, Inc., 2003.

[70] W.E. Wallace, NIST Chemistry WebBook, NIST Standard Reference Database Number 69, National Institute of Standards and Technology, Gaithersburg MD, n.d.

[71] K. Grossmann, R.G. Pavelko, N. Barsan, U. Weimar, Interplay of H_2, water vapor and oxygenat the surface of SnO_2 based gas sensors - An operando investigation utilizing deuterated gases, Sensors Actuators, B Chem. 166–167 (2012) 787–793. doi:10.1016/j.snb.2012.03.075.

[72] T. Cao, R. You, X. Zhang, S. Chen, D. Li, Z. Zhang, W. Huang, An: In situ DRIFTS mechanistic study of CeO_2 catalyzed acetylene semihydrogenation reaction, Phys. Chem. Chem. Phys. 20 (2018) 9659–9670. doi:10.1039/c8cp00668g.

[73] G.N. Vayssilov, M. Mihaylov, P.S. Petkov, K.I. Hadjiivanov, K.M. Neyman, Reassignment of the Vibrational Spectra of Carbonates , Formates , and Related Surface Species on Ceria : A Combined Density Functional and Infrared Spectroscopy Investigation, (2011) 23435–23454. doi:10.1021/jp208050a.

[74] N. Sheppard, Vibrational Spectroscopic the Chemisorption of Single-Crystal Surfaces, Ann. Rev. Phys. Chern. 39 (1988) 589–644.

[75] T.S. Marinova, D. V. Chakarov, Adsorption of ethylene on Ir(111), Surf. Sci. 192 (1987) 275–282. doi:10.1016/S0039-6028(87)81176-7.

[76] T.S. Marinova, P.K. Stefanov, Adsorption and thermal evolution of acetylene on a Cu(100) surface, Surf. Sci. 191 (1987) 66–74. doi:10.1016/S0039-6028(87)81048-8.

[77] K.L. Kostov and Ts.S. Marinova, Interaction of Ethylene and Acetylene With Oxygen on Ir(111) Surface, Surf. Sci. 184 (1987) 359–373.

[78] T.S. Marinova, P. Stefanov, Interaction of acetylene with an oxygen-covered Cu(100) surface, Surf. Sci. 219 (1989) 490–498. doi:10.1016/0039-6028(89)90523-2.

[79] J. Kappler, A. Tomescu, N. Barsan, U. Weimar, CO consumption of Pd doped SnO2 based sensors, Thin Solid Films. 391 (2001) 186–191. doi:10.1016/S0040-6090(01)00980-4.

9. Publications

Patent

[1] Alharbi, A. Weimar, Udo and Bârsan, N. Gassensor Und Verfahren Zur Selektiven Detektion von Acetylen Und Ethylen. 102019002782.5, 2019.

Papers in peer reviewed journals

[1] Alharbi, A. A.; Sackmann, A.; Weimar, U.; Bârsan, N. A Highly Selective Sensor to Acetylene and Ethylene Based on $LaFeO_3$. Sensors Actuators, B Chem. 2020, 303.

[2] Alharbi, A. A.; Sackmann, A.; Weimar, U.; Bârsan, N. Acetylene and Ethylene Sensing Mechanism for $LaFeO_3$ based Gas Sensors: Operando Insights. J. Phys. Chem. C. (Accepted). 2020.

Conferences

[1] Alharbi, A. & Weimar, U. and Bârsan, N. Investigation of the carbonate role in acetylene selectivity of perovskite-structure oxides based gas sensors. Eurosensors 2018 Conference, Graz, Austria, 9–12 September 2018.

[2] Alharbi, A. & Weimar, Udo and Bârsan, Nicolae. (2019). Gas sensing Mechanism Investigation of $LaFeO_3$ Perovskite-Type Oxides via Operando Technique. The 8th GOSPEL Workshop, Gas Sensors Based on Semiconducting Metal Oxides: Basic Understanding & Application Fields, Ferrara, Italy, 20–21 June 2019.